

1-1-2015

# Face Sheet/core Debonding In Sandwich Composites Under Static And Fatigue Loading

Manjinder Singh Warriach  
*Wayne State University,*

Follow this and additional works at: [https://digitalcommons.wayne.edu/oa\\_dissertations](https://digitalcommons.wayne.edu/oa_dissertations)

 Part of the [Mechanical Engineering Commons](#)

---

## Recommended Citation

Warriach, Manjinder Singh, "Face Sheet/core Debonding In Sandwich Composites Under Static And Fatigue Loading" (2015). *Wayne State University Dissertations*. 1386.

[https://digitalcommons.wayne.edu/oa\\_dissertations/1386](https://digitalcommons.wayne.edu/oa_dissertations/1386)

This Open Access Dissertation is brought to you for free and open access by DigitalCommons@WayneState. It has been accepted for inclusion in Wayne State University Dissertations by an authorized administrator of DigitalCommons@WayneState.

**FACE SHEET/CORE DEBONDING IN SANDWICH COMPOSITES UNDER  
STATIC AND FATIGUE LOADING**

by

**MANJINDER SINGH WARRIACH**

**DISSERTATION**

Submitted to the Graduate School

of Wayne State University,

Detroit, Michigan

in partial fulfillment of the requirements

for the degree of

**DOCTOR OF PHILOSOPHY**

2015

**MAJOR: MECHANICAL ENGINEERING**

Approved By:

\_\_\_\_\_  
Advisor

\_\_\_\_\_  
Date

\_\_\_\_\_  
\_\_\_\_\_  
\_\_\_\_\_  
\_\_\_\_\_

© COPYRIGHT BY  
MANJINDER SINGH WARRIACH  
2015  
All Rights Reserved

## DEDICATION

First and foremost to god

## ACKNOWLEDGMENTS

I would like to express my feeling of gratitude to my advisor Dr. Golam Newaz for giving me the opportunity to work under him. His ingenious guidance, supervision and moral support throughout work are admirably acknowledged. I would like to thank my committee member's Dr. Emmanuel Ayorinde, Dr. Trilochan Singh and Dr. Hwai-Chung Wu for their valuable suggestions during this work. I would like to thank Dr. Mohammad Hailat for his help in experimental work. I would like to thanks all my lab mates for their help and support. Finally, I would like to thank Mr. Bassam Kas-Mikha for his precision work in machining the necessary parts for the developed test fixture.

Face sheet material (E-glass/epoxy) and core material (Polyurethane foam) were provided by Jim Dallam and Daniel Allman of MAG-ias. Funding for this research has been made possible through a graduate teaching assistantship from the mechanical engineering department at Wayne State University.

## TABLE OF CONTENTS

DEDICATION.....	ii
ACKNOWLEDGMENTS.....	iii
LIST OF TABLES.....	vii
LIST OF FIGURES.....	viii
CHAPTER 1 INTRODUCTION.....	1
1.1 Sandwich structure.....	1
1.2 Beam theory for sandwich beam.....	3
1.3 Applications of sandwich structures.....	11
CHAPTER 2 LITERATURE REVIEW AND OBJECTIVES.....	13
2.1 Static delamination test.....	13
2.2 Fatigue delamination test.....	17
2.3 Objectives.....	21
CHAPTER 3 BASIC CONCEPTS AND ANALYTICAL MODELS.....	22
3.1 The fracture mechanics approach.....	22
3.1.1 Fracture modes.....	22
3.1.3 J-Integral.....	23
3.1.4 Virtual crack closure technique (VCCT).....	24
3.2 Analytical models.....	27
3.2.1 Single cantilever beam (SCB) test.....	27
3.2.2 Double cantilever beam (DCB) test.....	29
3.2.3 Cracked sandwich beam (CSB) specimen.....	32

3.2.4 Mixed mode bending (MMB) specimen.....	34
CHAPTER 4 MATERIALS AND SANDWICH CONSTRUCTION.....	40
4.1 Materials.....	40
4.1.1 Face sheet material.....	40
4.1.2 Core material.....	40
4.2 Sandwich construction.....	42
4.3 Specimen dimensions.....	43
CHAPTER 5 EXPERIMENTAL ASPECTS AND FINITE ELEMENT ANALYSIS.....	44
5.1 Experimental aspects.....	44
5.1.1 T-peel test.....	44
5.1.2 Wedge test.....	46
5.1.3 Mixed mode bending (MMB) test.....	48
5.1.4 Fatigue test using single cantilever beam (SCB) test.....	53
5.1.5 Fatigue test using mixed mode bending (MMB) test.....	56
5.2 Finite element analysis.....	62
CHAPTER 6 RESULTS AND DISCUSSION.....	69
6.1 T-peel test and wedge test static evaluation.....	69
6.2 Mixed mode bending (MMB) test static evaluation.....	75
6.3 Fatigue test using single cantilever beam (SCB) test.....	92
6.4 Fatigue test using mixed mode bending (MMB) test.....	95
6.5 Failure modes of sandwich composite.....	100
CHAPTER 7 CONCLUSIONS AND RECOMMENDATIONS.....	102
7.1 Conclusions.....	102

7.2 Recommendations for future work.....	105
References.....	106
Abstract.....	115
Autobiographical Statement.....	117



## LIST OF TABLES

Table 4.1: Mechanical properties of $0^{\circ}/90^{\circ}$ E-glass/epoxy [59].....	41
Table 4.2: Mechanical properties of Polyurethane foam.....	41
Table 6.1: Fracture toughness and standard deviation using the T peel test for different E-glass fiber/foam core sandwich composite samples.....	71
Table 6.2: Fracture toughness and standard deviation using the wedge test for different E-glass fiber/foam core sandwich composite samples.....	71
Table 6.3: Mean fracture toughness and standard deviation of wedge test and T peel test for E-glass fiber/foam core sandwich composite samples.....	71
Table 6.4: Comparison of fracture toughness values obtained from experimental and finite element results using different techniques for E-glass face/core foam sandwich composite specimen.....	72

## LIST OF FIGURES

Figure 1.1: Schematic of sandwich structure [1].....	1
Figure 1.2: Sandwich panel and I-beam [2].....	2
Figure 1.3: (a) Sandwich beam with transverse forces and bending moments, (b) a symmetrical cross section sandwich composite, (c) an unsymmetrical cross section sandwich composite[3].....	3
Figure 1.4: (a) Modes of deformation for sandwich composite beam, (b) position of local z-coordinates for the face sheets of symmetrical cross section sandwich[4].....	8
Figure 1.5: The Swedish military aircraft JAS39 Gripen [9].....	11
Figure 3.1: (a) mode I fracture, (b) mode II fracture, (c) mode III fracture.....	23
Figure 3.2: An arbitrary integration contour around a crack tip [47].....	24
Figure 3.3: Virtual crack closure technique for four noded elements.....	25
Figure 3.4: Virtual crack closure technique for four-noded elements [48].....	26
Figure 3.5: (a) deformation of DCB test specimen, (b) deformation of SCB test specimen [13].....	27
Figure 3.6: The schematic and loading of loading of the Sandwich double cantilever beam specimen [15].....	30
Figure 3.7: The elastic foundation model of the DCB specimen [47].....	30
Figure 3.8: The schematic and the loading of the cracked sandwich beam Specimen [15].....	32
Figure 3.9: The free body diagram of the debonded region of the CSB specimen [47].....	33
Figure 3.10: MMB test setup and sandwich specimen [47].....	35
Figure 3.11: Mixed mode bending specimen disintegrated into CSB specimen and DCB specimen, the loads and reactions on the sandwich specimen [47]...	36

Figure 3.12: Kinematics of MMB sandwich specimen [15].....	37
Figure 3.13: The vertical movement ( $\delta_{MMB}$ ) at the point of load application [47].....	37
Figure 4.1: Schematic representation of local axis of polyurethane foam.....	42
Figure 4.2: E-glass face sheet/polyurethane foam core sandwich composite test specimen. Dimensions are in mm.....	43
Figure 5.1: T-Peel test setup and SCB sandwich specimen.....	45
Figure 5.2: Typical load-displacement curve of T- peel test for foam core sandwich composite.....	46
Figure 5.3: Wedge test machine setup.....	47
Figure 5.4: Schematic of wedge test [61].....	48
Figure 5.5: Static test setup using mixed mode bending test and mixed mode bending sandwich specimen.....	49
Figure 5.6: Typical load-displacement curve of MMB foam core sandwich composite, at lever arm distance ( $c = 20\text{ mm}$ ) from the point of application of load.....	50
Figure 5.7: Typical load-displacement curve of MMB foam core sandwich composite, at lever arm distance ( $C = 30\text{ mm}$ ) from the point of application of load.....	51
Figure 5.8: Typical load-displacement curve of MMB foam core sandwich composite, at lever arm distance ( $c = 40\text{ mm}$ ) from the point of application of load.....	52
Figure 5.9: Typical load-displacement curve of MMB foam core sandwich composite, at lever arm distance ( $c = 50\text{ mm}$ ) from the point of application of load.....	53
Figure 5.10: Fatigue tension-tension test setup using single cantilever beam test.....	54
Figure 5.11: Typical tension-tension cyclic load.....	55
Figure 5.12: Crack length vs. number of cycles for foam core sandwich composite for various displacement levels corresponding to maximum displacement level at which initial delamination crack initiates.....	56
Figure 5.13: Fatigue test setup using mixed mode bending test and mixed mode bending sandwich specimen.....	57

Figure 5.14: Crack length vs. number of cycles for MMB foam core sandwich composites at a lever arm distance ( $c = 20 \text{ mm}$ ).....	59
Figure 5.15: Crack length vs. number of cycles for MMB foam core sandwich composites at a lever arm distance ( $c = 30 \text{ mm}$ ).....	60
Figure 5.16: Crack length vs. number of cycles for MMB foam core sandwich composites at a lever arm distance ( $c = 40 \text{ mm}$ ).....	61
Figure 5.17: Crack length vs. number of cycles for MMB foam core sandwich composites at a lever arm distance ( $c = 50 \text{ mm}$ ).....	62
Figure 5.18: Two dimensional finite element model of sandwich composite for T-peel test and close view near crack tip.....	66
Figure 5.19: Two dimensional finite element model of sandwich composite for MMB test and close view near crack tip.....	67
Figure 5.20: (a) Two dimensional finite element model of foam core sandwich specimen with initial crack. (b) Detail of finite element model.....	68
Figure 6.1: Critical fracture toughness using the T peel test for different E-glass face sheet/foam core sandwich composite samples.....	73
Figure 6.2: Critical fracture toughness using the wedge test for different E-glass face sheet/foam core sandwich composite samples.....	74
Figure 6.3: Comparison of fracture toughness values obtained from experimental and finite element results using different techniques for E-glass face sheet/foam core sandwich composite specimen.....	75
Figure 6.4: Compliance versus crack length ( $a/L$ ) at a lever arm distance ( $c = 20 \text{ mm}$ ) for E-glass face sheet/foam core sandwich composite specimen.....	78
Figure 6.5: Compliance versus crack length ( $a/L$ ) at a lever arm distance ( $c = 30 \text{ mm}$ ) for E-glass face sheet /foam core sandwich composite specimen.....	79
Figure 6.6: Compliance versus crack length ( $a/L$ ) at a lever arm distance ( $c = 40 \text{ mm}$ ) for E-glass face sheet/foam core sandwich composite specimen.....	80
Figure 6.7: Compliance versus crack length ( $a/L$ ) at a lever arm distance ( $c = 50 \text{ mm}$ ) for E-glass face sheet/foam core sandwich composite specimen.....	81

Figure 6.8: Comparison of compliance versus crack length ( $a/L$ ) at a lever arm distance ( $c = 20, 30, 40$ and $50$ mm) for E-glass face sheet/foam core sandwich composite specimen.....	82
Figure 6.9: Energy release rate versus crack length ( $a/L$ ) at a lever arm distance ( $c = 20$ mm) for E-glass face sheet /foam core sandwich composite specimen.....	83
Figure 6.10: Energy release rate versus crack length ( $a/L$ ) at a lever arm distance ( $c = 30$ mm) for E-glass face sheet/foam core sandwich composite specimen.....	84
Figure 6.11: Energy release rate versus crack length ( $a/L$ ) at a lever arm distance ( $c = 40$ mm) for E-glass face sheet/foam core sandwich composite specimen.....	85
Figure 6.12: Energy release rate versus crack length ( $a/L$ ) at a lever arm distance ( $c = 50$ mm) for E-glass face sheet/foam core sandwich composite specimen.....	86
Figure 6.13: Comparison of energy release rate versus crack length ( $a/L$ ) at a lever arm distance ( $c = 20, 30, 40$ and $50$ mm) for E-glass face sheet/foam core sandwich composite specimen.....	87
Figure 6.14: Global mode ratio versus crack length ( $a/L$ ) at a lever arm distance ( $c = 20$ mm) for E-glass face sheet/foam core sandwich composite specimen.....	88
Figure 6.15: Global mode ratio versus crack length ( $a/L$ ) at a lever arm distance ( $c = 30$ mm) for E-glass face sheet/foam core sandwich composite specimen.....	89
Figure 6.16: Global mode ratio versus crack length ( $a/L$ ) at a lever arm distance ( $c = 40$ mm) for E-glass face sheet/foam core sandwich composite specimen.....	90
Figure 6.17: Global mode ratio versus crack length ( $a/L$ ) at a lever arm distance ( $c = 50$ mm) for E-glass face sheet/foam core sandwich composite specimen.....	91
Figure 6.18: Comparison of global mode ratio versus crack length ( $a/L$ ) at a lever arm distance ( $c = 20, 30, 40$ and $50$ mm) for E-glass face sheet/foam core sandwich composite specimen.....	92

Figure 6.19: Crack growth rate versus energy release rate for E-glass face sheet/foam core sandwich composite specimens.....	94
Figure 6.20: Crack growth rate versus number of cycles for E-glass face sheet/foam core sandwich composite specimens.....	95
Figure 6.21: Crack growth rate versus energy release rate for E-glass face sheet/foam core at a lever arm distance ( $c = 20\text{ mm}$ ) for sandwich composite specimens.....	97
Figure 6.22: Crack growth rate versus energy release rate for E-glass face sheet/foam core at a lever arm distance ( $c = 30\text{ mm}$ ) for sandwich composite specimens.....	98
Figure 6.23: Crack growth rate versus energy release rate for E-glass face sheet/foam core at a lever arm distance ( $c = 40\text{ mm}$ ) for sandwich composite specimens.....	99
Figure 6.24: Crack growth rate versus energy release rate for E-glass face sheet/foam core at a lever arm distance ( $c = 50\text{ mm}$ ) for sandwich composite specimens.....	100
Figure 6.25: Fracture surfaces of top and bottom foam surfaces showing foam material indicative of ‘cohesive failure’.....	101

## CHAPTER 1

### INTRODUCTION

#### 1.1 Sandwich structure

A sandwich structure is a specialized form of layered shell structure. In sandwich structure, which two thin, stiff and strong face sheets are bonded together with a relatively thick low density core. Figure 1.1 shows the schematic of sandwich structure. ASTM definition of sandwich structure is as follows “A structural sandwich is a special form of a laminated composite comprising of a combination of different materials that are bonded to each so as to utilize the properties of each separate component to the structural advantage of the whole assembly”.

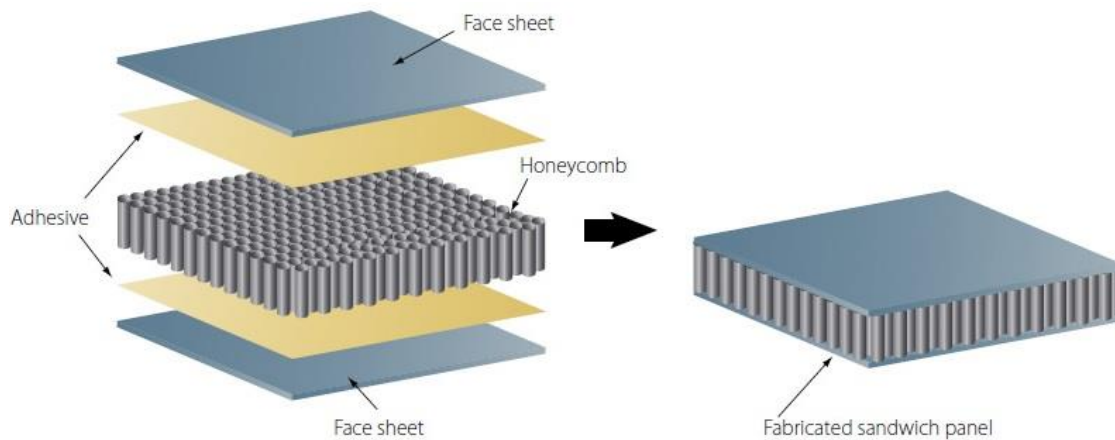


Figure 1.1: Schematic of sandwich structure (from Riley et al. [1])

The sandwich structure is considered as I-beam section, in that, face sheets are considered as flanges and core is considered as web as represented in figure 1.2. The face sheets are designed to carry the majority of the tensile and compressive loads created

from bending while the thicker core is designed to carry the shear loads created from transverse loading.

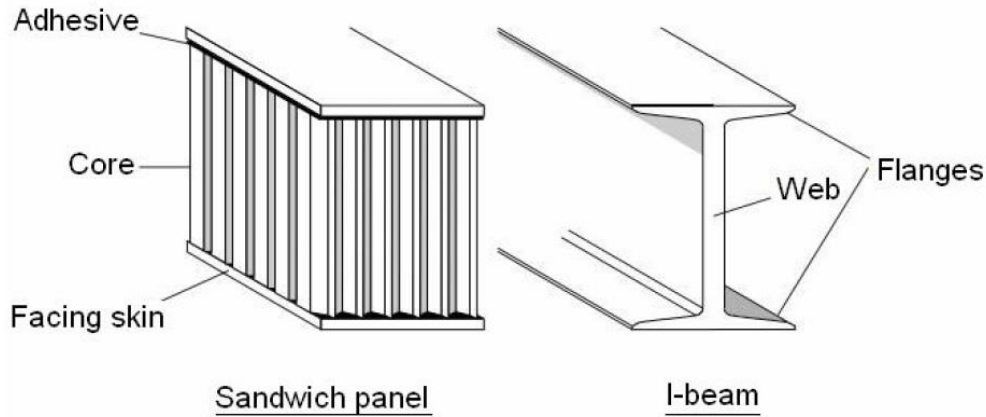


Figure 1.2: Sandwich panel and I-beam (from Bitzer [2])

Sandwich structures are best appropriate for structures which are liable to fail in buckling because of their good bending stiffness and strength to weight ratio. The bond between the face sheet and core should be extremely strong enough to resist build up tensile and shear stresses between skin and core. Sandwich structures, mainly fail due to core shear because the core is weak as compared to face sheet. The most important failure mode in sandwich structures other than core shear is a delamination between face and core. There are many reasons for debonding in sandwich structures like impact loads due to bird strike in aerospace structure and stone chipping in service, tool drop during maintenance and poor resin flow during manufacturing or under static and fatigue loading during the service lifetime of the structure due to accidental overloads. When debond occurs face sheet loses its lateral support from the core and structural stiffness reduces



because of the loss of shear load transfer between the faces. Thus material properties associated with inter-laminar fracture of face sheet/core interface are of great importance.

## 1.2 Beam theory for sandwich beam

Consider a simple sandwich beam subjected to bending moment,  $M_x$  and a transverse force  $T_x$ , as shown in figure 1.3 (a).

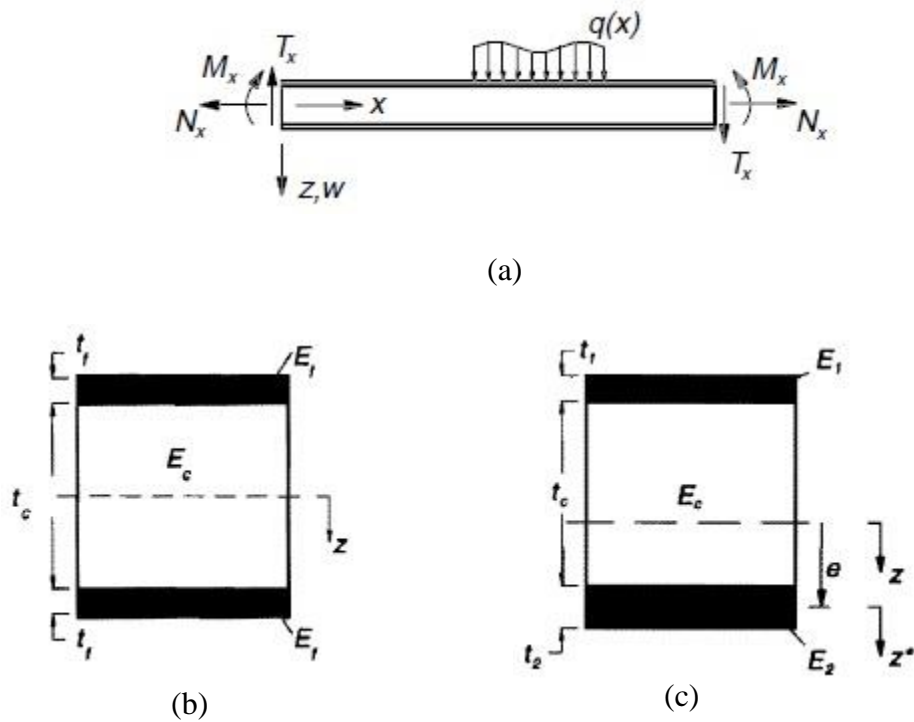


Figure 1.3: (a) Sandwich beam with transverse forces and bending moments, (b) a symmetrical cross section sandwich composite, (c) an unsymmetrical cross section sandwich composite.(from ref. Zenkert [3])

The strains can be written as

$$\varepsilon_x = \frac{\partial u}{\partial x} = \frac{z}{R_x} = -z \frac{\partial^2 w}{\partial x^2} \quad (1.1)$$

$$\gamma_{xz} = \frac{\partial u}{\partial z} + \frac{\partial w}{\partial x} \quad (1.2)$$

Where,  $u$  and  $v$  is the deformation in global  $x$  and  $z$  direction, the radius of curvature  $R_x$  is the inverse of curvature  $\kappa_x$ .

By considering only bending moment ( $M_x$ ). The strain from the neutral axis at a distance  $z$  can be defined as

$$\varepsilon_x = \frac{M_x z}{D} \quad (1.3)$$

Where,  $D$  is the flexural rigidity.

When the cross section of sandwich structure is symmetrical i.e., the face sheets of a sandwich structure are of similar material and equal thickness as shown in figure 1.3 (b).

The flexural rigidity ( $D$ )

for a symmetrical cross-section sandwich can be expressed as

$$D = \int E z^2 dz = \frac{E_f t_f^3}{6} + 2E_f t_f \left[ \frac{d}{2} \right]^2 + \frac{E_c t_c^3}{12} \quad (1.4)$$

$$= \frac{E_f t_f^3}{6} + \frac{E_f t_f d^2}{2} + \frac{E_c t_c^3}{12} = 2D_f + D_o + D_c \quad (1.5)$$

Where,  $t_f$  is the thickness of face-sheet,  $E_f$  is the modulus of elasticity of face sheet,  $t_c$  is the thickness of core,  $E_c$  is the modulus of core,  $2D_f$  is the bending stiffness of the face sheets about their respective neutral axes,  $D_o$  is the bending stiffness of the faces about the middle axis,  $D_c$  is the bending stiffness of the core,  $d = t_f + t_c$  (the distance between the centroids of the face sheets).

When the cross section of sandwich structure is unsymmetrical i.e., one of the face sheet has different material and/or of different thickness as shown in figure 1.3 (c).

The location of the neutral axis is defined as  $e$  and specified by the co-ordinate system for which first moment of area is zero when integrated over the total cross section.

$$\int \sigma_x dz = \int E \varepsilon_x dz = \int \frac{Ez}{R_x} = \frac{1}{R_x} \int Ez dz = 0 \quad (1.6)$$

The distance  $e$  from the median axis of the lower face sheet to the neutral axis is then computed from the following expression.

$$E_1 t_1 \left( \frac{t_1}{2} + t_c + \frac{t_2}{2} \right) + E_c t_c \left( \frac{t_c}{2} + \frac{t_2}{2} \right) = e [E_1 t_1 + E_c t_c + E_2 t_2] \quad (1.7)$$

The flexural rigidity can be expressed as

$$D = \frac{E_1 t_1^3}{12} + \frac{E_2 t_2^3}{12} + \frac{E_c t_c^3}{12} + E_1 t_1 (d - e)^2 + E_1 t_2 e^2 + E_c t_c \left( \frac{t_c + t_2}{2} - e \right)^2 \quad (1.8)$$

Where  $d = t_1/2 + t_c + t_2/2$  (distance between median lines of face sheets)

If the core is weak,  $E_c \ll E_f$ , then flexural rigidity can be written as

$$D = \frac{E_1 t_1^3}{12} + \frac{E_2 t_2^3}{12} + \frac{E_1 t_1 E_2 t_2 d^2}{E_1 t_1 + E_2 t_2} \quad (1.9)$$

For symmetrical sandwich cross section, the direct stress in face sheet can be determined by using their description given in equation (1.3) for thin face sheet and weak core as follows

$$\sigma_1 = -\frac{M_x (d - e) E_1}{D} = -\frac{M_x E_1 E_2 t_2 d}{D (E_1 t_1 + E_2 t_2)} \approx -\frac{M_x}{t_1 d} \quad (1.10)$$

$$\sigma_2 = \frac{M_x e E_2}{D} \approx \frac{M_x E_1 E_2 t_2 d}{D (E_1 t_1 + E_2 t_2)} \approx \frac{M_x}{t_2 d} \quad (1.11)$$

For equilibrium, the shear force should balance the change in the direct stress field.

$$\frac{d\sigma_x}{dx} + \frac{d\tau_{xz}}{dz} = 0 \rightarrow \tau_{xz}(z) = \int_z^{(d+t_f)/2} \frac{d\sigma_x}{dx} dz \quad (1.12)$$

$\tau_{xz}$  is zero at  $d/2 + t_f$  and the relation  $dM_x/dx = T_x$ , shear stress can be expressed as

$$\tau = \frac{T_x}{D} \int_z^{(d+t_f)/2} E z dz = \frac{T_x B(z)}{D} \quad (1.13)$$

Where,  $B(z)$  is the first moment of area and can be described as

$$B(z) = \int_z^{(d+t_f)/2} E z dz \quad (1.14)$$

The shear stress in the face sheets and the core of a symmetrical cross section sandwich is expressed as

$$\tau_f(z) = \frac{T_x}{(D_0+2D_f)} \frac{E_f}{2} \left( \frac{t_c^2}{4} + t_c t_f + t_f^2 - z^2 \right) \quad (1.15)$$

$$\tau_c(z) = \frac{T_x}{D} \left[ \frac{E_f t_f d}{2} + \frac{E_c}{2} \left( \frac{t_c^2}{4} - z^2 \right) \right] \quad (1.16)$$

The maximum shear stress occurs in the neutral axis, i.e., for  $z = 0$ , and minimum stress is at the interface face sheet/core, and are expressed as follows

$$\tau_{c,max}(z = 0) = \frac{T_x}{D} \left( \frac{E_f t_f d}{2} + \frac{E_c t_c^2}{8} \right) \quad (1.17)$$

$$\tau_{c,min} = \tau_{f,max} = \frac{T_x}{D} \left( \frac{E_f t_f d}{2} \right) \quad (1.18)$$

The shear stresses for unsymmetrical cross section sandwich can be expressed as

For  $z < 0$  (distance between the top of face sheet 1 and core from neural axis)

$$\tau_{f1}(z) = \frac{T_x E_1}{D} \frac{1}{2} \left[ \left( d - e + \frac{t_1}{2} \right)^2 - z^2 \right] \quad (1.19)$$

$$\tau_c(z) = \frac{T_x}{D} \left[ E_1 t_1 (d - e) + \frac{E_c}{2} \left( d - e - \frac{t_1}{2} \right)^2 - z^2 \right] \quad (1.20)$$

For  $z > 0$  (distance between the bottom of face sheet 2 and core from neural axis)

$$\tau_{f2}(z) = \frac{T_x E_2}{D} \frac{1}{2} \left[ \left( e + \frac{t_2}{2} \right)^2 - z^2 \right] \quad (1.21)$$

$$\tau_c(z) = \frac{T_x}{D} \left[ E_2 t_2 e + \frac{E_c}{2} \left( e - \frac{t_2}{2} \right)^2 - z^2 \right] \quad (1.22)$$

For weak core, the core shear stress is constant; the maximum core shear stress can be expressed as

$$\tau_{c,max} = \frac{T_x}{D} \frac{E_1 t_1 E_2 t_2 d}{E_1 t_1 + E_2 t_2} \quad (1.23)$$

For thin face sheets, the above equation can be expressed as

$$\tau_{c,max} = \frac{T_x}{d} \quad (1.24)$$

The equations (1.10, 1.11 and 1.24) validates the statement about load bearing capacity and stress distribution in a sandwich composite as mentioned by Zenkert [4] that “the faces carry bending moments as tensile and compressive stresses and the core carries transverse forces as shear stresses”.

For a sandwich composite beam with thin face sheets the total curvature due to the presence of bending and shear deformation can be expressed as

$$\frac{d^2 w}{dx^2} = -\frac{M_x}{D} + \frac{1}{S} \frac{dT_x}{dx} \quad (1.25)$$

Where,  $S$  is the shear stiffness. The shear stiffness is described as

$$S = \frac{Gh}{k} \quad (1.26)$$

Where,  $G$  is the shear modulus,  $h$  is the height of the beam and  $k$  is shear factor. For sandwich composite beam with thin face sheets,  $t_f \ll t_c$  and weak core,  $E_c \ll E_f$  the stiffness according to Zenkert [4] can be expressed as

$$S = \frac{G_c d^2}{t_c} \quad (1.27)$$

For a sandwich composite beam, the in-plane and out of plane deformations can be expressed as

$$u(z) = u_0 + z\psi_x \quad (1.28)$$

$$w = w_b + w_s \quad (1.29)$$

$$\psi_x = -\frac{dw_b}{dx} \quad (1.30)$$

Where,  $u_0$  is the deflection of mid plane,  $\psi_x$  is the rotation of cross section,  $w_b$  is the deformation due to bending moment,  $w_s$  is the deformation due to shear force.

The modes of deformation for sandwich composite beam are represented in figure 1.4 (a).

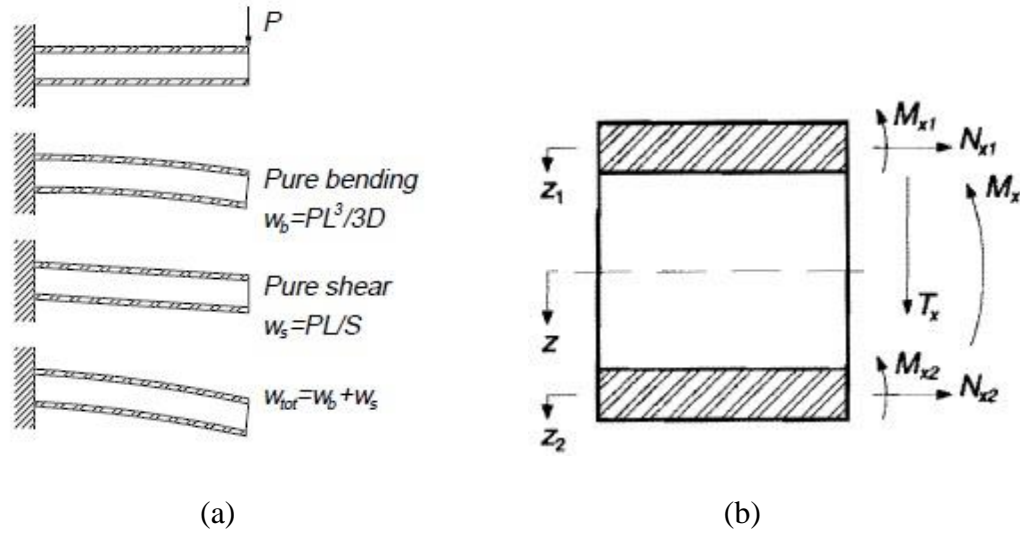


Figure 1.4: (a) Modes of deformation for sandwich composite beam, (b) position of local  $z$ -coordinates for the face sheets of symmetrical cross section sandwich (from ref. Zenkert [4])

To obtain the general governing equation for sandwich composite beam, first consider that the sandwich composite beam has no in-plane deformation. Then the in-plane stresses according to Plantema [5] can be expressed as

$$\sigma_1 = -E_1 z \frac{d^2 w_b}{dx^2} - E_1 z_1 \frac{d^2 w_s}{dx^2} \quad (1.31)$$

$$\sigma_2 = -E_2 z \frac{d^2 w_b}{dx^2} - E_2 z_2 \frac{d^2 w_s}{dx^2} \quad (1.32)$$

Where,  $z_1$  is a local co-ordinate calculated from the median axis of the top face sheet and  $z_2$  is a local co-ordinate calculated from the median axis of the bottom face sheet as shown in figure 1.4 (b). The local bending moment in the face sheets can be expressed as

$$M_{x1} = -D_{f1} \frac{d^2 w_b}{dx^2} \quad (1.33)$$

$$M_{x2} = -D_{f2} \frac{d^2 w_b}{dx^2} \quad (1.34)$$

Where,  $D_{f1}$  and  $D_{f2}$  are the flexural rigidities of the top and bottom face sheets about their median axes, respectively.

In the same manner, the in-plane forces can be expressed as

$$N_{x1} = E_{f1} t_{f1} (d - e) \frac{d^2 w_b}{dx^2} \quad (1.35)$$

$$N_{x2} = -E_{f2} t_{f2} e \frac{d^2 w_b}{dx^2} \quad (1.36)$$

The total bending moment can be expressed as

$$M_x = (D_o + D_{f1} + D_{f2} + D_c) \frac{d^2 w_b}{dx^2} = D \frac{d^2 w_b}{dx^2} \quad (1.37)$$

For equilibrium, the vertical forces and moments can be expressed as

$$q + \frac{dT_x}{dx} + N_x \frac{d^2 w}{dx^2} = 0 \quad (1.38)$$

$$T_x = \frac{dM_x}{dx} \quad (1.39)$$

The governing equation for sandwich composite beam derived by Hoff [6] is as follows

$$2D_f \frac{d^6 w}{dx^6} - \frac{DS}{D_o} \frac{d^4 w}{dx^4} = \left( \frac{d^2}{dx^2} - \frac{S}{D_o} \right) \left( q + N_x \frac{d^2 w}{dx^2} \right) \quad (1.40)$$

For sandwich composite with thin face sheets equation (1.40) can be written as

$$D_o \frac{d^4 w}{dx^4} = \left( 1 - \frac{D_o}{S} \frac{d^2}{dx^2} \right) \left( q + N_x \frac{d^2 w}{dx^2} \right) \quad (1.41)$$

By adding time dependent inertia terms in equation (1.38 and 1.39), equation (1.38) and equation (1.39) can be expressed as

$$-T_x + R \frac{d^3 w_b}{dx dt^2} + \frac{\partial M_x}{\partial x} = 0 \quad (1.42)$$

$$q + \frac{\partial T_x}{\partial x} + N_x \frac{\partial^2 w}{\partial x^2} - \rho^* \frac{\partial^2 w}{\partial t^2} = 0 \quad (1.43)$$

Where,  $\rho^*$  is the surface mass of the beam and  $R$  is the rotary inertia. These parameters can be described as

$$\rho^* = \int \rho dz \quad (1.44)$$

$$R = \int \rho z^2 dz \quad (1.45)$$

Where,  $\rho$  is the density of the material.

For sandwich composite with thin face sheets the governing equation can be expressed as

$$D_0 \frac{\partial^4 w}{\partial x^4} + \left( \frac{D_0}{S} \frac{\partial^2}{\partial x^2} - 1 - \frac{R}{S} \frac{\partial^2}{\partial t^2} \right) \left[ q + N_x \frac{\partial^2 w}{\partial x^2} - \rho^* \frac{\partial^2 w}{\partial t^2} \right] - R \frac{\partial^4 w}{\partial x^2 \partial t^2} = 0 \quad (1.46)$$

This equation is generally known as the Timoshenko beam equation as derived by Timoshenko [7].



### 1.3 Applications of sandwich structures

Sandwich structures are used in truck containers which are used for transportation of cold goods because of high thermal insulation and low structural weight (from ref. Zenkert [3]). The face sheet of Mine-sweepers or mine-counter-measure vessels is made up of foam core sandwich structures because of their damage tolerant attribute to underwater detonations (from ref. Hellbratt [8]). Sandwich structures are used in military and civil aircrafts and the applications include control surfaces, doors, wings radomes, tailplanes, stabilizers etc. Antennas and solar panels of space structures are made up of sandwich structure (from ref. Zenkert [3]). The canard wing, the vertical stabilizer and access doors of Swedish military aircraft JAS 39 Gripen shown in figure1.5 are composite sandwich structures made up of CFRP as facesheet and aluminum honeycomb core (from ref. Pickett [9] and Turner [10]).



Figure 1.5: The Swedish military aircraft JAS39 Gripen [9]

The hull of navy ship YS200 is made up of carbon fiber reinforced polymer (CFRP) sandwich due to low structural weight, non -magnetic properties and high energy absorption capability (from ref. Zenkert [3]). The wellhead protection structure for North Sea oil pumps is composed of composite sandwich because of their peculiar properties like high impact strength and low corrosion (from ref. Zenkert [3]). Sandwich structures composed of aramid and glass fiber reinforced Vinylester/polyester as facesheet and PVC foam as core are widely used in surface-effect ships because of their low structural weight (from ref. Olsson [11]). The external structure of Stockholm Globe Arena is made of sandwich structure in which aluminum face sheet is bonded to the core material (from ref. van Tooren [12]).

## CHAPTER 2

### LITERATURE REVIEW AND OBJECTIVES

#### 2.1. Static delamination test

Rinker et al. [13] numerically investigated the effect of residual thermal stress on face sheet debonding in CFRP/PMI sandwich structure under static loading. They used single cantilever beam (SCB) test and cracked sandwich beam (CSB) test for Mode I and Mode II respectively. Their results showed the effect of residual stress was significant in CSB test but not in DCB test. Also they numerically studied the effect of friction between face sheet and core in cracked sandwich beam test. They reported that the energy release rate decreased and stiffness increased at higher friction coefficient. Later they numerically calculated fracture toughness using virtual crack closure technique (VCCT) and found 7 % mode mixity in SCB test and 25 % mode mixity in CSB test.

Aviles and Carlsson [14] derived expressions to calculate compliance and energy release rate of double cantilever beam test for sandwich structures using built-In beam analysis and elastic foundation. They reported that good agreement was seen between the results obtained from experiment, elastic foundation model and finite element analysis (FEA) but not with beam analysis. They also studied the effect of core modulus, beam length and face sheet thickness on the compliance using FEA and built-In beam analysis. They found that core modulus, and in case of sufficiently long specimen change in the length of beam, had no effect on the compliance. They also reported that compliance increased moderately and sharply when the ratio of face sheet thickness to crack length was greater and less than 0.025 respectively. Finally, they establish expression for

maximum crack length and effective crack size to avoid nonlinear end effects and consider the foundation effect for soft core material in the beam foundation.

Quispitupa et al. [15] formulated expression for compliance and energy release rate of mixed mode bending (MMB) specimen for sandwich structures. They analytically and numerically showed that compliance and energy release rate values were in close agreement. They found that compliance and energy rate increased and analysis became mode I dominant with increase in lower arm distance. They studied the effect of face sheet thickness, core thickness, core modulus on compliance and energy release rate. They noted that for thin face sheet mode I was dominant, compliance and energy release rate values were higher. Compliance of the system decreased with increase in core thickness and for high core modulus. Finally, they noted that for soft core materials mode mixity ration was not constant and higher for long crack length. Saha et al. [16] studied the effect of infusion of different types of nanoparticles in the foam core on fracture toughness using tilted sandwich debond (TSB) configuration. They found that nanoparticles delayed the crack propagation and improve fracture toughness by 69 %.

Wang et al. [17] carried out experiment on metal foam core sandwich using modified cracked sandwich beam test. Their results indicated that Interfacial peel strength was lower than interlaminar fracture strength and delamination was at interface but unsynchronously on the two sides of the specimen. Ural et al. [18] investigated titanium honeycomb core sandwich at room temperature and high altitude subsonic temperature (-54°C) to predict Interfacial fracture toughness using double cantilever beam test. They found that fracture toughness was 24% less at high altitude subsonic temperature as

compared to room temperature. Liechti and Marton [19] studied the effect of room temperature and high temperature (180°C) on fracture toughness in titanium honeycomb core sandwich beam using steel reinforcement attached mechanically to the face sheet using double cantilever sandwich beam test. Their results showed that fracture toughness was higher at room temperature, toughness decreased with increase in crack length. They also reported that failure was cohesive and adhesive at room and high temperature respectively.

Li and Carlsson [20] established analytical expression for compliance and energy release rate of the tilted sandwich debond (TSD) specimen using elastic foundation approach. Later they performed parametric study on a sandwich made up of Glass/Vinylester face and H200 PVC foam core to evaluate the influence of material and geometrical parameters on compliance and energy release rate. They showed that core modulus and thickness strongly influence the compliance of the system. Finally they reported that crack propagated in Stick-slip manner but remained at the interface for all desired tilt angles. Li and Carlsson [21] introduced tilted sandwich debond specimen to evaluate fracture toughness of foam core sandwich panels. The bottom surface of a sandwich was attached to an inclined surface and load applied to the top to propagate the crack. They conclude that the crack propagated in the core parallel to the interface for all tilt angles above critical tilt angle and fracture toughness was not influenced by crack length. Finally they reported that critical tilt angle decreased with increase in the initial crack length.

Smith and Shivakumar [22] modified the cracked sandwich beam by adding a roller support at the free end of the specimen to prevent large rotations. Studied the effect of core densities of PVC foam and face sheet material on fracture toughness. Their results indicated that crack growth was stable in high density cores ( $130-200 \text{ kg/m}^3$ ) but stick-slip growth was seen in low density cores ( $80-100 \text{ kg/m}^3$ ). Finally they reported that fracture was independent of crack length and face sheet material. Berggreen and Carlsson [23] modified the tilted sandwich debond (TSD) specimen to extend the limited range of mode-mixites of TSD specimen by reinforcing the upper face sheet with stiff metal plate. Prasad and Carlsson [24, 25] reported cracked kinked into the core and propagated along the interface when shear stress was positive and negative ahead of the crack tip. Berggreen et al. [26] and Lundsgaard-Larsen et al. [27] reported that crack kinked into the face sheet when the shear stress was negative ahead of the crack tip. Gdoutos [28] conducted finite element analysis and reported that for strong interfacial bonds in sandwich composites, crack can divert into the core and run parallel to the interface in Mode I.

Hojo et al. [29] conducted experiment on carbon fiber/epoxy laminates with self-same epoxy interleaf to study the effect of resin-rich layer thickness ( $50 \mu\text{m}$ ) on fracture toughness under Mode I and Mode II using double cantilever beam specimen and three point end notched flexure specimen. Their results indicated that there was no change in fracture toughness under Mode I but fracture toughness value was 3.4 times higher that of with interleaf under Mode II. Hojo et al. [30] carried out experiment on Zanchor-reinforced CF/epoxy laminates to predict fracture toughness using double cantilever

beam specimen. They found that the fracture toughness value was 3.5 times higher with Zanchor reinforcement.

## 2.2 Fatigue delamination test

Shipsha et al. [31] conducted experiments to study effect of two core materials on fatigue crack growth rates under Mode I and Mode II loading in foam core sandwich. Their results indicated that crack growth rates were higher by a factor of 10 for both Mode I and Mode II for core material with lower density. In addition, crack growth rates were higher under Mode I as compared to under Mode II for both core materials. Rinker et al. [13] investigated numerically the effect of residual thermal stress on face sheet debonding in CFRP/PMI sandwich structure using single cantilever beam test and cracked sandwich beam specimen for Mode I and Mode II, respectively. Their results indicated that the effect of residual thermal was significant in CSB test and in DCB test. Because of the residual thermal stress Paris law constants were higher.

Berkowitz and Johnson [32] carried out experiments to study the effect of hot temperature(77°C), room temperature(21°C) and cold temperature (-54°C) on crack growth rate in a nomex honeycomb sandwich structure using modified double cantilever beam specimen. Their results indicated that the cold temperature reduced the fatigue crack growth rate significantly as compared to room temperature but hot temperature had very small impact on fatigue crack growth rate. Kanny and Mahfuz [33] conducted experiments to study the effect of frequency on fatigue behavior on two different PVC core sandwich structures. Their results indicated that fatigue strength was higher for high

density core and at high frequency the number of cycle to failure increased. They also noted a significant increase in core temperature in low density core at high frequency as compared to low frequency because of this substantial difference was seen in crack path. Finally , they reported that crack growth rate for low density core was faster at low frequency as compared to high frequency.

Newaz et al. [34] conducted experiments to study the effect of room temperature and high temperature on crack growth rate in unidirectional carbon/polyetheretherketone (PEEK) composites using Mode I fatigue loading under load controlled conditions. Their results indicated that crack growth rate was high at room temperature but crack growth rate decreased significantly at high temperature due to the process zone ahead of the crack front. They characterized crack growth rate at elevated temperature using relaxation controlled growth model. Trethewey et al. [35] conducted experiments on various unidirectional composites to predict fatigue crack growth behavior using end notched flexure (ENF) specimen. They reported that crack growth resistance was higher for tough thermoplastic resin plastics as compared to brittle thermoset system and friction in the delaminated area was a potential energy absorbing mechanism.

Hojo et al. [29] conducted experiment on carbon fiber/epoxy laminates with self-same epoxy interleaf to study the effect of resin-rich layer thickness(50  $\mu\text{m}$ ) on the delamination fatigue crack growth behavior under Mode I and Mode II using double cantilever beam specimen and 4- point end notched flexure specimen respectively. They reported that there was no change in delamination fatigue threshold value under Mode I. However, the delamination fatigue threshold value increased by 2 times at stress ratio (R)



= 0.1 and 2.3 times at stress ratio( $R$ ) = 0.5 under Mode II. Hojo et al. [30] carried out experiment on Zanchor- reinforced CF/epoxy laminates to investigate fatigue crack growth behavior using double cantilever beam specimen. They reported that threshold value increased by 3.4 and 5 times at stress( $R$ ) = 0.1 and 0.5 respectively with Zanchor reinforcement. Peng et al. [36] studied the effect of ply orientations on fatigue delamination crack growth rate behavior in multidirectional Carbon/bismaleimide composites. They reported that the normalized threshold value was independent of the inplane-adjacent fiber orientation. Moreover, they concluded that rising delamination resistance was mainly caused by fiber bridging and intra- ply fracture.

Shivakumar et al. [37] proposed a fatigue life model for Mode I delaminated composite laminates considering the effects of fracture resistance with debond growth. Later they verified the model to predict the delamination length in woven roving glass/vinylester delaminated composites under block cyclic loading. Nakai and Hiwa [38] conducted experiment on two types of unidirectional CF/epoxy laminates (i.e. T300/3601 and M40J//2500) to study delamination fatigue crack growth behavior in air and water. They noted that in T300/3601 laminates the crack growth was cycle and time dependent in air and water respectively, and in M40J/2500 laminates the crack growth was cycle dependent in both air and water. Finally, they reported that the crack growth rate was higher in air than that in water for both laminates. Sjögren and Asp [39] conducted experiment on HTA/6376C carbon fiber/epoxy laminates to study the effect of high temperature (100°C) on delamination growth behavior. They reported that strain energy release rate threshold was only 10 % of the critical energy release rate value in static test.

Shindo et al. [40] carried out experiment on glass fiber reinforced polymer woven laminates under Mode I using DCB to study the effect of low temperature on delamination crack growth behavior. Their results indicated that delamination growth rates were much lower at low temperature as compared to room temperature. Later they reported that at room temperature the fiber-matrix debonding was the fatigue delamination growth mechanism but at low temperature fiber- matrix debonding and brittle fracture of matrix were the fatigue delamination growth mechanism. Shipsha et al. [41] carried out experiments to understand fatigue crack growth in foam core materials for sandwich structures under constant load amplitude tests, under manual shedding of load amplitude tests, K-increasing technique and K-decreasing test. Hojo et al. [42] conducted experiment on Alumina fiber (ALF) / epoxy laminates at 77K in liquid nitrogen to study delamination fatigue crack growth behavior. They reported that maximum energy release rate threshold value for fatigue crack growth at 77 K was 3.4 times higher than that at room temperature. Hirose et al. [43, Hirose et al. [44, Hirose and Hojo [45], Minakuchi et al. [46] proposed a semi-cylindrical shape crack arrester which was blended in the core and attached to the skin, to restrain crack propagation at the interface in foam core sandwich composites and reported that crack arrester has no adverse effect on the structural properties of the sandwich beam.

For sandwich composites, delamination growth has not been studied extensively in terms of Mode I energy release rate using two different types of tests to check result validity. Also, until now limited literature is available for fatigue delamination crack growth under constant displacement amplitude loading for composite sandwich

structures. In this study, the delamination crack growth behavior for E-glass face sheet/polyurethane foam core sandwich structure for the mode I and mixed mode under static and fatigue loading is characterized.

### 2.3 Objectives

The main goal of this research is to study the face sheet debonding from core experimentally under static and fatigue loading in sandwich structures made up of polyurethane foam as the core and E-glass/epoxy composite laminate as face sheet. The research is primarily divided into two parts. In the first part, static tests are conducted on sandwich composites using T-peel test and wedge test for mode I loading and using mixed mode bending test for mixed mode loading at room temperature and humidity to evaluate fracture toughness of the sandwich composite. In the second part, fatigue tests are conducted on sandwich structures under constant displacement amplitude mode I and mixed mode loading at room temperature and humidity to measure interfacial crack growth rates. The effect of lever arm distance ( $c$ ) under mixed mode loading on global mode ratio ( $G_{II}/G_I$ ) is studied. The results are plotted to estimate the energy release rate threshold and to extract Paris law constants to predict the failure of sandwich composite under investigation. Finally, finite element analyses are conducted using ABAQUS to validate the experimental results.

## CHAPTER 3

### FRACTURE CONCEPTS AND ANALYTICAL MODELS

#### 3.1 The fracture mechanics approach

The main intention of employing a fracture mechanics approach is to define the crack growth resistance from aforementioned crack or imperfection in terms of material parameters.

##### 3.1.1 Fracture modes

Most of the cracks depict a mixed mode fracture behavior. The corresponding contribution of mode I and mode II component depend on the geometry, load and boundary conditions and material properties of the component under consideration. The fracture mechanics approach concentrates mainly on the three fundamental types of failure modes as represented in figure 3.1. The mode I fracture is the opening mode, in this mode crack surfaces move perpendicular to the crack plane and opens the crack. The mode II fracture is the shearing mode, in this mode crack surfaces slide over each other in the in-plane shear stress parallel to the crack direction. The mode III fracture is tearing mode, in this mode crack surfaces slide over each other in the out of plane shear stress perpendicular to the crack direction.

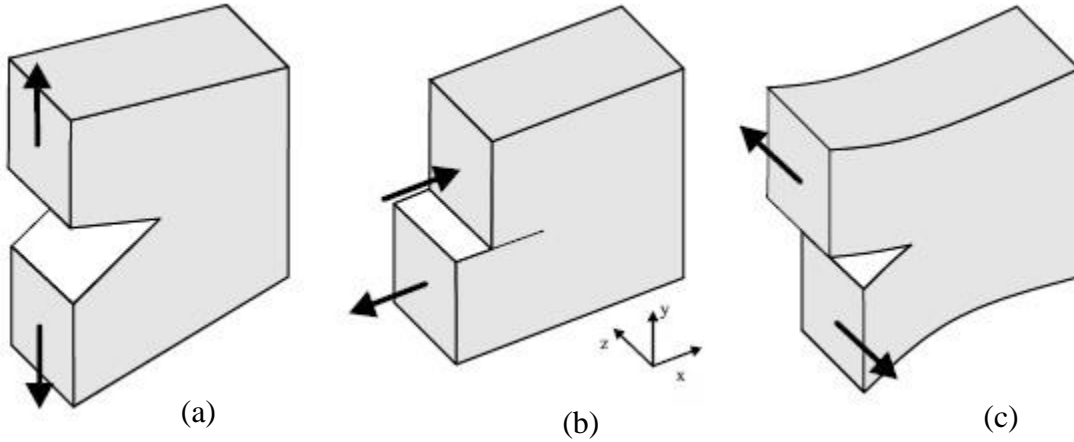


Figure 3.1: (a) mode I fracture, (b) mode II fracture, (c) mode III fracture.

### 2.1.2 J-Integral

Rice (1968) proposed J-integral parameter to describe nonlinear material behavior ahead of crack tip. The J-integral is defined as path-independent contour integral that evaluates the strength of the singular stresses and strains in the vicinity of crack tip as shown in figure 3.2.

The J-integral is given by

$$J = \int_{\Gamma} \left( \phi dx_2 - \sigma_{ij} n_j \frac{\partial u_i}{\partial x_j} ds \right) \quad (3.1)$$

Where,  $\Gamma$  is any counter clockwise path enclosing the crack faces,  $\phi$  is the strain energy density,  $n_j$  is the outward directed normal vector on the path,  $x_j$  is a coordinate along the crack path,  $u_i$  is the displacement vector and  $ds$  is the element of  $\Gamma$ .

The strain energy density is defined by

$$\Phi = \int_0^{\varepsilon} \sigma_{ij} d\varepsilon_{ij} \quad (3.2)$$

Where,  $\sigma_{ij}$  and  $\varepsilon_{ij}$  are the stress and strain tensors, respectively.

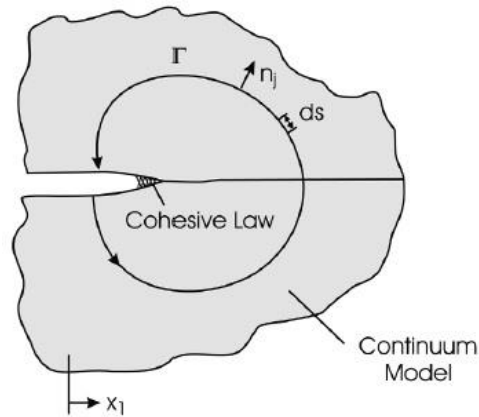


Figure 3.2: An arbitrary integration contour around a crack tip (from ref. Carlsson and Kardomateas [47]).

### 3.1.3 Virtual crack closure technique (VCCT)

The VCCT is based on Irwin assumption that the energy released to extend the crack by small amount is equal to the energy required to close the crack, state of crack tip does not change during crack extension. Figure 3.3 and 3.4 represents the virtual crack closure technique for four-noded and eight-noded elements, respectively. When the crack tip is located at node  $k$ , the displacement behind the crack tip at node  $i$  is approximately equal to the displacement behind the crack tip at node  $l$  when the crack tip is at node  $i$ .

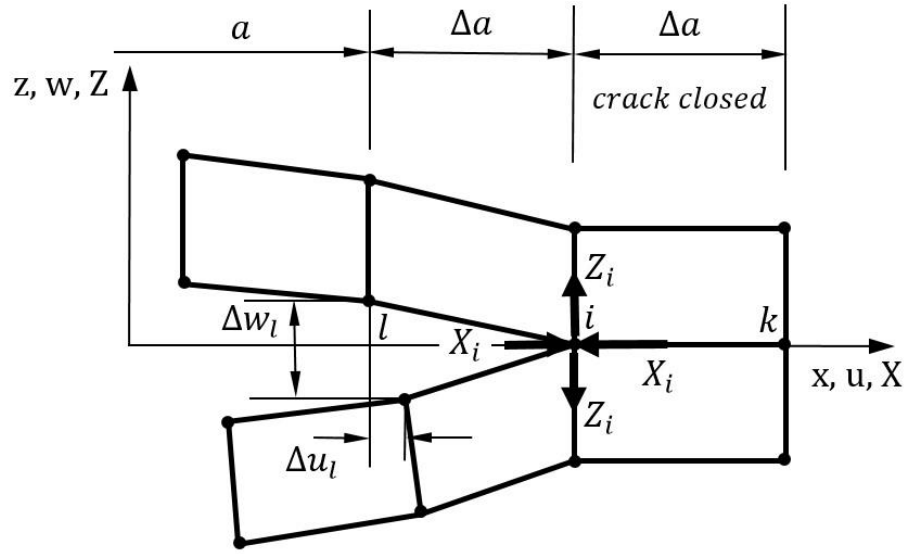


Figure 3.3: Virtual crack closure technique for four noded elements

The components of strain energy release rate  $G_I, G_{II}$  for 2 dimensional analysis for four noded element are as follows.

$$G_I = -\frac{1}{2\Delta a} Z_i \Delta w_l \quad (3.3)$$

$$G_{II} = -\frac{1}{2\Delta a} X_i \Delta u_l \quad (3.4)$$

Where,  $\Delta a$  is the length of the elements at the crack front,  $Z_i$  and  $X_i$  are opening and shear forces at nodal point  $i$  and  $\Delta w_l$  and  $\Delta u_l$  are the differences in the opening and shear nodal displacement at node  $l$ . The forces (opening and shear) and displacement (opening and shear) are calculated from the analysis results to calculate energy release rate.

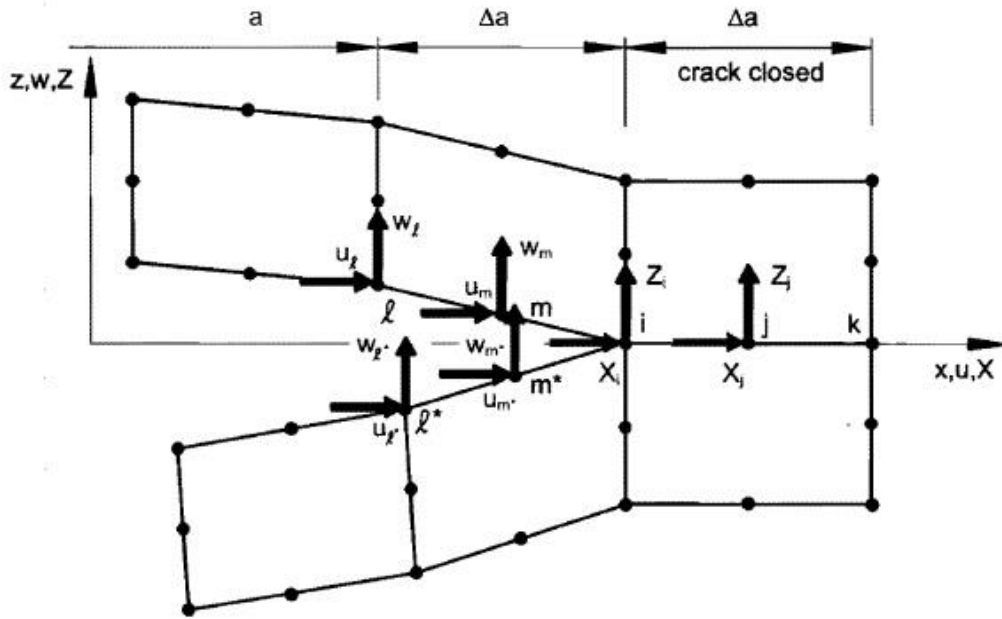


Figure 3.4: Virtual crack closure technique for four-noded elements (from ref. Krueger [48]).

The components of strain energy release rate  $G_I$ ,  $G_{II}$  for 2 dimensional analysis for eight-noded element are as follows.

$$G_I = -\frac{1}{2\Delta a} [Z_i(w_l - w_{l^*}) + Z_j(w_m - w_{m^*})] \quad (3.5)$$

$$G_{II} = -\frac{1}{2\Delta a} [X_i(u_l - u_{l^*}) + X_j(u_m - u_{m^*})] \quad (3.6)$$

Where,  $\Delta a$  is the length of the elements at the crack front,  $X_i$  and  $Z_i$  are the sliding and opening forces at nodal point  $i$ ,  $X_j$  and  $Z_j$  are the sliding and opening forces at nodal point  $j$ ,  $u_l$  and  $u_m$  are the sliding displacements at the upper crack face at nodal point  $l$  and  $m$ , respectively.  $w_l$  and  $w_m$  are the opening displacements at the upper crack face at nodal point  $l$  and  $m$ , respectively.  $u_{l^*}$  and  $u_{m^*}$  are the sliding displacements at the lower crack face at nodal point  $l^*$  and  $m^*$ , respectively.  $w_{l^*}$  and  $w_{m^*}$  are the opening displacements at the lower crack face at nodal point  $l^*$  and  $m^*$ , respectively.



### 3.2 Analytical models

#### 3.2.1 Single cantilever beam (SCB) test

Single cantilever beam (SCB) specimen was developed by Cantwell and Davies [49] and later used by Cantwell and Davies [50] to estimate the fracture toughness of glass fiber reinforced sandwich composite from the experimental compliance method. Till now no analytical model to evaluate fracture toughness has been presented for SCB specimen. The elastic foundation analysis (EFA) derived for double cantilever beam (DCB) test by Aviles and Carlsson [14] and Quispitupa et al. [15] and for tilted sandwich debond(TSD) specimen by Li and Carlsson [20] are modified to calculate compliance and energy release rate for SCB test.

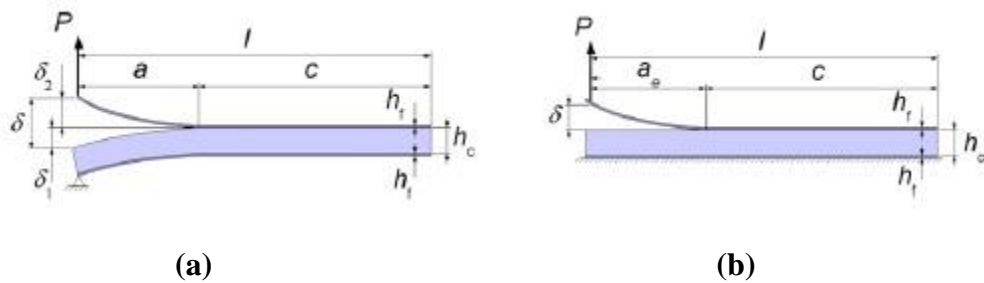


Figure 3.5: (a) deformation of DCB test specimen, (b) deformation of SCB test specimen.(from ref. Rinker et al. [13])

Figure 3.5 shows the deformation of DCB test specimen and deformation of SCB test specimen. Aviles and Carlsson [14] and Quispitupa et al. [15] set up a method to evaluate deflection ( $\delta$ ), compliance ( $C$ ), and energy release rate( $G$ ) against crack length in DCB test by employing an elastic foundation analysis(EFA). Total deflection( $\delta$ ) of DCB test consists of deformation of the cracked top face sheet ( $\delta_2$ ) and the combined deformation of the core and lower face sheet ( $\delta_1$ ). From figure 3.5 (b) it is evident that

( $\delta_1$ ) is zero as bottom of the specimen is fixed in case of SCB test. The deflection ( $\delta$ ) and compliance ( $C$ ) of the SCB test completely depends on deformation of the cracked top face sheet ( $\delta_2$ ).

The deformation of the cracked top face sheet ( $\delta_2$ ) can be expressed as

$$\delta = \delta_2 = \frac{P}{3D_f} \left[ a^3 + 3a^2\eta^{1/4} + 3a\eta^{1/2} + \frac{3}{2}\eta^{3/4} \right] \quad (3.7)$$

The compliance ( $C_{SCB}$ ) of the SCB test can be expressed as

$$C_{SCB} = \frac{1}{3D_f} \left[ a^3 + 3a^2\eta^{1/4} + 3a\eta^{1/2} + \frac{3}{2}\eta^{3/4} \right] \quad (3.8)$$

Where,  $P$  is the applied load,  $a$  is the crack length,  $\eta$  is the parameter for the elastic foundation modulus and  $D_f$  is the bending stiffness of the face sheet determined using classical laminate theory.

The parameter for elastic foundation modulus ( $\eta$ ) can be described as

$$\eta = \frac{2D_f h_c}{bE_c} \quad (3.9)$$

Where,  $b$  is the width of specimen,  $h_c$  is the height of core and  $E_c$  is the elastic modulus of core.

The energy release rate ( $G_{SCB}$ ) can be expressed as

$$G_{SCB} = \frac{P^2}{2bD_f} \left[ a^2 + 2a\eta^{1/4} + \eta^{1/2} \right] \quad (3.10)$$

Li and Carlsson [20] calculated the elastic foundation analysis (EFA) for tilted sandwich debond (TSD) specimen. By considering, the tilt angle zero degree in case of SCB test.

The compliance ( $C_{SCB}$ ) can be expressed as

$$C_{SCB} = \frac{4\beta}{K} \left( \frac{1}{3}\beta^3 a^3 + \beta^2 a^2 + \beta a + \frac{K}{4\beta k G_{13,f} h_f} a + \frac{1}{2} \right) \quad (3.11)$$

The energy release rate ( $G_{SCB}$ ) can be expressed as

$$G_{SCB} = \frac{4\beta P^2}{2bK} \left( \beta^2 a^2 + 2\beta^2 a + \beta + \frac{K}{4\beta k G_{13,f} h_f b} \right) \quad (3.12)$$

Where,  $G_{13,f}$  is the out of plane shear stiffness of the facesheet,  $h_f$  is the thickness of the facesheet and  $k = 5/6$  is a shear correction factor.

$\beta$  can be described as

$$\beta = \left( \frac{K}{4D_f} \right)^{1/4} \quad (3.13)$$

$$K = \frac{E_c b}{h_c} \quad (3.14)$$

### 3.2.2 Double cantilever beam (DCB) specimen

The double cantilever beam (DCB) specimen is very well-known test for determining the delamination fracture toughness of laminated composites, containing initial delamination symmetrically at the mid plane, under Mode I. Prasad and Carlson [51] were the first to adopt DCB specimen for foam core sandwich beams. Aviles and Carlsson [14] established elastic foundation model (EFM) of sandwich double cantilever beam specimen to evaluate compliance and energy release rate. The schematic and loading of loading of the Sandwich double cantilever beam specimen is shown in figure 3.6. The upper segment (debonded face sheet) is treated as a cantilever beam with flexural modulus,  $E_{f1}$  and thickness  $h_{f1}$ . The lower segment consists of lower face with flexural modulus,  $E_{f2}$  and thickness  $h_{f2}$ , united to a core with elastic modulus,  $E_c$ , shear modulus,  $G_{xz}$  and thickness  $h_c$ . The deviation of the upper and lower segment of the specimen is denoted as  $\delta_{DCB\_upper}$  and  $\delta_{DCB\_lower}$  as shown in figure 3.6.

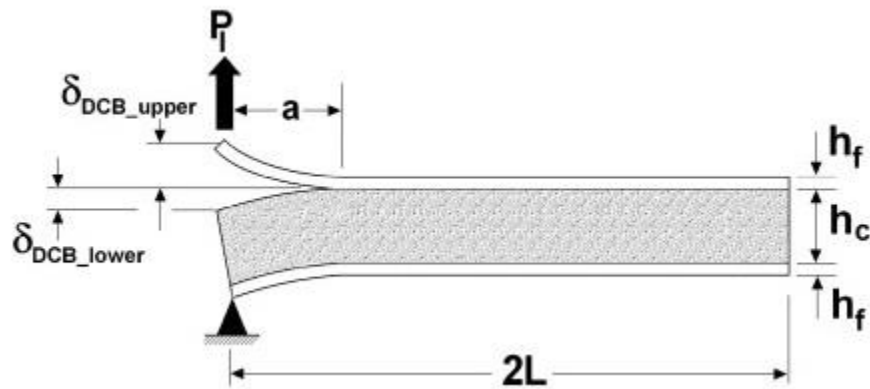


Figure 3.6: The schematic and loading of loading of the Sandwich double cantilever beam specimen ( from ref. Quispitupa et al. [15]).

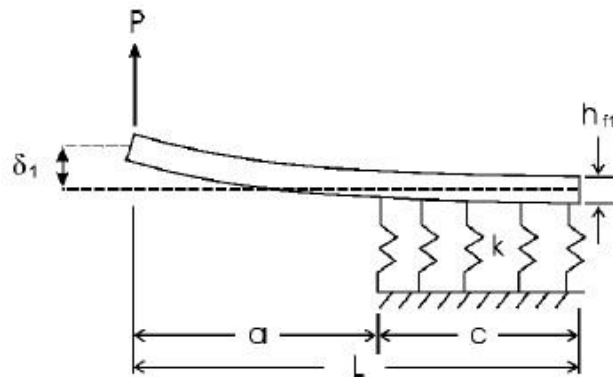


Figure 3.7: The elastic foundation model of the DCB specimen (from ref. Carlsson and Kardomateas [47]).

The elastic foundation model of the DCB specimen is shown in figure 3.7. The intact part of the upper face sheet, reinforced by the core is pictured by the elastic foundation. The total length of the specimen and crack length is  $L$  and  $a$ , respectively. The foundation modulus  $k$  is the basis for elastic foundation. The investigation is based on the Euler-Bernoulli theory and the Winkler foundation model adapted by Kanninen [52] for isotropic and symmetric DCB specimens. The wrinkler model presumes that the

reaction forces are proportional to the beam displacement at any point in the elastic foundation. The foundation modulus  $k$  can be linked to the extensional out-of-plane stiffness of the core as indicated by Allen [53] and Kanninen [52].

$$k = \frac{2E_c b}{h_c} \quad (3.15)$$

Where,  $b$  is the width of the specimen. Quispitupa et al. [15] disagreed that the elastic foundation modulus  $k$  effectively considers that one half of the core is effective as a support which is not practical in case of thick cores. Quispitupa et al. [15] suggested the elastic foundation modulus for a sandwich DCB specimen as follows.

$$k = \frac{2E_c b}{h_{f1}} \quad (3.16)$$

The analytical formulations for compliance and energy release rate of a symmetric DCB specimen derived by Aviles and Carlsson [14] are as follows.

$$C_{DCB} = \frac{a}{b} \left[ \frac{1}{h_c G_{xz}} + \frac{a^2}{3(D - \frac{B^2}{A})} \right] + \frac{4}{E_f h_f^3 b} \left[ a^3 + 3a^2 \eta^{1/4} + 3a^2 \eta^{1/2} + \frac{3}{2} \eta^{3/2} \right] \quad (3.17)$$

$$G_{DCB} = \frac{P_I^2}{2b^2} \left[ \frac{1}{h_c G_{xz}} + \frac{a^2}{(D - \frac{B^2}{A})} + \frac{12}{E_f h_f^3} [a^2 + 2a\eta^{1/4} + \eta^{1/2}] \right] \quad (3.18)$$

Where,  $P_I$  is the mode I load and A, B, D terms are the 1-D beam extensional, coupling, and bending stiffness for the lower part of the DCB specimen, given by

$$A = E_{f2} h_{f2} + E_c h_c \quad (3.19)$$

$$B = h_{f2} h_c \left( \frac{E_c - E_{f2}}{2} \right) \quad (3.20)$$

$$D = \frac{1}{12} [E_{f2} (h_{f2}^3 + 3h_{f2} h_c^2) + E_c (h_c^3 + 3h_{f2}^2 h_c)] \quad (3.21)$$

$\eta$  is the elastic foundation modulus parameter, given by

$$\eta = \frac{h_{f1}^3 b E_{f1}}{3k} \quad (3.22)$$

### 3.2.3 Cracked sandwich beam (CSB) specimen

The cracked sandwich beam (CSB) specimen was first suggested by Carlsson et al. [54] to evaluate the mode II fracture toughness of sandwich structure at the face/core interface. Figure 3.8 shows the schematic and the loading of the cracked sandwich beam specimen.

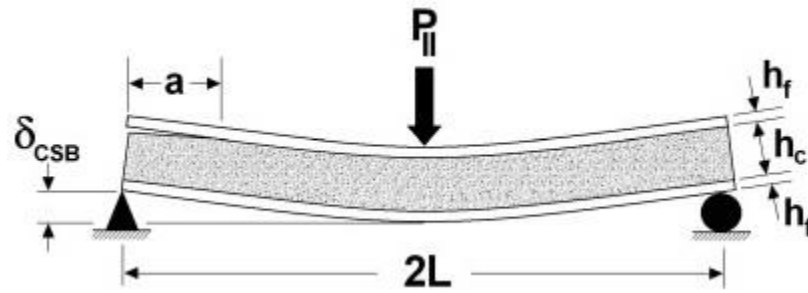


Figure 3.8: The schematic and the loading of the cracked sandwich beam specimen (from ref. Quispitupa et al. [15]).

The CSB specimen is an enhanced form of the mode II end-notched-flexure (ENF) test designed by Barrett and Foschi [55] for investigating wooden beams and afterwards used for composite laminates by Russell and Street [56]. Carlsson et al. [54] studied the CSB specimen by applying first order shear deformation beam theory and formulated the expression for the energy release rate ( $G_{CSB}$ ) and compliance ( $C_{CSB}$ ) for a symmetric sandwich beam as follows.

$$C_{CSB} = \frac{L^3}{6bD_i} + \frac{L}{2h_c b G_{xz}} + \frac{a^3}{12b} \left[ \frac{1}{D_d} - \frac{1}{D_i} \right] \quad (3.23)$$

Where,  $L$  is half length of span,  $b$  is the width of the specimen,  $h_c$  is the thickness of the core,  $G_{xz}$  is the shear modulus of the core,  $D_d$  and  $D_i$  are the bending stiffness of the debonded and the intact region of the specimen, respectively.

$$D_i = \frac{E_f h_f}{2} (h_c + h_f)^2 + \frac{E_f h_f^3}{6} + \frac{E_c h_c^3}{12} \quad (3.24)$$

Where,  $h_c$  is the thickness of face sheet,  $E_c$  and  $E_f$  are modulus of elasticity for core and face sheet, respectively.

Figure 3.9 shows the free body diagram of the debonded region of the CSB specimen. The beam 1 and 2 represents the upper face sheet and lower face sheet glued to the core, respectively. The bending stiffness of the debonded region is calculated from figure 3.9 and is as follows.

$$D_d = (1 - \alpha_1) D_2 \quad (3.25)$$

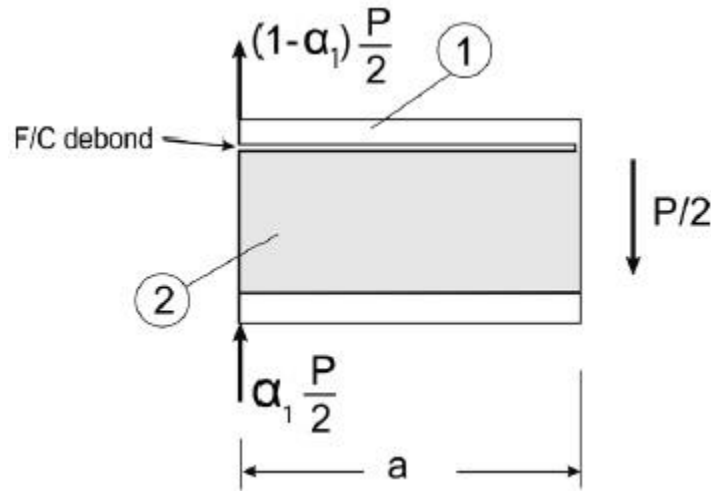


Figure 3.9: The free body diagram of the debonded region of the CSB specimen (from ref. Carlsson and Kardomateas [47]).

Where,  $\alpha_1$  is the load subdividing parameter and given by

$$\alpha_1 = \left[ \frac{\frac{a^3}{3} \frac{1}{D_2} + \frac{a}{KG_f h_f + G_{xz} h_c}}{\frac{a^3}{3} \frac{1}{D_2} + \frac{a}{KG_f h_f + G_{xz} h_c} + \frac{a^3}{3} \frac{1}{D_1} + \frac{a}{KG_f h_f}} \right] \quad (3.26)$$

$$D_1 = \frac{E_f h_f^3}{12} \quad (3.27)$$

$$D_2 = D - \frac{B^2}{A} \quad (3.28)$$

Where,  $D_1$  and  $D_2$  are bending stiffness for upper and lower beams of the debonded region of CSB specimen, respectively as shown in figure 3.9. The A, B, D terms are the 1-D beam extensional, coupling, and bending stiffness for the lower part of the debonded sandwich beam,  $K = 1.2$  is the shear correction factor suggested by Carlsson et al. [54],  $a$  is the crack length,  $G_f$  is the shear modulus of face sheet.

The energy release rate ( $G_{CSB}$ ) of CSB specimen is as follows

$$G_{CSB} = \frac{P_{II}^2 a^2}{8b^2} \left[ \frac{1}{D_d} - \frac{1}{D_i} \right] \quad (3.29)$$

Where,  $P_{II}$  is the load in mode II.

### 3.2.4 Mixed mode bending (MMB) specimen

Reeder and REWS [57] developed mixed mode bending (MMB) test for mixed mode delamination fracture characterization of unidirectional composites. Quispitupa et al. [15] revised the test to accommodate sandwich specimens, as shown in figure 3.10.



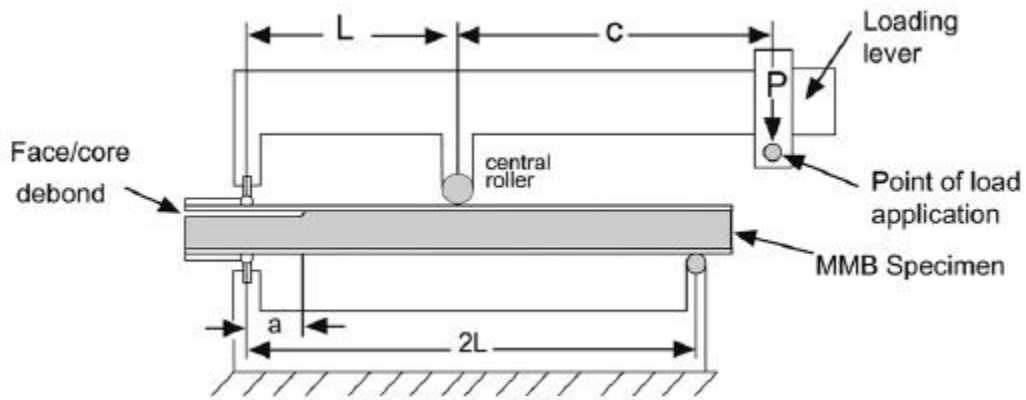


Figure 3.10: MMB test setup and sandwich specimen  
(from ref. Carlsson and Kardomateas [47]).

The MMB sandwich specimen containing a through width edge crack at the upper face/core interface was analyzed. A vertical downward acting load  $P$  was applied to the lever arm imparts an upward directed load at the left end of the debonded face sheet and downward directed load at the center. The MMB can be viewed as superposition of the cracked sandwich beam specimen (CSB) and Double cantilever beam specimen (DCB), the loads and reactions on the sandwich specimen are shown in figure 3.11.

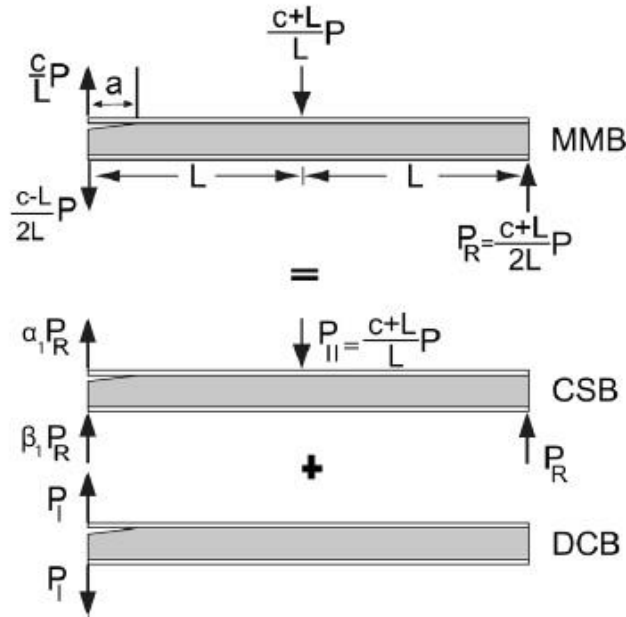


Figure 3.11: Mixed mode bending specimen disintegrated into CSB specimen and DCB specimen, the loads and reactions on the sandwich specimen (from ref. Carlsson and Kardomateas [47]).

Theoretical expressions for MMB compliance ( $C_{MMB}$ ) and energy release rate ( $G_{MMB}$ ) for symmetric sandwich specimens were developed on the basis of load subdividing and derived solutions of compliance and energy release rate for CSB and DCB specimens. Figure 3.12 illustrates the kinematics deformation of MMB specimen in such an arrangement which is identical to the asymmetric composite beams used by Ozdil and Carlsson [58]. The dotted lines shows deformed specimen if only  $P_I$  is applied. The vertical movement at the center of the beam ( $\delta_{CSB}$ ) equivalent to  $P_{II}$  load is given by

$$\delta_{CSB} = \Delta + \delta_C \quad (3.30)$$

The vertical movement  $\Delta$  is figured out from figure 3.12 using similar triangles technique

$$\frac{\Delta}{L} \approx \frac{\delta_{DCB\_lower}}{2L} \quad (3.31)$$

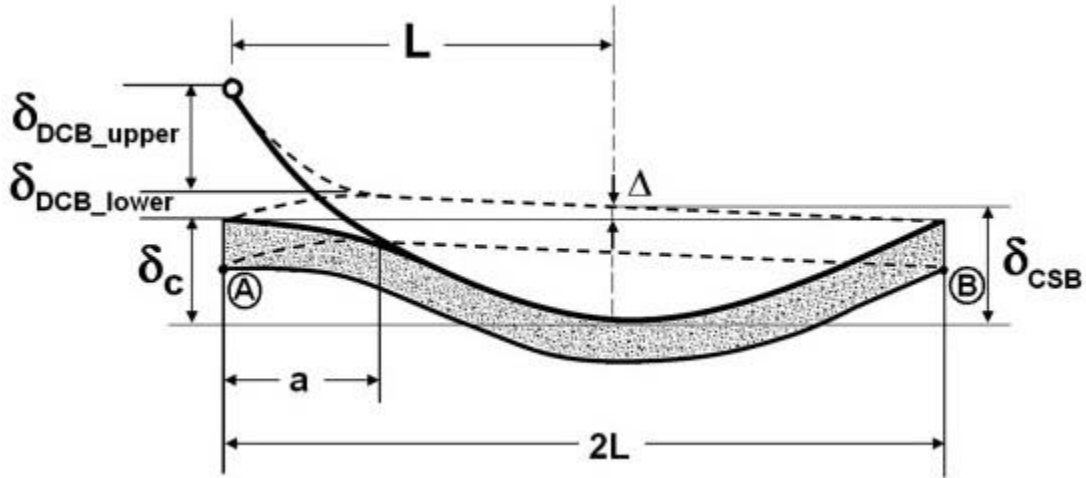


Figure 3.12: Kinematics of MMB sandwich specimen (from ref. Quispitupa et al. [15]).

$\delta_{DCB\_upper}$  and  $\delta_{DCB\_lower}$  are the opening vertical movements of the upper and lower beams of the MMB specimen related to the mode I load ( $P_I$ ) are given by

$$\delta_{DCB} = \delta_{DCB\_lower} + \delta_{DCB\_upper} \quad (3.32)$$

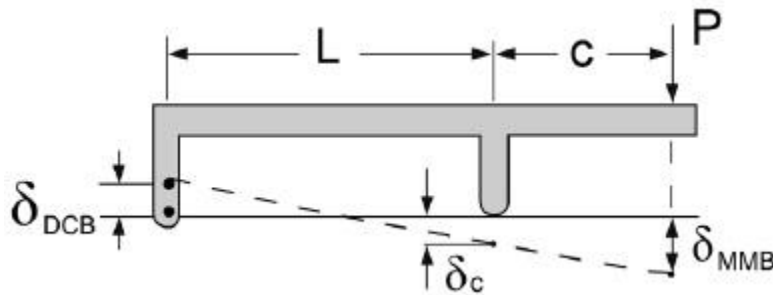


Figure 3.13: The vertical movement ( $\delta_{MMB}$ ) at the point of load application (from ref. Carlsson and Kardomateas [47]).

The vertical movement at the point of load application at a distance  $C$  from the center of the MMB specimen shown in figure 3.13 is specified by

$$\delta_{MMB} = \delta_c + \frac{c}{L}(\delta_c + \delta_{DCB}) \quad (3.33)$$

By substituting the values  $\delta_c$  and  $\delta_{DCB}$  into  $\delta_{MMB}$  gives the following relationship for the vertical movement at the point of load application.

$$\delta_{MMB} = \frac{c}{L}\delta_{DCB\_upper} + \frac{c-L}{2L}\delta_{DCB\_lower} + \left(\frac{c+L}{L}\right)\delta_{CSB} \quad (3.34)$$

The vertical displacements  $\delta_{DCB\_lower}$ ,  $\delta_{DCB\_upper}$  and  $\delta_{CSB}$  can be formulated in terms of compliances as follows

$$\delta_{DCB\_lower} = P_I C_{DCB\_lower} \quad (3.35a)$$

$$\delta_{DCB\_upper} = P_I C_{DCB\_upper} \quad (3.35b)$$

$$\delta_{CSB} = P_{II} C_{CSB} \quad (3.35c)$$

The loads acting on DCB and CSB specimens from figure 3.11 are as follows

$$P_I = \frac{c}{L}P - \alpha_1 P_R \quad (3.36a)$$

$$P_{II} = \left(1 + \frac{c}{L}\right)P \quad (3.36b)$$

$$P_R = \left(\frac{c+L}{2L}\right)P \quad (3.36c)$$

By combining equation 3.35(a-c) with equation 3.36(a-c) gives the compliance of MMB specimen as follows

$$C_{MMB} = \left[\frac{c}{L}C_{DCB\_upper} + \frac{c-L}{2L}C_{DCB\_lower}\right]\left(\frac{c}{L} - \alpha_1 \frac{c+L}{2L}\right) + \left(\frac{c+L}{L}\right)^2 C_{CSB} \quad (3.37)$$

$$C_{DCB\_upper} = \frac{4}{E_f h_f^3 b} \left[ a^3 + 3a^2 \eta^{1/2} + 3a \eta^{1/2} + \frac{3}{2} \eta^{3/4} \right] \quad (3.38)$$

$$C_{DCB\_lower} = \frac{a}{b} \left[ \frac{1}{h_c G_{xz}} + \frac{a^2}{3\left(D - \frac{B^2}{A}\right)} \right] \quad (3.39)$$

Where,  $C_{DCB_{upper}}$  is the compliance of the upper sub-beam of the double cantilever beam and  $C_{DCB_{lower}}$  is the compliance of the lower sub-beam of the double cantilever beam.

The energy release rate of the MMB specimen can be expressed as

$$G_{MMB} = \frac{P^2}{2b^2} \left[ \frac{c}{L} \left( \frac{c}{L} - \alpha_1 \frac{c+L}{2L} \right) \frac{12}{E_f h_f^3} \left[ a^2 + 2a\eta^{1/4} + \eta^{1/2} \right] + \frac{c-L}{2L} \left( \frac{c}{L} + \alpha_1 \frac{c+L}{2L} \right) \left( \frac{1}{h_c G_{xz}} + \frac{a^2}{\left( D - \frac{B^2}{A} \right)} \right) + \left( \frac{c+L}{L} \right)^2 \left( \frac{a^2}{8} \left[ \frac{1}{D_d} - \frac{1}{D_i} \right] \right) \right] \quad (3.40)$$

The global mode ratio is defined by  $G_{CSB}/G_{DCB} = G_{II}/G_I$

$$\frac{G_{II}}{G_I} = \left( \frac{P_{II}a}{2P_I} \right)^2 \frac{\left[ \frac{1}{D_d} - \frac{1}{D_i} \right]}{\frac{1}{h_c G_{xz}} + \frac{a^2}{\left( D - \frac{B^2}{A} \right)} + \frac{12}{E_f h_f^3} \left[ a^2 + 2a\eta^{1/4} + \eta^{1/2} \right]} \quad (3.41)$$

## CHAPTER 4

### MATERIALS AND SANDWICH CONSTRUCTION

#### 4.1 Materials

##### 4.1.1 Face sheet material

The material used for facesheet in sandwich construction is E-glass/epoxy prepreg layer with density  $1926.3 \text{ Kg/m}^3$ . Each layer of the prepreg was a cross-ply of two plies stitched together those were oriented at  $0^\circ$  and  $90^\circ$ . The resin used in the prepreg was Epon 202. The material properties of E-glass/epoxy prepreg layer are taken from a Wayne State University Master's thesis by Phadatare [59]. The same material is used in this work as reported in the thesis. The table 1.1 shows the properties of E-glass/epoxy composite made from this prepreg.

##### 4.1.2 Core material

The material used for core in sandwich construction was polyurethane closed cell foam with density  $248 \text{ Kg/m}^3$ . The mechanical property tests like tension, compression and shear were conducted to predict mechanical properties of polyurethane which are required in further analytical and numerical calculations. The table 2.2 shows the mechanical properties of polyurethane used in analytical and numerical calculations. Figure 4.1 shows the schematic representation of local axis.

Table 4.1: Mechanical properties of 0°/90° E-glass/epoxy [59]

Property Name	Values
Density (kg/m <sup>2</sup> )	1926.3
Tensile modulus, E <sub>xt</sub> , E <sub>yt</sub> , E <sub>zt</sub> (GPa)	19.88, 19.88, 12.59
Compressive modulus, E <sub>xc</sub> , E <sub>yc</sub> , E <sub>zc</sub> (GPa)	7.42, 7.42, 12.59
Shear modulus , G <sub>xy</sub> , G <sub>yz</sub> , G <sub>zx</sub> (GPa)	4.04, 3.37, 3.37
In-Plane tensile strength, X <sub>t</sub> , Y <sub>t</sub> (MPa)	545.8, 545.8
In-Plane compressive strength, X <sub>c</sub> , Y <sub>c</sub> (MPa)	288.8, 288.8
Shear strength, S <sub>xy</sub> , S <sub>yz</sub> , S <sub>zx</sub> (MPa)	31.64, 71.96, 71.96
Poisson's ratio v <sub>21</sub> , v <sub>31</sub> , v <sub>32</sub>	0.11, 0.18, 0.18

Table 4.2: Mechanical properties of Polyurethane foam

Property Name	Value
Density(Kg/m <sup>3</sup> )	248
Tensile modulus, E <sub>xt</sub> , E <sub>yt</sub> , E <sub>zt</sub> (MPa)	171.43 , 171.43, 127.88
Compressive modulus, E <sub>xc</sub> , E <sub>yc</sub> , E <sub>zc</sub> (MPa)	118 , 118.69 , 65.52
Shear modulus , G <sub>xz</sub> , G <sub>xy</sub> , G <sub>yz</sub> (MPa)	57.81 ,47.98 , 62.64
Poisson's ratio v <sub>xy</sub> ,v <sub>xz</sub> ,v <sub>yz</sub>	0.10 , 0.11 , 0.10
Tensile strength, X <sub>t</sub> , Y <sub>t</sub> , Z <sub>t</sub> (MPa)	3.82 , 3.82 , 2.41
Shear strength , S <sub>xz</sub> , S <sub>xy</sub> , S <sub>yz</sub> (MPa)	2.01 , 1.80 , 2.15

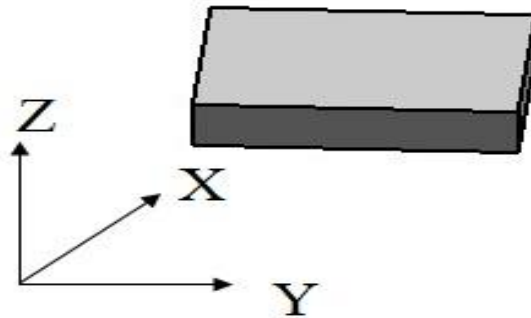


Figure 4.1: Schematic representation of local axis of polyurethane foam

#### 4.2 Sandwich construction

In processing sandwich composite panels, ten layers of E-glass/epoxy prepreg were layered up on both sides of a polyurethane foam core. To simulate initial crack at the interface 50.4 mm long Teflon sheet of thickness 0.0762 mm was inserted between face sheet and core on one side of sandwich panel and cured in vacuum press molding TMP equipment in our laboratory with temperature and pressure capability of 350°C and about 350 kPa, respectively. The curing process includes, treating the sandwich composite panel under vacuum and 344.7 kPa pressure applied on the sandwich composite panel at 135°C for 20 minutes. The sandwich composite panel is then cooled by passing mist, followed by water over the platen for 15 minutes each. After curing, the sandwich panels were post cured in an oven at 80°C for 5 hours. For all composites, there was resin diffusion from the face sheet into the core during processing and closer examination showed that the diffusion thickness into the core was about 0.5 mm from the actual face sheet and core interface.



### 4.3 Specimen dimensions

The panels were cut into specimens (200 mm long, 25.4 mm wide) using a band saw for testing. The specimen geometry is shown in figure 4.2. The thickness of the samples was 27.6 mm.

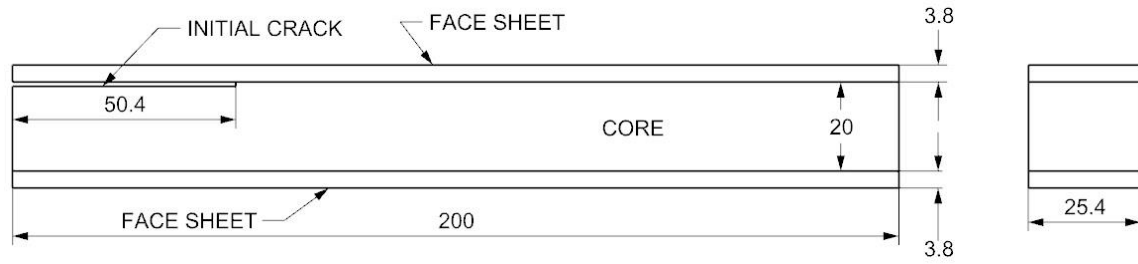


Figure 4.2: E-glass face sheet/polyurethane foam core sandwich composite test specimen. Dimensions are in mm.

## CHAPTER 5

### EXPERIMENTAL ASPECTS AND FINITE ELEMENT ANALYSIS

#### 5.1 Experimental aspects

##### 5.1.1 T-peel test

The setup used to conduct T-peel test was single cantilever beam (SCB) test shown in figure 5.1. T-peel tests were conducted using MTS hydraulic testing machine with a load capacity of 100KN. The bottom surface of the specimen was fixed to the steel plate with epoxy which in turn was fastened to the T- shaped fixture designed for this work with the help of 6 bolts. A L-shaped bracket was attached to the top surface with the help of 2 bolts to grip the debonded end of face sheet of the specimen and apply displacement. All the tests were conducted under displacement control with a crosshead displacement rate of 0.025mm/sec. The specimen was loaded in a cyclic manner for 8-10 times and crack growth was monitored and marked after looking through optical micrometer and measured using Vernier caliper for each cycle. The load and displacement values for the entire test were recorded after every one-tenth of a second with the help of computerized controlled acquisition system. The typical load-displacement curve for foam core sandwich specimen is shown in figure 5.2. The curve was linear before crack initiation occurs during each cycle. The fracture toughness ( $G_c$ ) was calculated from load displacement curve using area method and two analytical solutions given in equation (3.10) and equation (3.12). Eight-ten fracture toughness values were obtained from a single specimen. In total five specimens were tested.



Figure 5.1: T-Peel test setup and SCB sandwich specimen.

The area for each load and unload cycle was calculated using trapezoid rule. The expression given in equation (5.1) from Anderson [60] was used to calculate fracture toughness using area method.

$$G_c = \frac{1}{b} \left( \frac{\Delta E}{\Delta a} \right) \quad (5.1)$$

Where,  $\Delta E$  is area under load-displacement curve,  $\Delta a$  is crack extension,  $b$  is width of specimen.

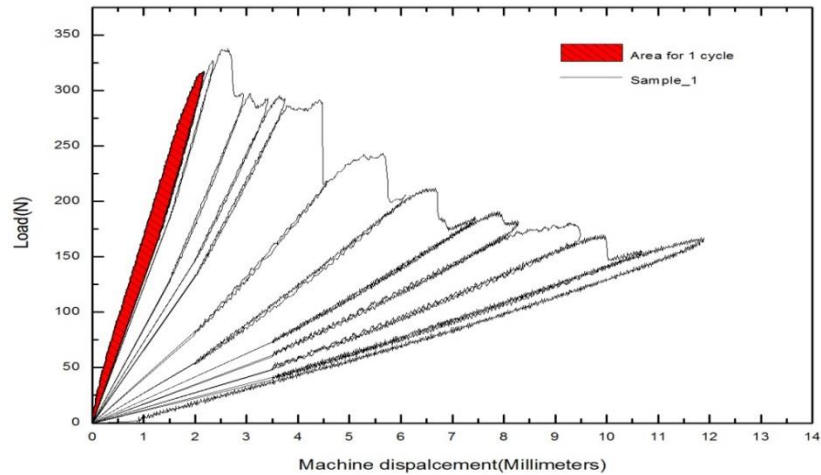


Figure 5.2: Typical load-displacement curve of T-peel test for foam core sandwich composite.

### 5.1.2 Wedge test

The experimental setup used to conduct wedge test and schematic of wedge test is shown in figure 5.3 and 5.4, respectively. The specimen from one side was fixed to the steel plate with epoxy to prevent buckling of the specimen. The specimen along with the steel plate was gripped in the vice to keep the specimen perfectly parallel to the wedge and the vice was kept on the bottom plunger of the hydraulic testing machine MTS 8810. The wedge made up of steel (thickness = 3mm and length = 228.6 mm) 15° tapered only on one side to avoid damage to core of specimen was inserted between the core and the partially debonded face. Before the start of test, initial position readings are marked on the specimen at the crack front and at the point of application of wedge (at point “O” and point “C” in figure 5.4). The wedge was mounted in the stationary plunger and displacement was given to the plunger on which vice with specimen was kept at a rate of

0.025mm/sec. The crack front location was marked on the specimen for every 10 mm displacement of the plunger. The same procedure was repeated for 8-10 times per sample and crack front location was monitored and marked on the specimen after looking through optical micrometer and measured using Vernier caliper. In total 5 samples were tested. The load displacement data was not recorded for this type of test. The Obreimoff's relation given in equation (5.2) from Lawn [61] was used to calculate fracture toughness.

$$G_c = \frac{3Ed^3h^2}{16C^4} \quad (5.2)$$

Where,  $E$  is the modulus elasticity of skin,  $d$  is the thickness of skin,  $h$  is the thickness of wedge,  $C$  is the crack front distance from the point of application of wedge.

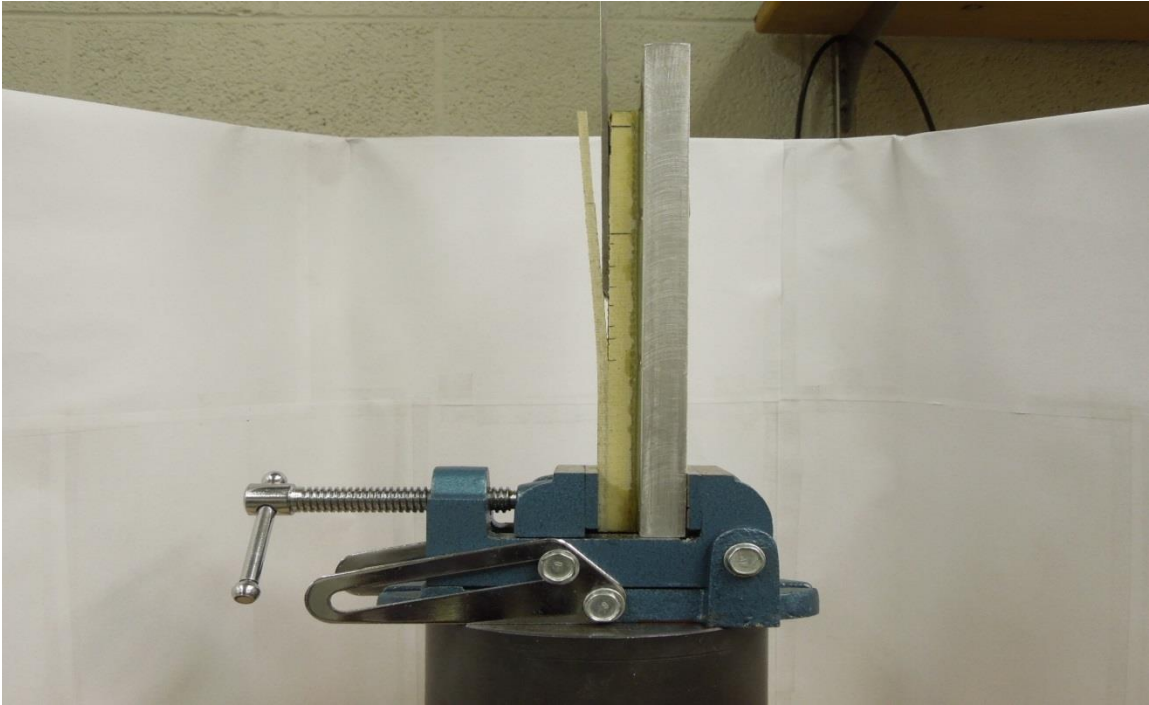


Figure 5.3: Wedge test machine setup

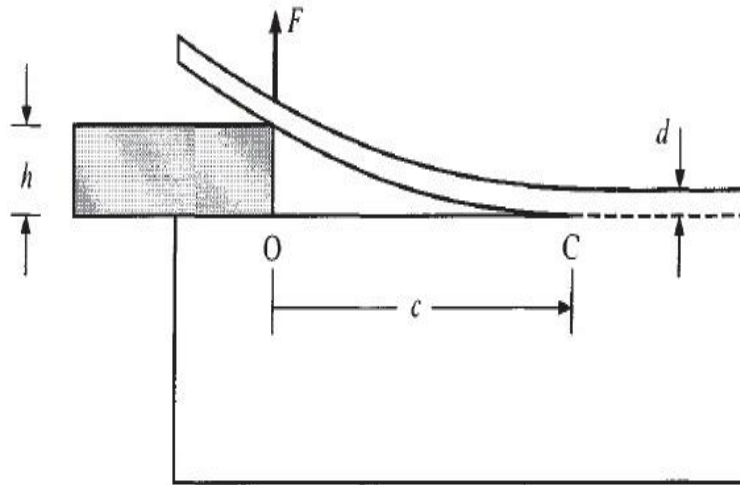


Figure 5.4: Schematic of wedge test [61]

### 5.1.3 Mixed mode bending (MMB) test

The experimental setup to conduct a mixed mode bending test recently modified by Quispitupa et al. [15] for sandwich specimen is shown in figure 5.5. The tests were conducted using MTS 8810 hydraulic testing machine with a load capacity of 200KN. Mixed mode bending tests of sandwich composites was conducted in accordance with the ASTM D6671-01 [62]. Specially machined hinges were fixed on both sides of the specimen above the cracked region of the MMB sandwich specimen in such a way that the initial crack length ( $a$ ) measured from the point of load application to the crack tip was 25 mm, load application. All the tests were conducted under displacement control with a span length of  $2L = 152.4\text{mm}$ . The load is applied (at the point of load application "O" as shown in figure 5.5) through the steel loading yoke (fixed in the stationary plunger), saddle fixed on the loading arm and imparted to the specimen via rollers and

hinges. The MMB test rig was kept on the stationary plunger and displacement was given to the plunger at a constant rate of 0.025mm/sec.

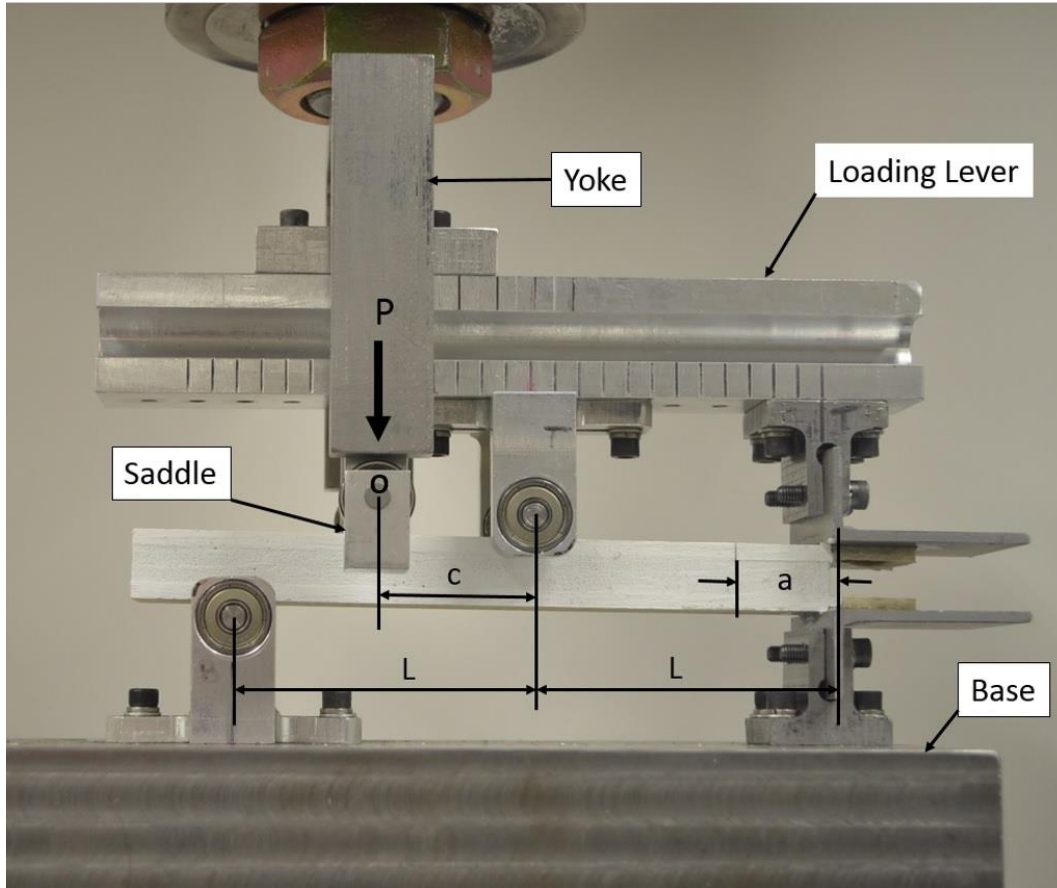


Figure 5.5: Static test setup using mixed mode bending test and mixed mode bending sandwich specimen.

The mode mixity was changed by adjusting the lever arm distance  $c$  (20, 30, 40, 50 mm). The critical load at the beginning of the crack propagation was marked according to the instructions given in ASTM D6671-01 [62] and confirmed by visual observation. The crack growth was monitored and marked after looking through optical micrometer and measured using Vernier caliper for each cycle. In crack length measurement compliance of the system is not considered as recommended by Manca et

al. [63]. The load and displacement values for the entire test were recorded after every one-tenth of a second with the help of computerized controlled acquisition system. The typical load-displacement curves for foam core sandwich specimen at different lever arm distance ( $c$ ) 20, 30, 40, 50 mm are shown in figure 5.6-5.9, respectively. The curves were linear before crack initiation occurs in all tests. The energy release rate ( $G_{MMB}$ ) and compliance ( $C_{MMB}$ ) was calculated using equation (3.40 and 3.47). Ten-twelve energy release rate values were obtained from a single specimen. In total 12 specimens were tested, three sample at each lever arm distance ( $c$ ) 20, 30, 40 and 50 mm.

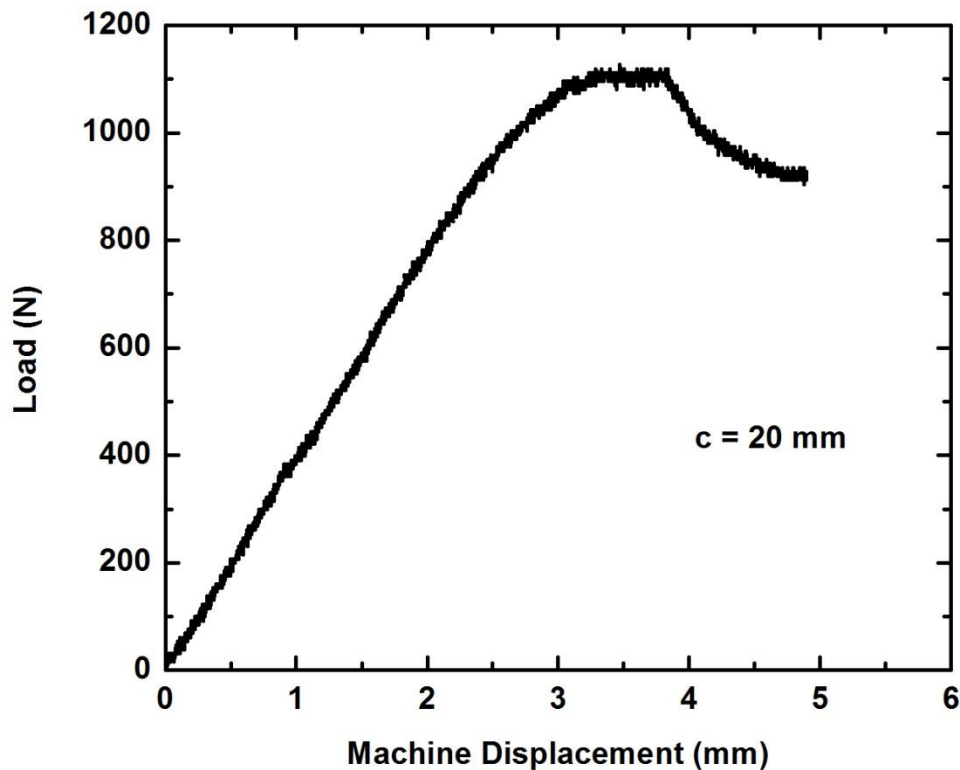


Figure 5.6: Typical load-displacement curve of MMB foam core sandwich composite, at lever arm distance ( $c = 20$  mm) from the point of application of load.



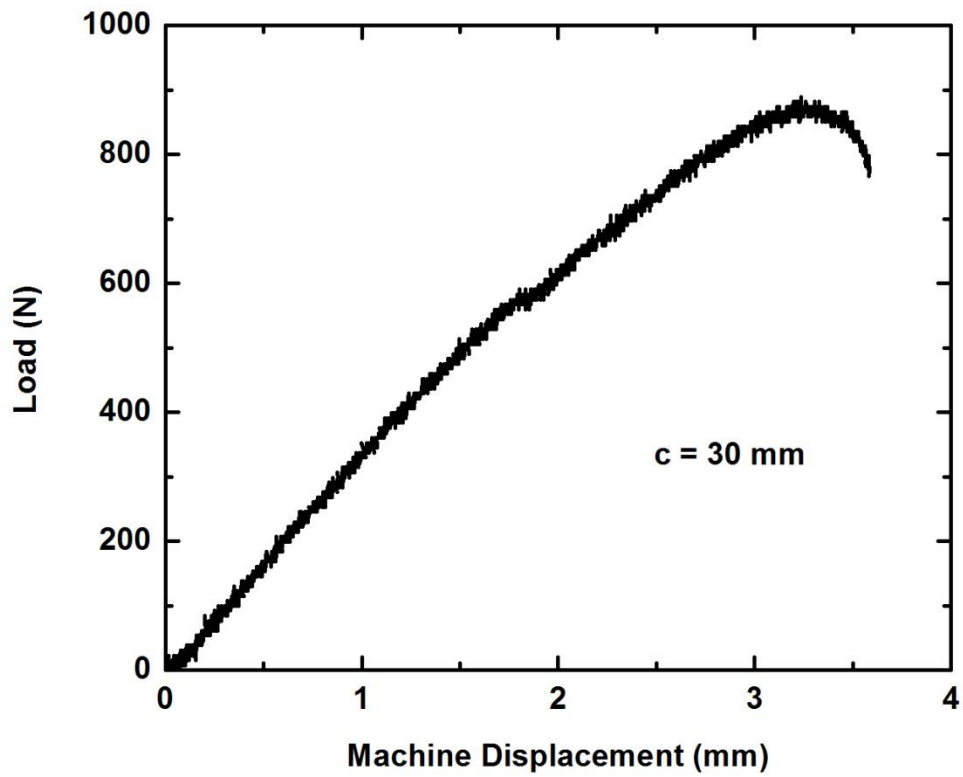


Figure 5.7: Typical load-displacement curve of MMB foam core sandwich composite, at lever arm distance ( $c = 30 \text{ mm}$ ) from the point of application of load.

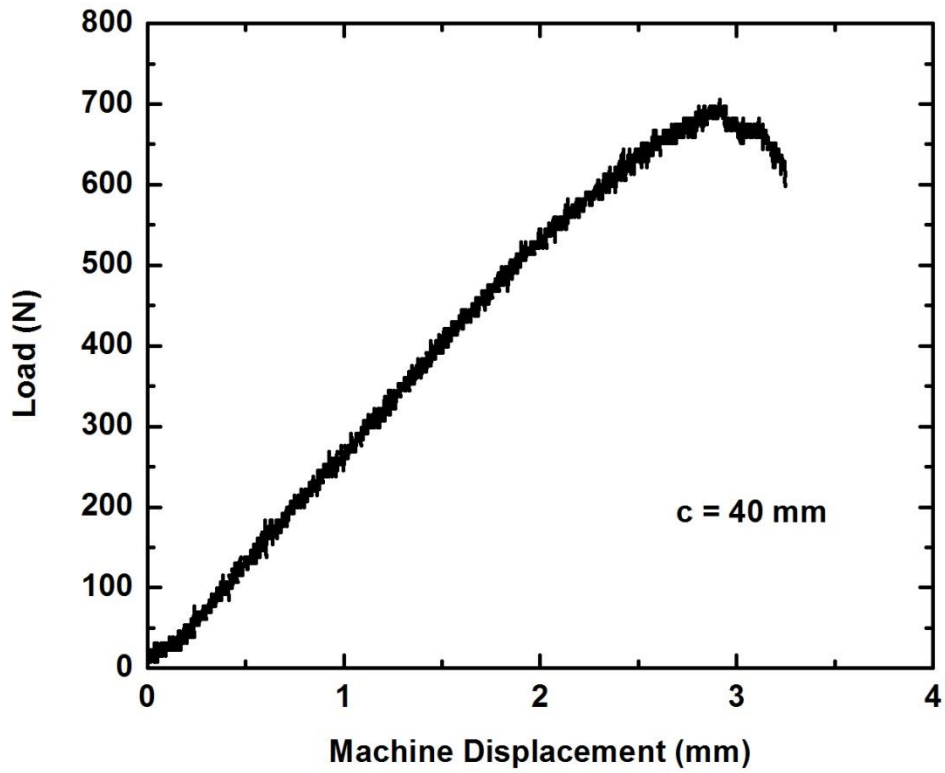


Figure 5.8: Typical load-displacement curve of MMB foam core sandwich composite, at lever arm distance ( $c = 40 \text{ mm}$ ) from the point of application of load.

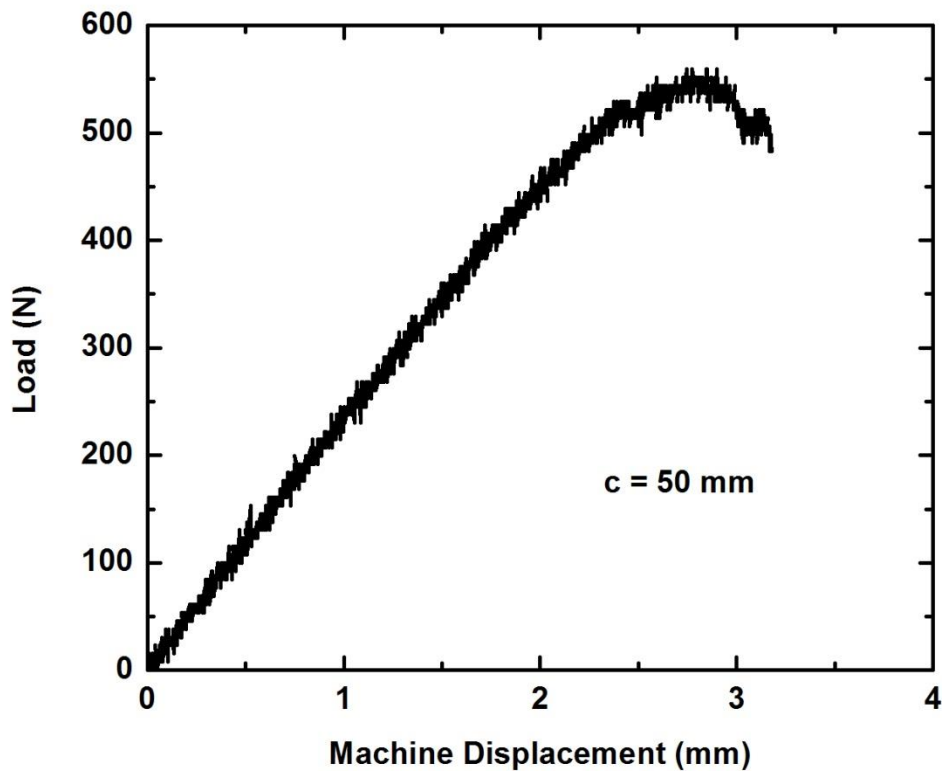


Figure 5.9: Typical load-displacement curve of MMB foam core sandwich composite, at lever arm distance ( $c = 50 \text{ mm}$ ) from the point of application of load.

#### 5.1.4 Fatigue test using single cantilever beam test

All fatigue test specimens were first statically pre-cracked to determine maximum load and displacement. The setup used to conduct the static and fatigue tests using single cantilever beam (SCB) configuration is shown in figure 5.10. All tests were conducted using MTS hydraulic testing machine with a load capacity of 100 KN. The bottom surface of the specimen was fixed to the steel plate with epoxy which in turn was fastened to the T- shaped fixture designed for this work with the help of 6 bolts. A L-shaped bracket was attached to the top surface with the help of 2 bolts to grip the

debonded end of face sheet of the specimen and apply displacement. All the tests were conducted under displacement control with a crosshead displacement rate of 0.025mm/sec.



Figure 5.10: Fatigue tension-tension test setup using single cantilever beam test.

Tests were stopped immediately after small crack growth looking through optical micrometer and measured using a Vernier caliper for each cycle. The load and displacement values for the entire test were recorded after every one-tenth of a second with the help of computerized controlled acquisition system. The fatigue specimens were mounted in the same manner as static ones and were subjected to constant sinusoidal displacement amplitude at a frequency of 2 Hz. and displacement ratio of  $R = 0.1$  was used. The specimens were tested at a different displacement ratio range from 32% to 90%

of the static fracture displacement level of the single cantilever beam test. Typical tension-tension cyclic load is shown in figure 5.11.

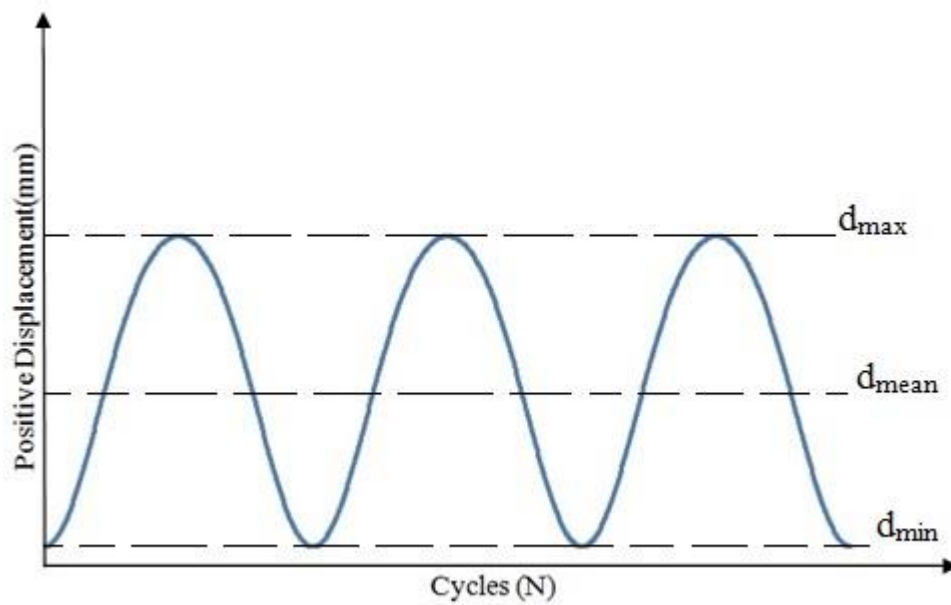


Figure 5.11: Typical tension-tension cyclic load

The crack growth was recorded after certain increments of cycles. All samples were run to 1 million of cycles. No crack propagation was noticed below 32% of the static fracture displacement of the single cantilever beam test. The crack growth versus number of cycle data was recorded and plotted for all test samples as shown in figure 5.12. For all test samples data as analyzed in terms of crack growth rate from figure 5.12. For applied peak and minimum cyclic displacements, both the energy release rate,  $G_I$  and its range,  $\Delta G_I$  for various lengths were estimated using VCCT and contour integral using ABAQUS [64].

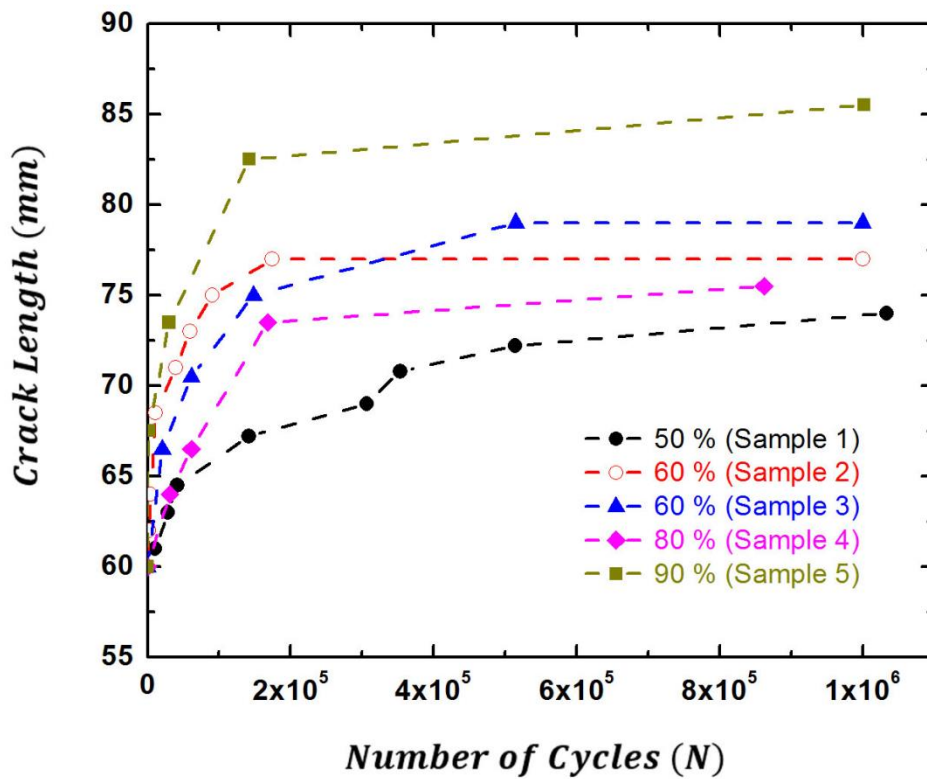


Figure 5.12: Crack length vs. number of cycles for foam core sandwich composites for various displacement levels corresponding to maximum displacement level at which initial delamination crack initiates.

### 5.1.5 Fatigue test using mixed mode bending (MMB) test

All fatigue test specimens were first statically pre-cracked to determine maximum load and displacement. The setup used to conduct the static and fatigue tests using mixed mode bending (MMB) configuration is shown in figure 5.13. All tests were conducted using MTS 8810 hydraulic testing machine with a load capacity of 200 KN. Mixed mode bending tests of sandwich composites was conducted in accordance with the ASTM D6671-01 [62]. Specially machined hinges were fixed on both sides of the specimen

above the cracked region of the MMB sandwich specimen in such a way that the initial crack length ( $a$ ) measured from the point of load application to the crack tip was 25 mm, load application. All the tests were conducted under displacement control with a span length of  $2L = 152.4\text{mm}$ . The load is applied (at the point of load application “ $O$ ” as shown in figure 5.13) through the steel loading yoke (fixed in the stationary plunger), saddle fixed on the loading arm and imparted to the specimen via rollers and hinges. The MMB test rig was kept on the stationary plunger and displacement was given to the plunger at a constant rate of  $0.025\text{mm/sec}$ .

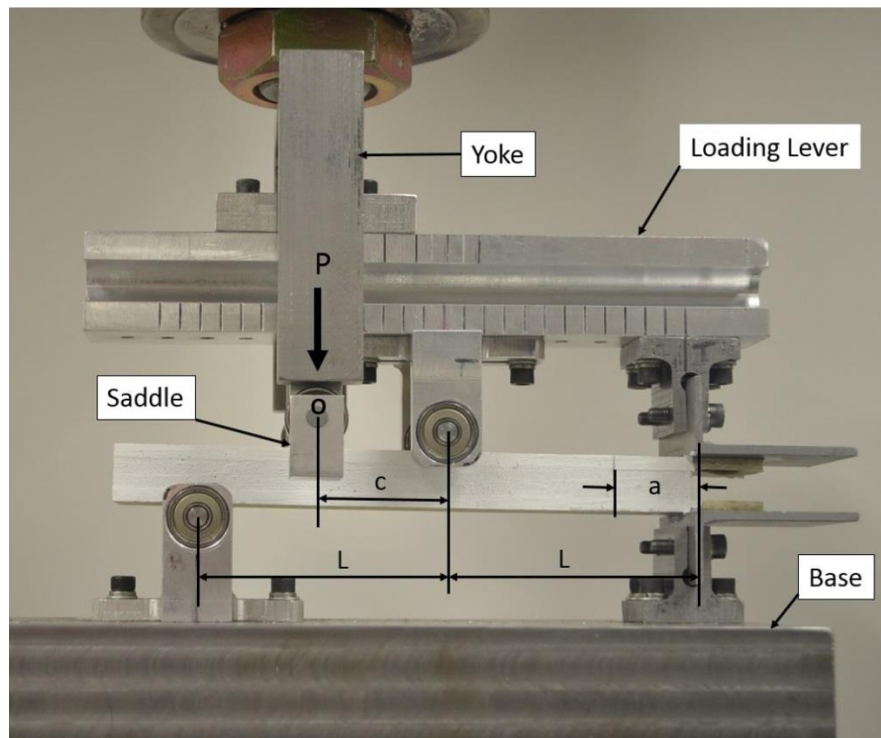


Figure 5.13: Fatigue test setup using mixed mode bending test and mixed mode bending sandwich specimen.

Tests were stopped immediately, after small crack growth, looking through optical micrometer and measured using a Vernier caliper for each cycle. The load and

displacement values for the entire test were recorded after every one-tenth of a second with the help of computerized controlled acquisition system.

The fatigue specimens were mounted in the same manner as static ones and were subjected to constant sinusoidal displacement amplitude at a frequency of 2 Hz. and displacement ratio of  $R = 0.1$  was used. The specimens were tested at 70% of the static fracture displacement level of the mixed mode bending test, at different mode-mixity by changing the lever arm distance ( $c = 20, 30, 40, 50mm$ ). Typical tension- tension cyclic load is shown in figure 5.11. The crack growth was recorded after every 200-250 cycles. Also the crack length was determined by equating the measured and calculated compliance. All samples were run to 7000-8000 of cycles. The crack growth versus number of cycle data was recorded and plotted for all test samples at different lever arm distance ( $c = 20, 30, 40, 50 mm$ ) as shown in figures 5.14-5.17. For all test samples data was analyzed in terms of crack growth rate from figure 5.14-5.17. For applied peak and minimum cyclic displacements, both the energy release rate,  $G$  and its range,  $\Delta G$  for various lengths were estimated using equation (3.40).



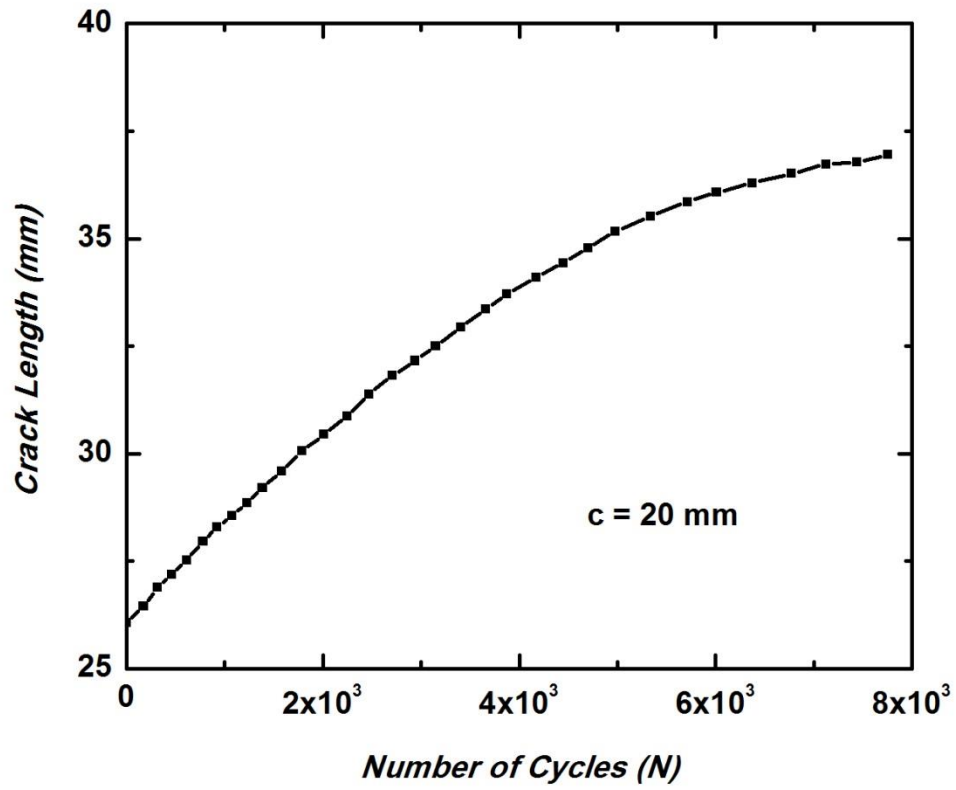


Figure 5.14: Crack length vs. number of cycles for MMB foam core sandwich composites at a lever arm distance ( $c = 20 \text{ mm}$ ).

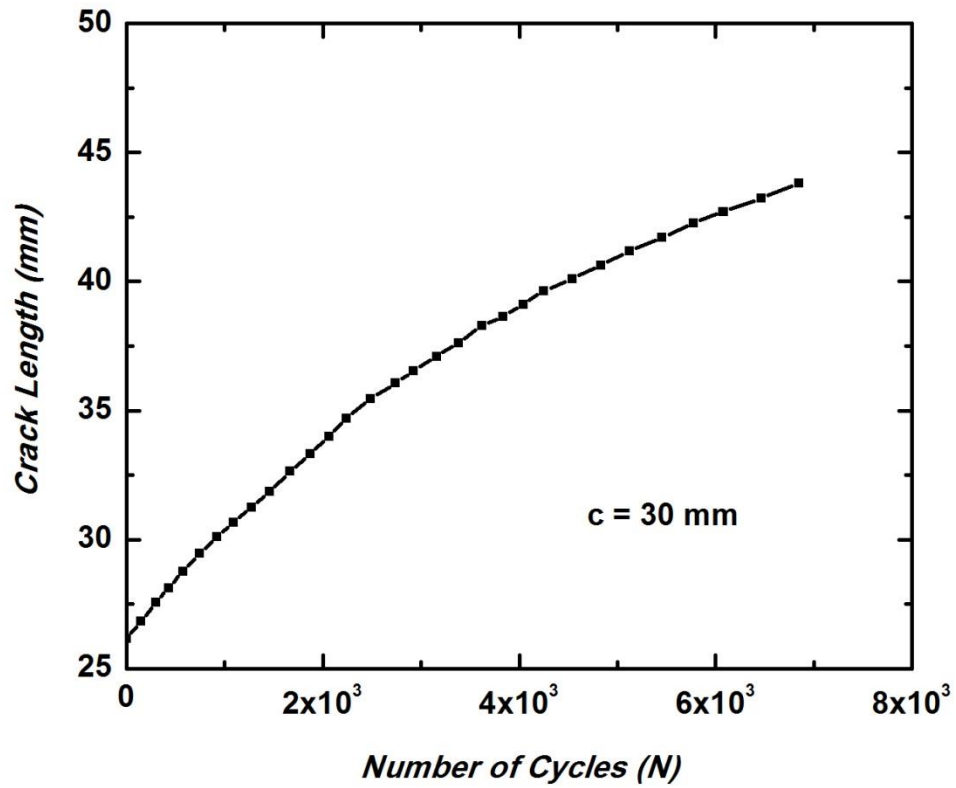


Figure 5.15: Crack length vs. number of cycles for MMB foam core sandwich composites at a lever arm distance ( $c = 30 \text{ mm}$ ).

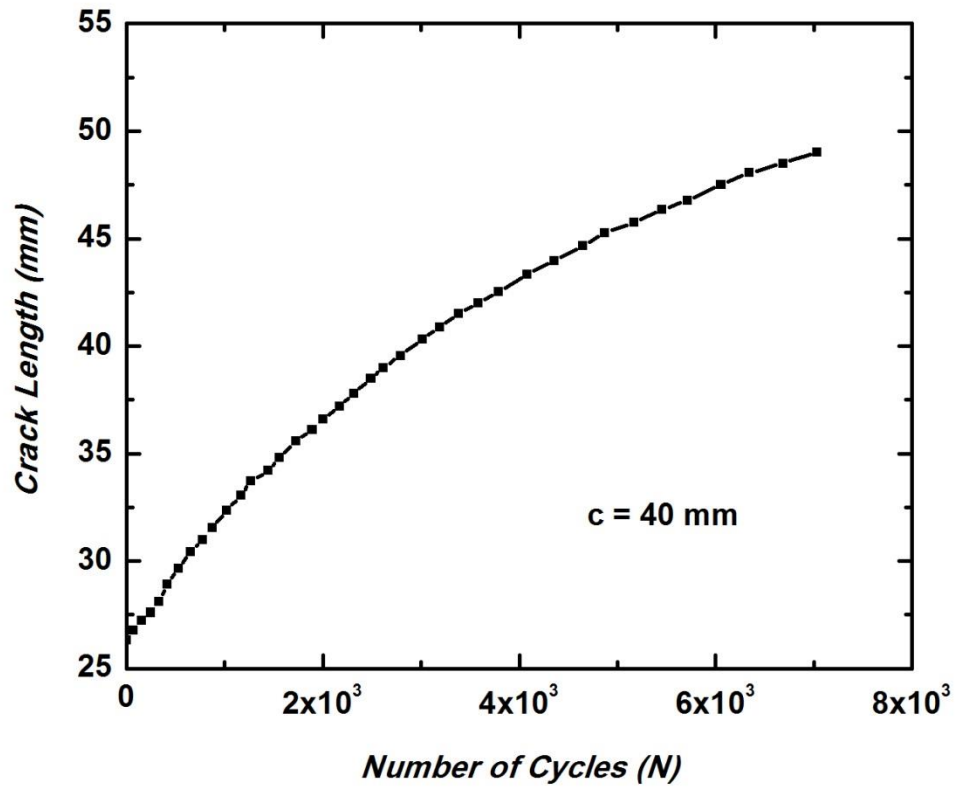


Figure 5.16: Crack length vs. number of cycles for MMB foam core sandwich composites at a lever arm distance ( $c = 40 \text{ mm}$ ).

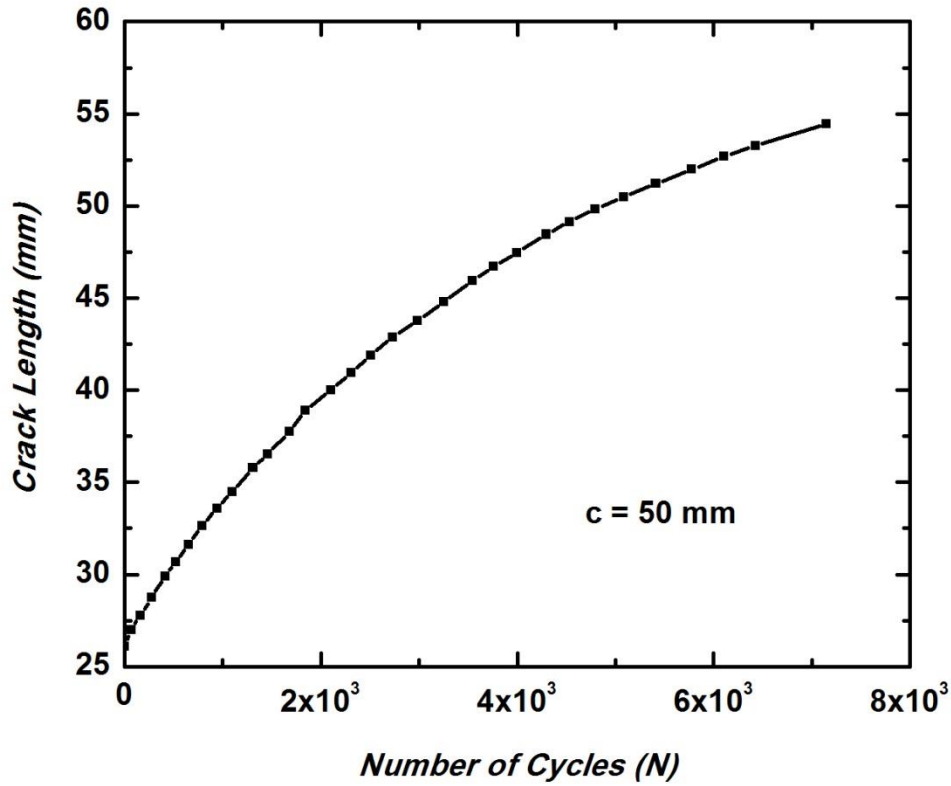


Figure 5.17: Crack length vs. number of cycles for MMB foam core sandwich composites at a lever arm distance ( $c = 50 \text{ mm}$ ).

## 5.2 Finite element analysis

Finite element analysis were performed in order to evaluate fracture toughness under Mode I using SCB specimens and to evaluate compliance, energy release rate and phase angles for mixed mode using MMB specimens. The energy release rate was calculated by employing equation 5.3 (from ref. Hutchinson and Suo [65]) from the respective crack flank displacements ( $\delta_x$  and  $\delta_y$ )

$$G = \frac{\pi(1+4\varepsilon^2)}{2x(c_1+c_2)} (\delta_y^2 + \delta_x^2) \quad (5.3)$$

Where,  $\delta_y$  and  $\delta_x$  are the opening and sliding relative displacements of the crack flanks at a short distance  $x$  behind the crack tip,  $c_1$  and  $c_2$  are stiffness parameter of the material above and below the bimaterial crack and is given by

$$c_m = \frac{k_m+1}{G_m} \quad (5.4)$$

Where,  $m$  = material number (1 = face and 2 = core),  $k_m = 3 - 4\nu_m$  for plane strain and  $k_m = (3 - \nu_m)/(1 + \nu_m)$  for plane stress,  $\nu_m$  is Poisson's ratio and  $G_m$  is the shear modulus for material  $m$  suggested by Dundurs [66]. The oscillatory index  $\varepsilon$  can be calculated using the expression proposed by Liechti and Chai [67].

$$\varepsilon = \frac{2}{2\pi} \ln \frac{(1-\beta)}{(1+\beta)} \quad (5.5)$$

Where,  $\beta$  is a non-dimensional combination of the moduli of the materials above and below the interface as proposed by Dundurs [66].

$$\beta = \frac{G_1(k_2-1)-G_2(k_1-1)}{G_1(k_2+1)+G_2(k_1+1)} \quad (5.6)$$

And also using two different techniques namely, J-Integral evaluation method and virtual crack closure technique (VCCT).

Two Dimensional finite element models for SCB and MMB specimens were created using HyperMesh [68] as preprocessor and solved using ABAQUS [64]. For J-Integral evaluation method, both SCB and MMB specimen's 2D finite element models were created using solid plane strain second order (CPE8) elements. The core is assumed to be linear elastic. The face sheets were modelled as orthotropic elastic material. The number of elements used through thickness for face sheet and core are 9 and 42, respectively. The crack was modeled 0.5mm below but parallel to the interface as seen

during mechanical testing. The area around the crack tip is modelled using quarter point elements to include singularity of  $1/\sqrt{r}$ . Due to path independence of the J-Integral in elasticity, many calculations are possible at each position along crack front. Each calculation may be believed of as a contour line passing through a ring of elements close the crack front. Eight rings of elements were created around the crack tip to request eight contour integral. The initial crack was modelled by placing double nodes along the predetermined crack path. The load and boundary conditions were applied accordingly as shown in figure 5.18 and figure 5.19 for SCB and MMB Specimen, respectively. The energy release rate was calculated directly from the results as J-Integral is a direct method to evaluate energy release rate. Energy release rates were calculated for different experimental crack sizes.

For virtual crack closure technique, both SCB and MMB specimen's 2D finite element models were created using solid plane strain second order (CPE8) elements as shown in figure 5.20. The core is assumed to be linear elastic. The face sheets were modelled as orthotropic elastic material. The number of elements used through thickness for face sheet and core are 9 and 42, respectively. The crack was modeled 0.5mm below but parallel to the interface as seen during mechanical testing. Cohesive elements with zero thickness were implemented through interaction cohesive behavior. Top and bottom surfaces are defined to establish contact area in the plane of delamination. A node set was created to represent the initially bonded region in the plane of delamination. In the contact property definition elastic properties of the interface were defined using uncoupled traction-separation behavior. The quadratic traction-interaction failure

criterion was chosen for damage initiation. A mixed mode, energy based damage evolution law based on the Benzeggagh-Kenane (BK) criterion shown in equation (5.7) was used for damage propagation proposed by Krueger [69].

$$G_c = G_{Ic} + (G_{IIc} - G_{Ic}) * \left(\frac{G_{II}}{G_T}\right)^\eta \quad (5.7)$$

Where,

$G_{Ic}$  and  $G_{IIc}$  are fracture toughness for mode I and mode II respectively,  $\frac{G_{II}}{G_T}$  is mixed mode ratio,  $\eta$  is cohesive property parameter and is 2.13 for our case.

For damage stabilization, viscosity parameter was used to overcome convergence difficulties due to softening behavior and stiffness degradation. The load and boundary conditions were applied accordingly as shown in figure 5.14 and figure 5.15 for SCB and MMB Specimen, respectively. From the finite element analysis results, normal force at the crack tip and vertical displacement one node behind the crack tip were calculated after certain increments of cycles to calculate energy release rate using equation (3.5) for mode I and using equation (3.5 and 3.6) for mixed mode. For computational estimation of fracture toughness, experimental crack sizes were used.

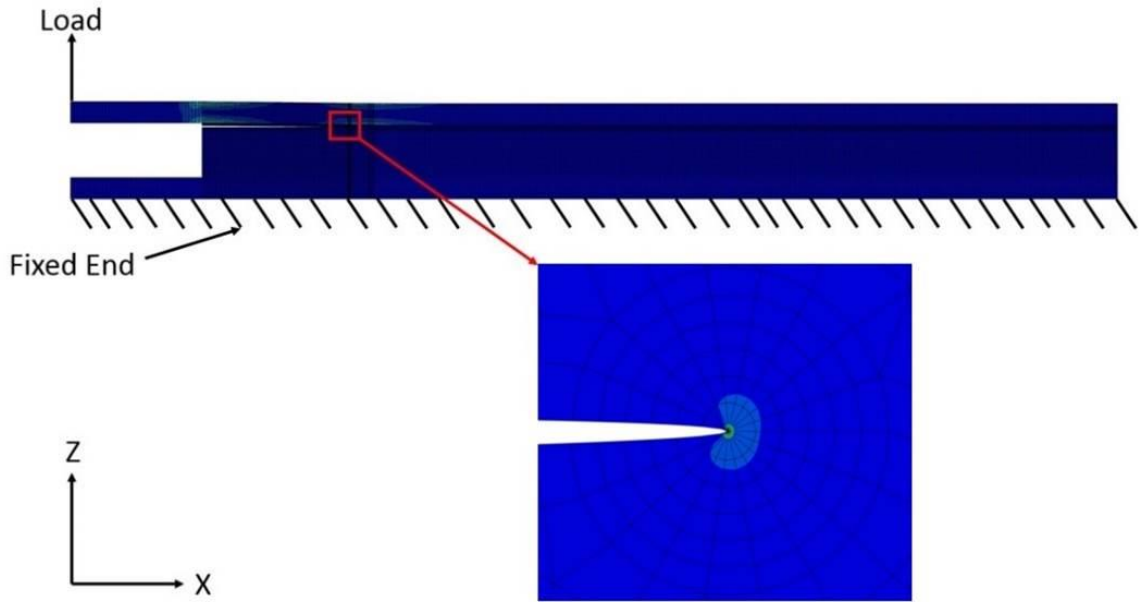


Figure 5.18: Two dimensional finite element model of sandwich composite for T-peel test and close view near crack tip.



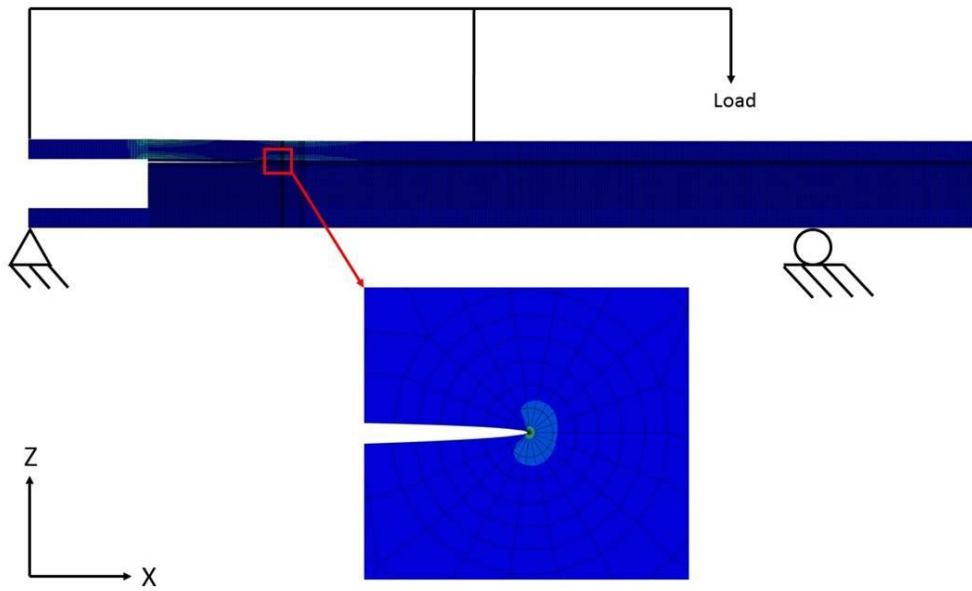


Figure 5.19: Two dimensional finite element model of sandwich composite for MMB test and close view near crack tip.

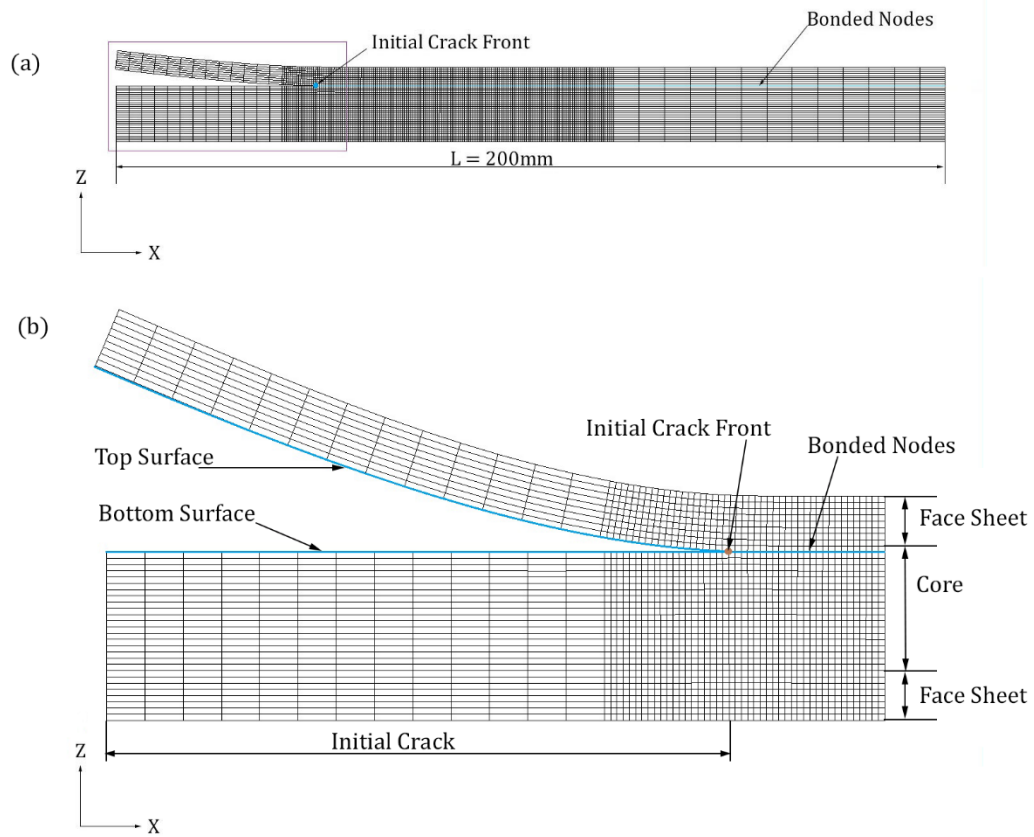


Figure 5.20: (a) Two dimensional finite element model of foam core sandwich specimen with initial crack. (b) Detail of finite element model.

## CHAPTER 6

### RESULTS AND DISCUSSION

#### 6.1. T-peel test and wedge test static evaluation

The fracture toughness was calculated using equation (5.1 and 5.2) for peel and wedge test, respectively. It was seen that crack propagated in the core 0.5 mm below but parallel to interface because of the penetration of the resin in the open cells of the foam. Fracture toughness of the system was much higher than the fracture toughness of the core material even though the crack propagated in the core. The crack growth was stable in wedge test. However, in T-peel test stick-slip behavior was also observed for some cycles. A very little variation in calculated fracture toughness values was seen in each specimen due to the non-homogeneity of the core material.

The fracture toughness and standard deviation for each specimen was calculated and shown in table 6.1 and 6.2 for peel and wedge test, respectively. Figure 6.1 and 6.2 shows the deviation of fracture toughness from the mean value for each sample for peel test and wedge test, respectively. The mean fracture toughness and standard deviation calculated from the mean fracture toughness and mean standard deviation value of each sample for t-peel and wedge test are  $0.72 \pm 0.06 \text{ KJ/m}^2$  and  $0.62 \pm 0.06 \text{ KJ/m}^2$ , respectively are also presented in table 6.3. It was also seen that fracture toughness was independent of crack length. The fracture toughness was also evaluated by using two analytical expressions mentioned in equation (3.10) and equation (3.12). The fracture toughness value was  $0.75 \text{ KJ/m}^2$  and  $0.72 \text{ KJ/m}^2$  using equation (3.10) and equation

(3.12), respectively. The fracture toughness value estimated for T-peel test using finite element analysis by employing VCCT technique equation (3.5), crack surface displacement extrapolation (CSDE) method equation (5.3) and direct J-integral evaluation method was  $0.76\text{KJ/m}^2$ ,  $0.74\text{KJ/m}^2$  and  $0.78\text{KJ/m}^2$ , respectively. The fracture toughness value estimated for wedge test using finite element analysis by employing VCCT technique equation (3.5), crack surface displacement extrapolation (CSDE) method equation (5.3) and direct J-integral evaluation method was  $0.67\text{KJ/m}^2$ ,  $0.64\text{KJ/m}^2$  and  $0.69\text{KJ/m}^2$ , respectively. Table 6.4 and figure 6.3 shows the comparison of fracture toughness values obtained from experimental and finite element results using different techniques. The fracture toughness values obtained from finite elements analysis by applying different technique are in excellent agreement for both the T-peel test and wedge test. However, the fracture toughness value estimated from finite element methods are slightly above the fracture toughness value calculated experimentally for both t-peel test and wedge test. The high fracture toughness value obtained from finite element analysis may be attributed to core material defined in finite element analysis (core was modelled using isotropic elastic material for simplicity) and there may be very contribution of mode II during experimental testing. It is mentioned in the literature that till now no test is available for pure mode I and mode II for sandwich composites. It was found that the fracture toughness of sandwich structure was considerably higher than the energy release rate value ( $0.32\text{KJ/m}^2$ ) of core material. Finally, it was seen that the fracture toughness value obtained from t-peel and wedge test experimentally was in close agreement.

Table 6.1: Fracture toughness and standard deviation using the T peel test for different E-glass fiber/foam core sandwich composite samples.

Sample No.	Energy release rate( $KJ/m^2$ )	Standard deviation
1	0.7756	0.116
2	0.7134	0.0889
3	0.7445	0.1164
4	0.6091	0.1458
5	0.768	0.1527

Table 6.2: Fracture toughness and standard deviation using the wedge test for different E-glass fiber/foam core sandwich composite samples.

Sample No.	Energy Release Rate( $KJ/m^2$ )	Standard deviation
1	0.7167	0.1189
2	0.6905	0.1259
3	0.5506	0.1239
4	0.572	0.1054
5	0.6057	0.1028

Table 6.3: Mean fracture toughness and standard deviation of wedge test and T peel test for E-glass fiber/foam core sandwich composite samples.

Test method	Mean energy release rate( $KJ/m^2$ )	Standard deviation
Wedge test	0.6271	0.065412
T-Peel test	0.72212	0.0605

Table 6.4: Comparison of fracture toughness values obtained from experimental and finite element results using different techniques for E-glass face/core foam sandwich composite specimen.

Method	T-Peel test Fracture toughness ( $KJ/m^2$ )	Wedge test Fracture toughness ( $KJ/m^2$ )
Experimental	0.73	0.62
Elastic foundation analysis of DCB	0.75	-
Elastic foundation analysis of TSD	0.72	-
Finite element using VCCT	0.76	0.67
Finite element using CSDE	0.75	0.64
J-Integral evaluation method	0.78	0.69

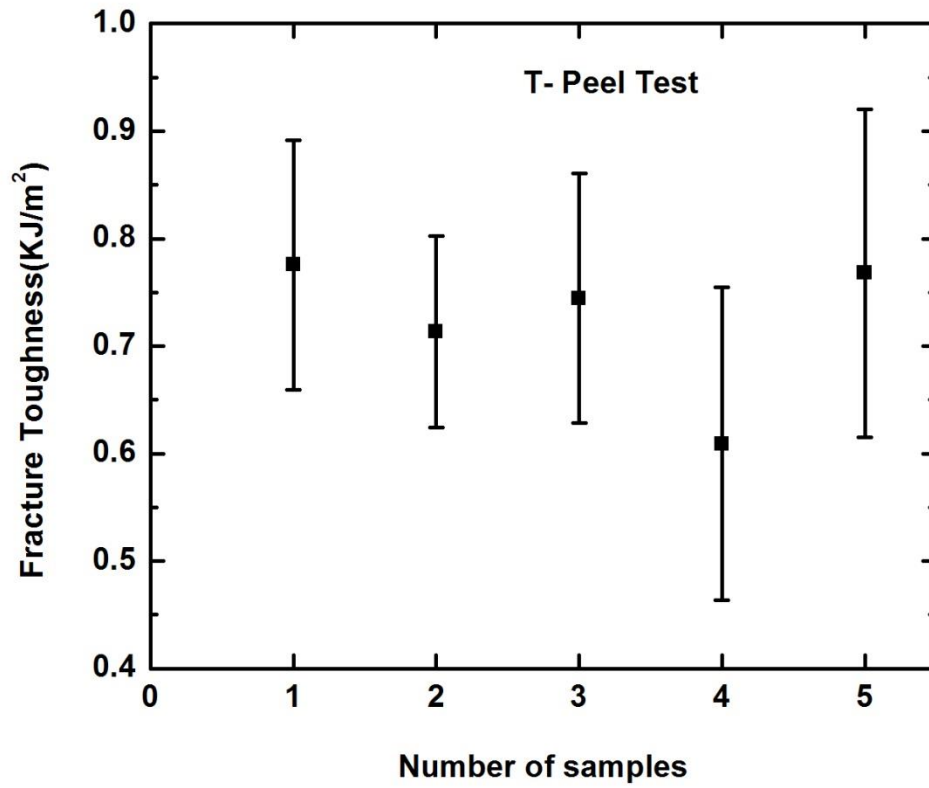


Figure 6.1: Critical fracture toughness using the T peel test for different E-glass fiber/foam core sandwich composite samples.

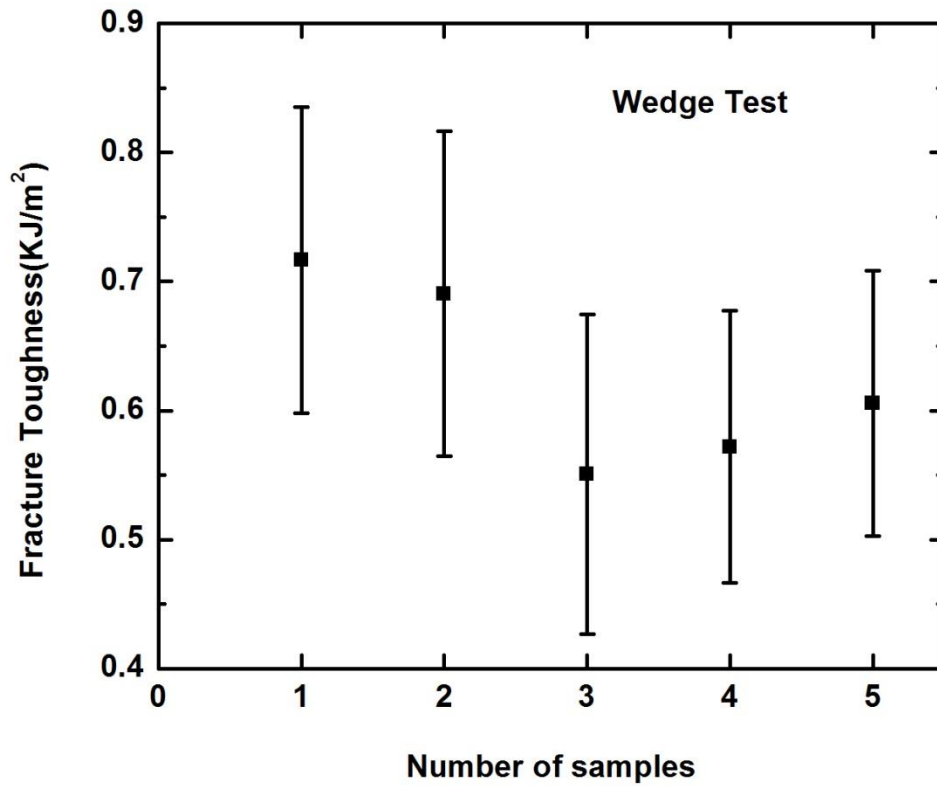


Figure 6.2: Critical fracture toughness using the wedge test for different E-glass fiber/foam core sandwich composite samples.



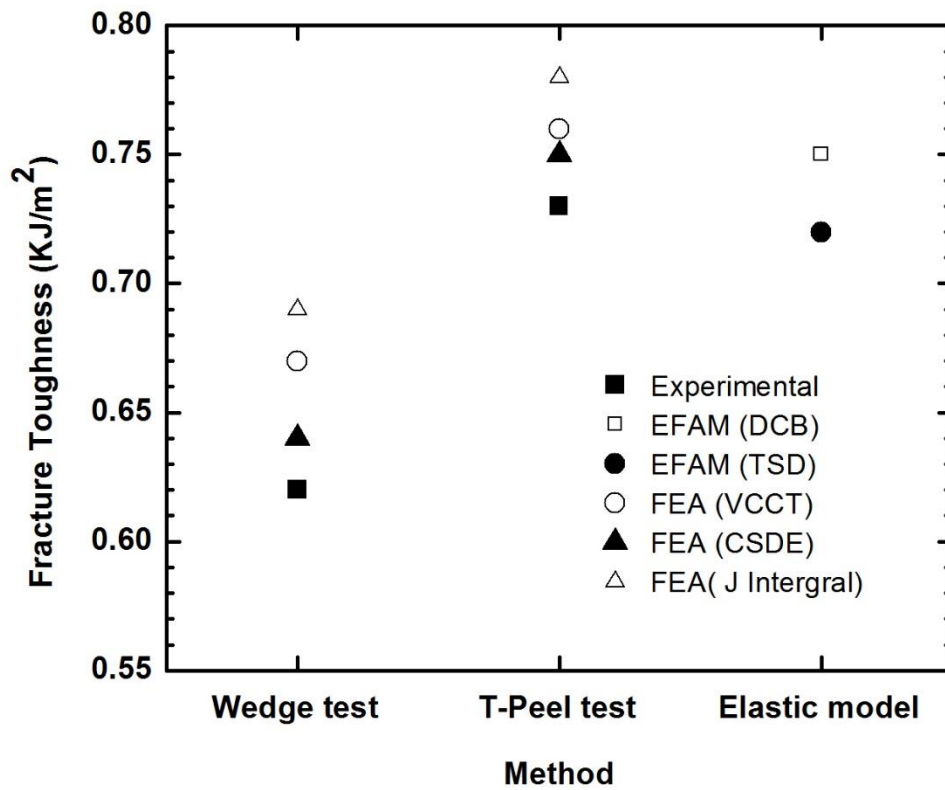


Figure 6.3: Comparison of fracture toughness values obtained from experimental and finite element results using different techniques for E-glass face/core foam sandwich composite specimen.

## 6.2. Mixed mode bending (MMB) test static evaluation

The compliance, energy release rate and global mode ratio for MMB test was calculated using equation (3.37, 3.40 and 3.41). It was seen that crack propagated in the core 0.5mm below but parallel to interface because of the penetration of the resin in the open cells of the foam. Fracture toughness of the system was much higher than the fracture toughness of the core material even though the crack propagated in the core. The

crack growth was stable for the entire range of crack length at different values of lever arm distance ( $c$ ) in MMB test. Figure 6.4 - 6.7 represents the compliance calculated using beam analysis and from finite element results using virtual crack closure technique (VCCT) for a range of crack length at different values of lever arm distance( $c$ ). The compliance of the MMB test increases with increasing crack length. It was seen that compliance of the MMB test increases with increasing lever arm distance( $c$ ). Figure 6.8 represents the comparison of compliance for different values of lever arm distance ( $c$ ) for a range of crack length for a similar geometry (same specimen dimensions). The compliance ( $C_{MMB}$ ) calculated using beam analysis and the finite element analysis are in excellent agreement. Figure 6.9 - 6.12 represents the energy release rate calculated using beam analysis and from finite element results using virtual crack closure technique (VCCT) for a range of crack length at different values of lever arm distance( $c$ ). The energy release rate of MMB test increases for increasing crack length. It was seen that energy release rate of the MMB test increases with increasing lever arm distance( $c$ ). Figure 6.13 represents the comparison of energy release rate for different values of lever arm distance ( $c$ ) for a range of crack length for a similar geometry (same specimen dimensions). The energy release rate ( $G_{MMB}$ ) calculated using beam analysis and the finite element results are in excellent agreement. Figure 6.14 - 6.17 represents the global mode ratio ( $G_{II}/G_I$ ) calculated using beam analysis and from finite element results using virtual crack closure technique (VCCT) for a range of crack length at different values of lever arm distance( $c$ ). The global mode ratio ( $G_{II}/G_I$ ) of MMB test increases for increasing crack length. It was seen that global mode ratio ( $G_{II}/G_I$ ) of the MMB test

decreases with increasing lever arm distance( $c$ ) and mode I becomes more dominant. Figure 6.18 represents the comparison of global mode ratio ( $G_{II}/G_I$ ) for different values of lever arm distance ( $c$ ) for a range of crack length for a similar geometry (same specimen dimensions). The global mode ratio ( $G_{II}/G_I$ ) calculated using beam analysis and the finite element results is in excellent agreement.

For a different material system, an E-glass fiber DBLT-850/PVC core sandwich structure, similar results has been reported in literature by Quispitupa et al. [15]. This sandwich structure has higher compliance, energy release rate and global mode ratio for delamination crack growth as compared to the polyurethane foam core sandwich structure investigated in this study.

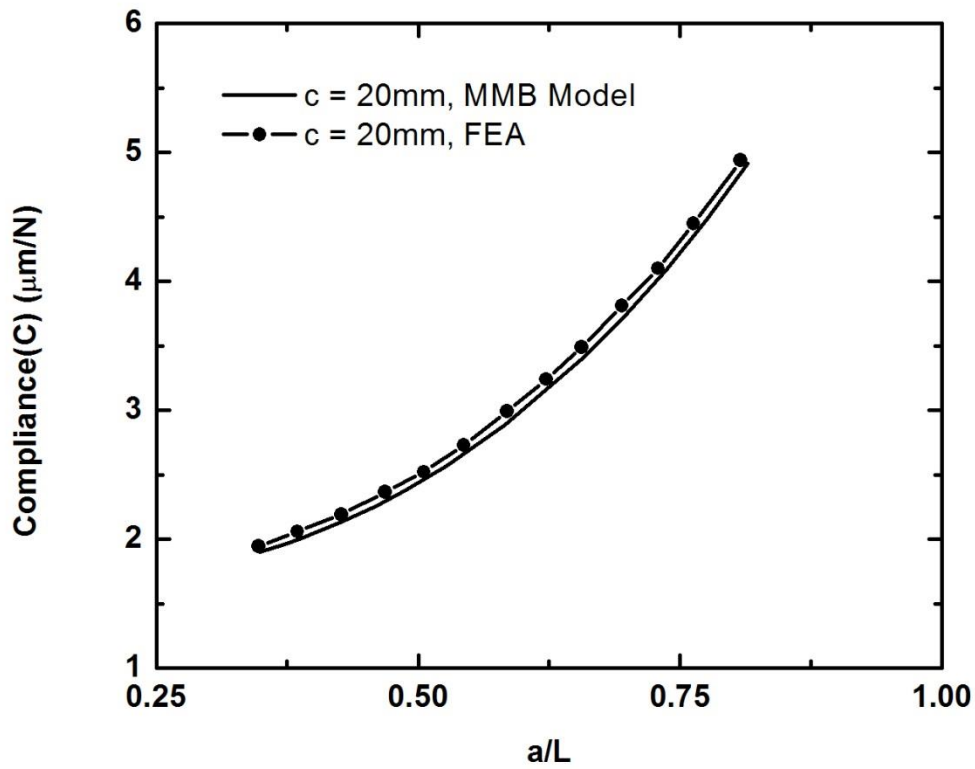


Figure 6.4: Compliance versus crack length ( $a/L$ ) at a lever arm distance ( $c = 20 \text{ mm}$ ) for E-glass face sheet/foam core sandwich composite specimen.

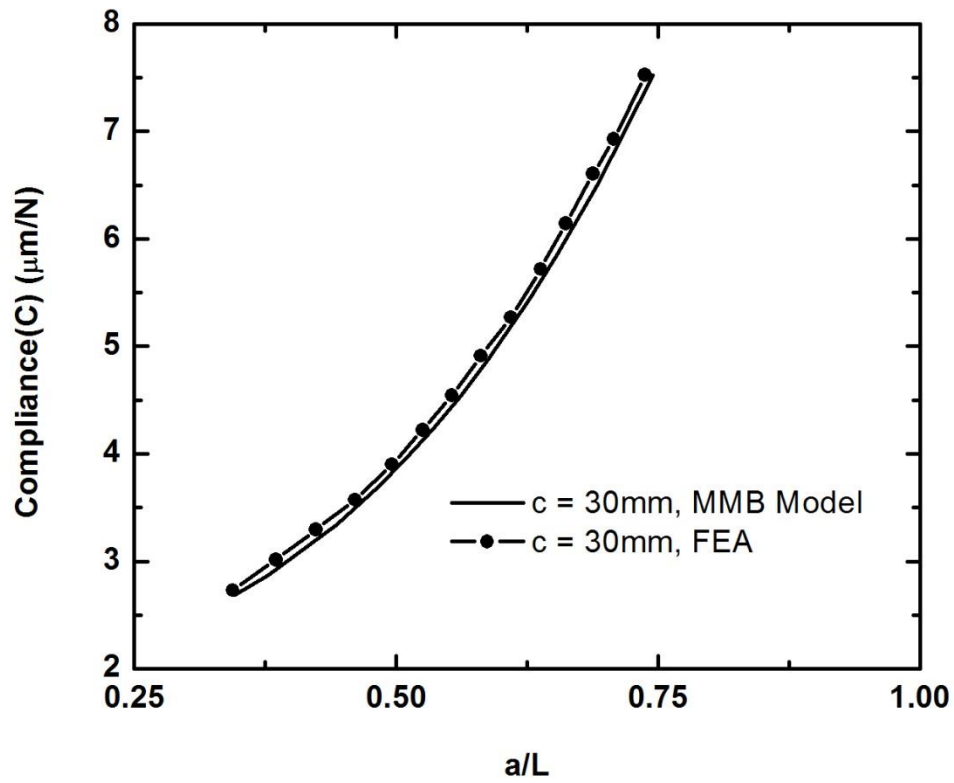


Figure 6.5: Compliance versus crack length ( $a/L$ ) at a lever arm distance ( $c = 30 \text{ mm}$ ) for E-glass face sheet/foam core sandwich composite specimen.

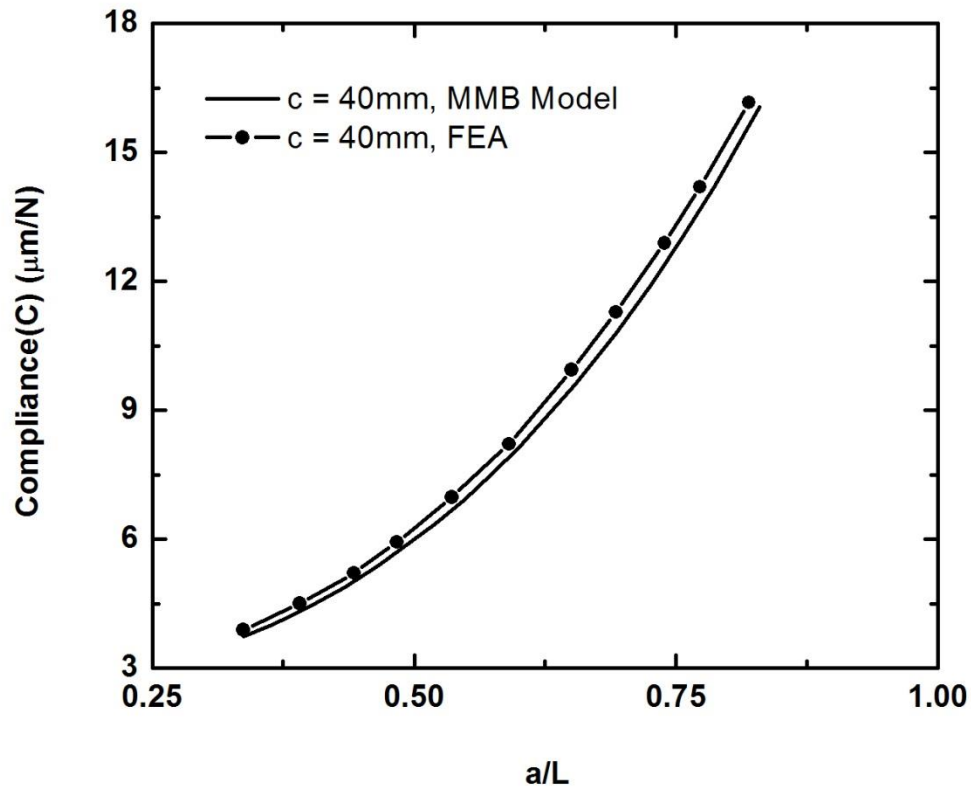


Figure 6.6: Compliance versus crack length ( $a/L$ ) at a lever arm distance ( $c = 40 \text{ mm}$ ) for E-glass face sheet/foam core sandwich composite specimen.

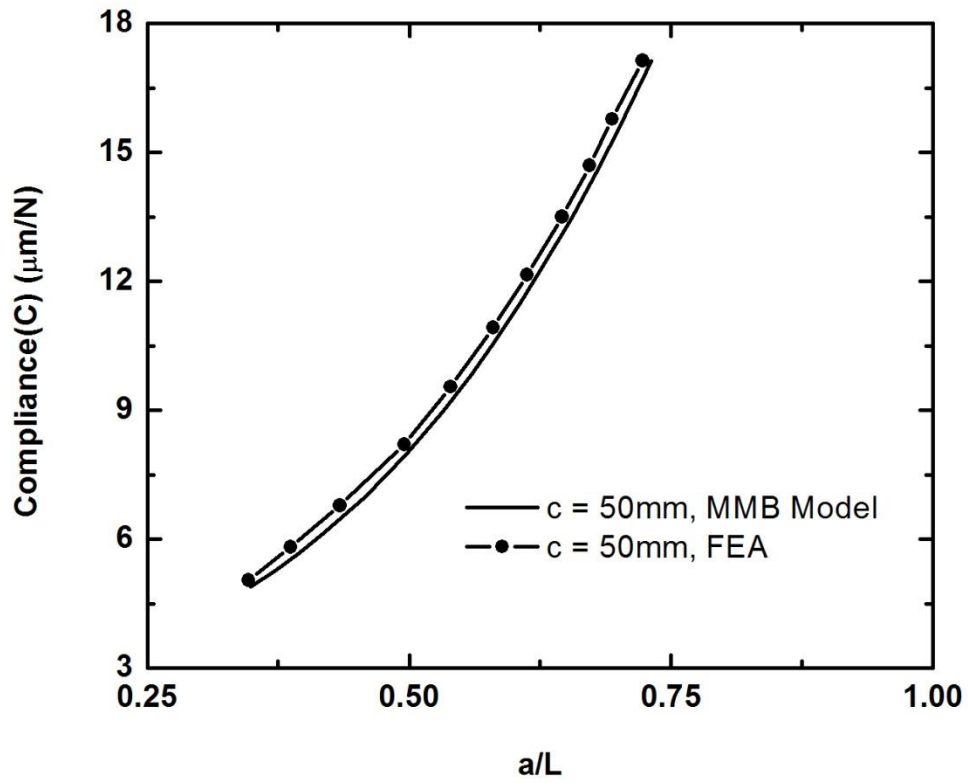


Figure 6.7: Compliance versus crack length ( $a/L$ ) at a lever arm distance ( $c = 50 \text{ mm}$ )

for E-glass face sheet/foam core sandwich composite specimen.

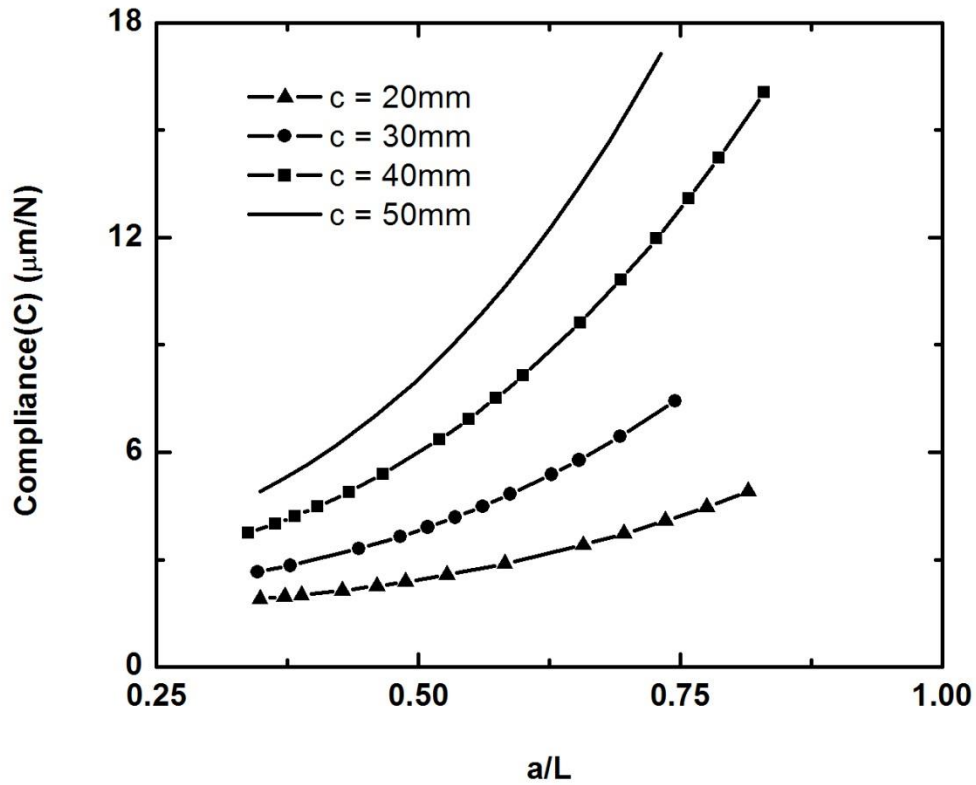


Figure 6.8: Comparison of compliance versus crack length ( $a/L$ ) at a lever arm distance ( $c = 20, 30, 40$  and  $50$  mm) for E-glass face sheet/foam core sandwich composite specimen.



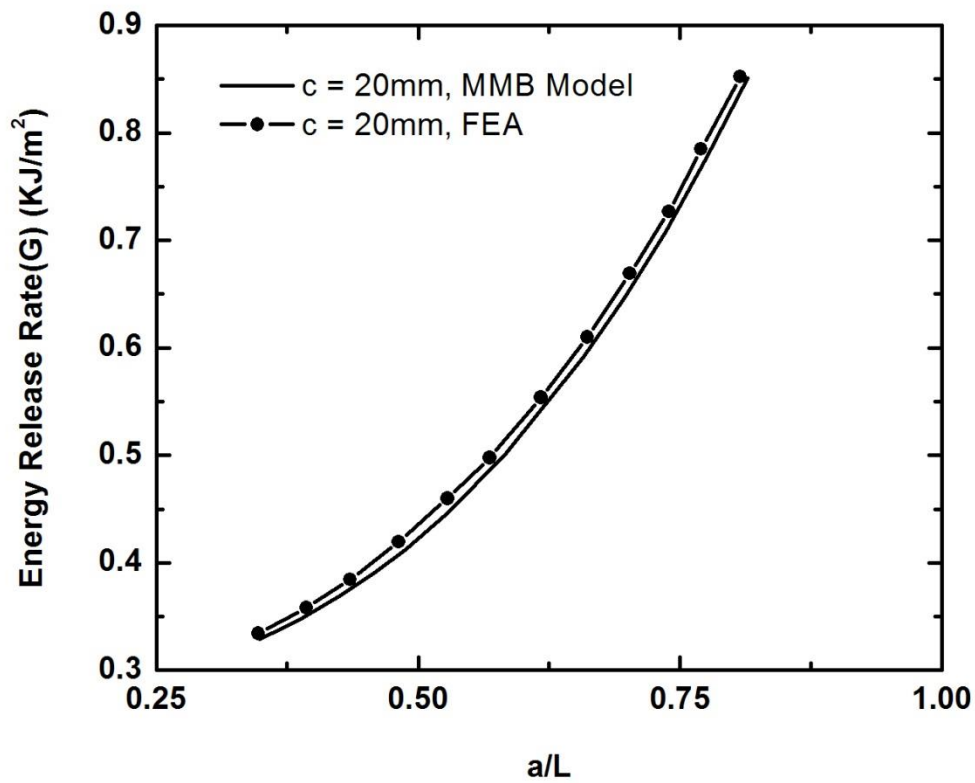


Figure 6.9: Energy release rate versus crack length ( $a/L$ ) at a lever arm distance ( $c = 20 \text{ mm}$ ) for E-glass face sheet/foam core sandwich composite specimen.

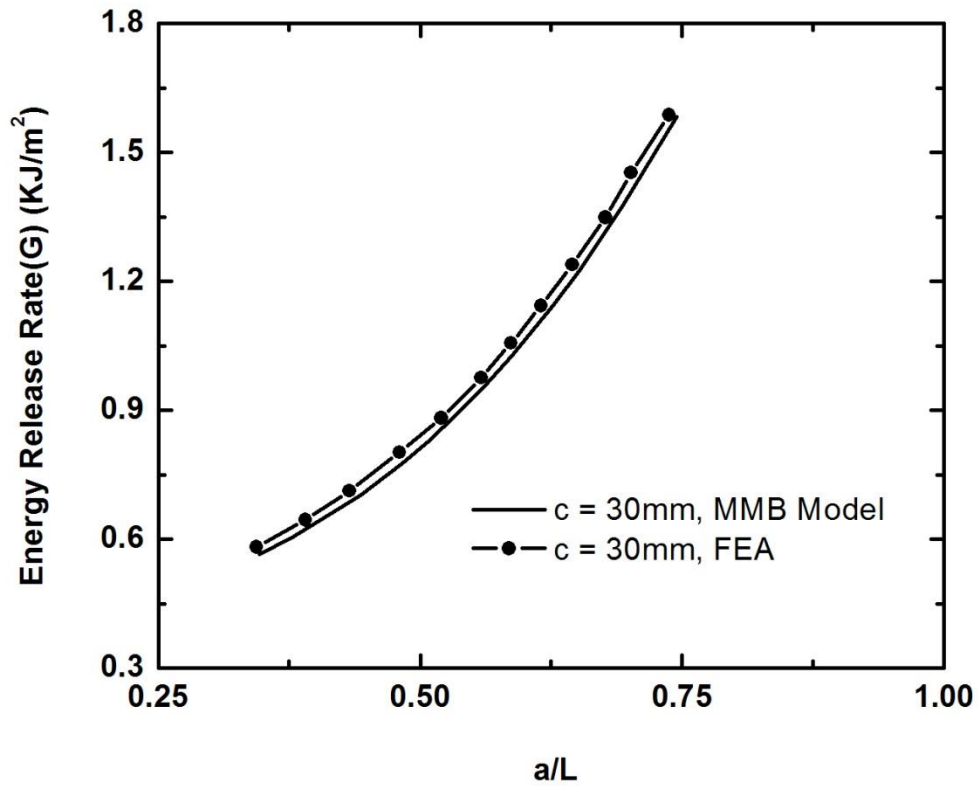


Figure 6.10: Energy release rate versus crack length ( $a/L$ ) at a lever arm distance ( $c = 30 \text{ mm}$ ) for E-glass face sheet/foam core sandwich composite specimen.

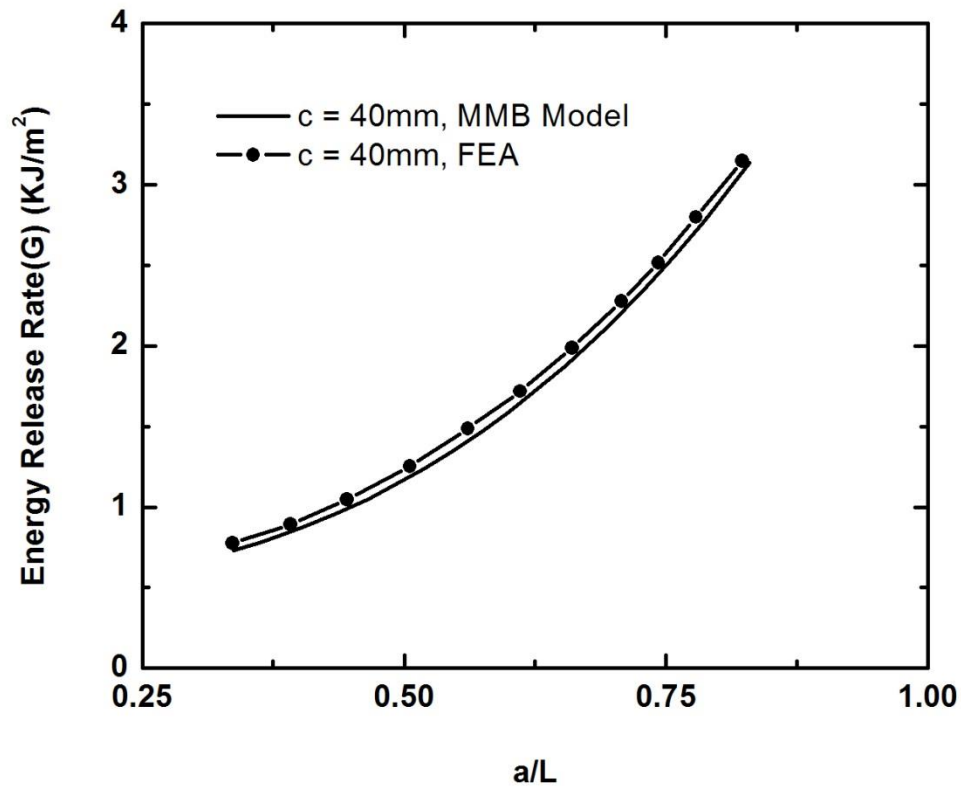


Figure 6.11: Energy release rate versus crack length ( $a/L$ ) at a lever arm distance ( $c = 40 \text{ mm}$ ) for E-glass face sheet/foam core sandwich composite specimen.

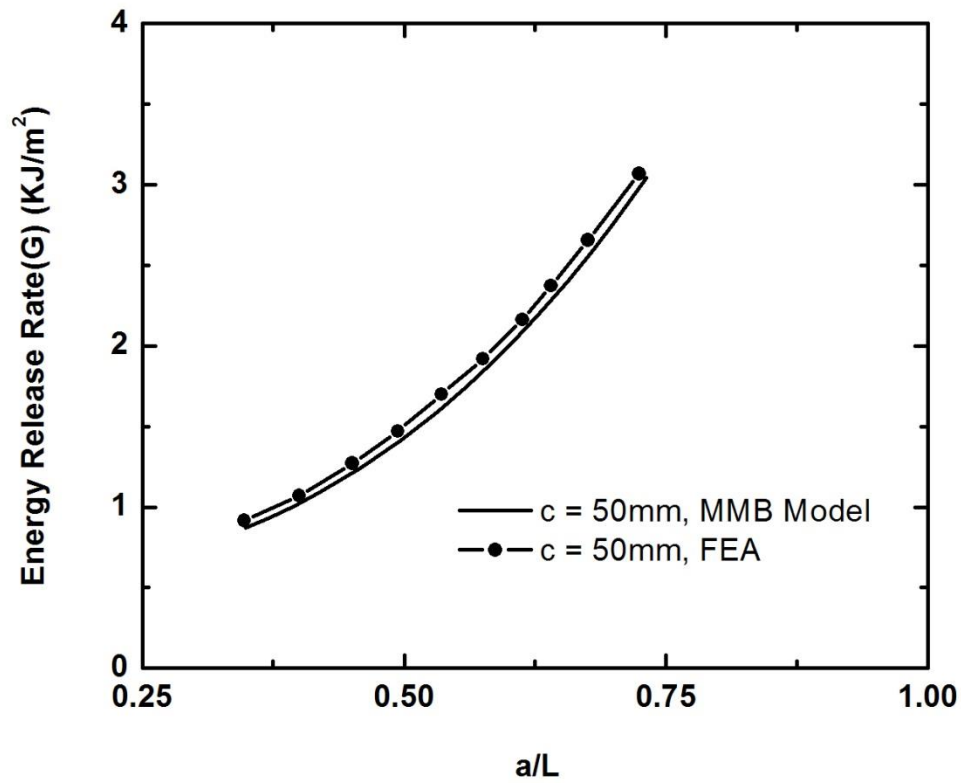


Figure 6.12: Energy release rate versus crack length ( $a/L$ ) at a lever arm distance ( $c = 50 \text{ mm}$ ) for E-glass face sheet/foam core sandwich composite specimen.

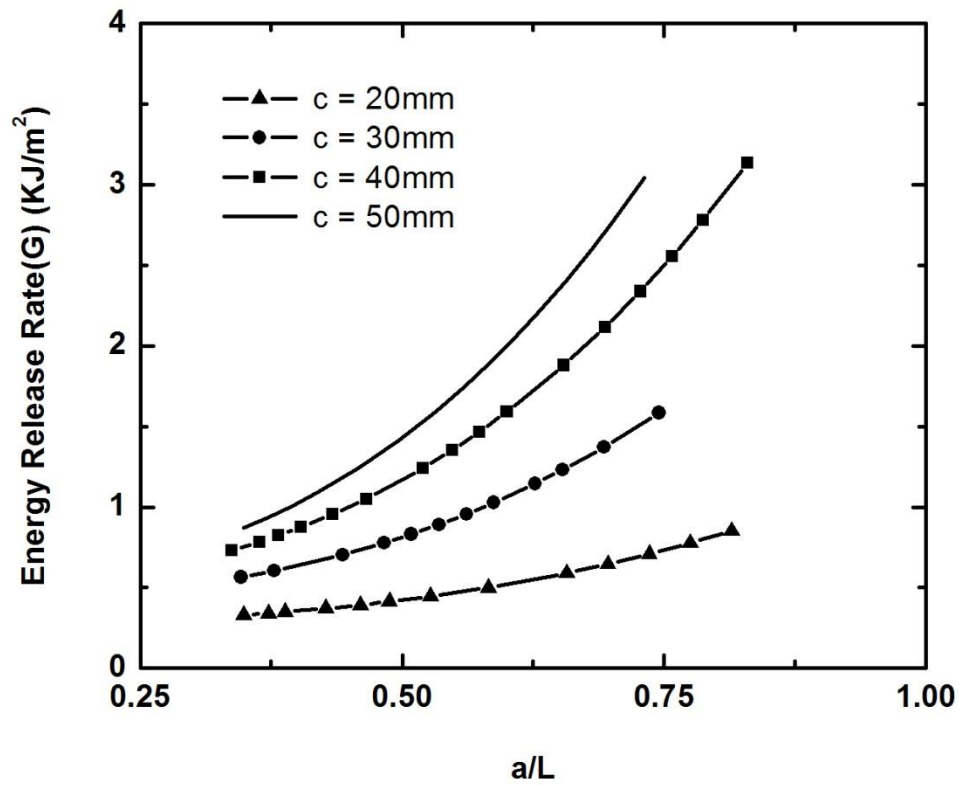


Figure 6.13: Comparison of energy release rate versus crack length ( $a/L$ ) at a lever arm distance ( $c = 20, 30, 40$  and  $50$  mm) for E-glass face sheet/foam core sandwich composite specimen.

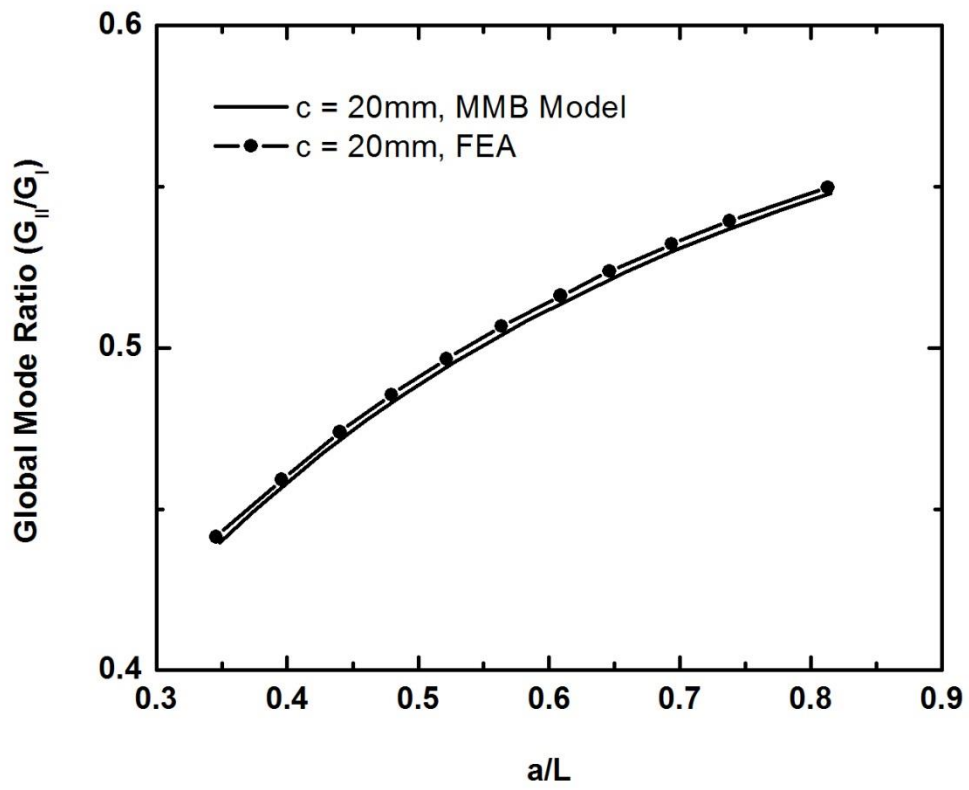


Figure 6.14: Global mode ratio versus crack length ( $a/L$ ) at a lever arm distance ( $c = 20\text{ mm}$ ) for E-glass face sheet/foam core sandwich composite specimen.

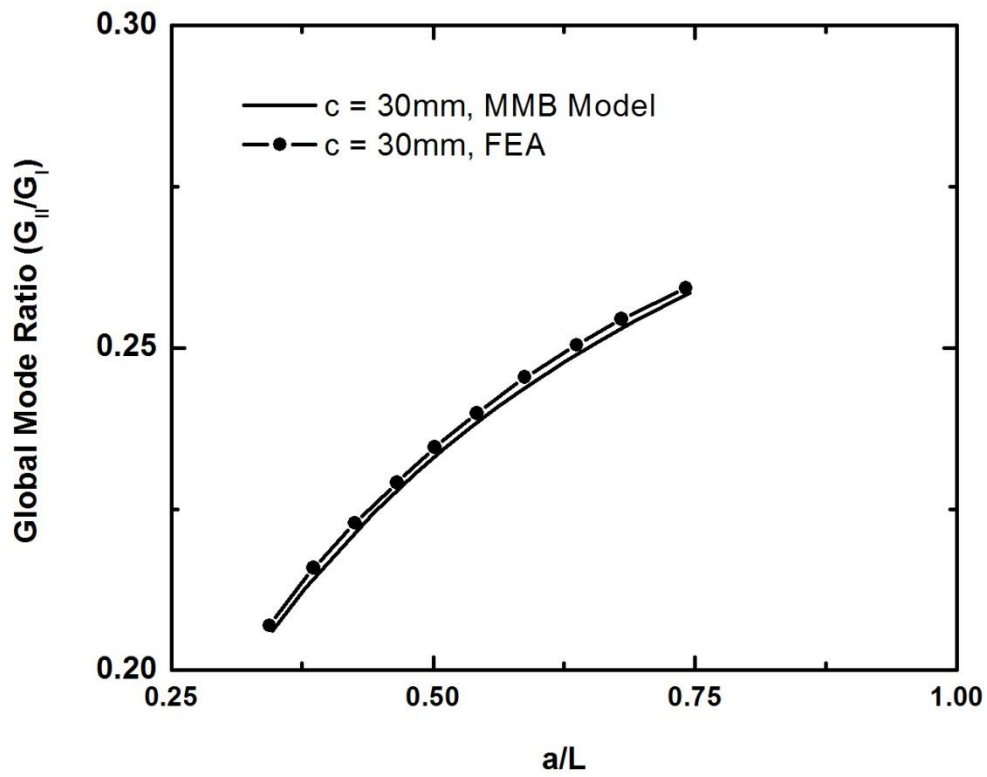


Figure 6.15: Global mode ratio versus crack length ( $a/L$ ) at a lever arm distance ( $c = 30 \text{ mm}$ ) for E-glass face sheet/foam core sandwich composite specimen.

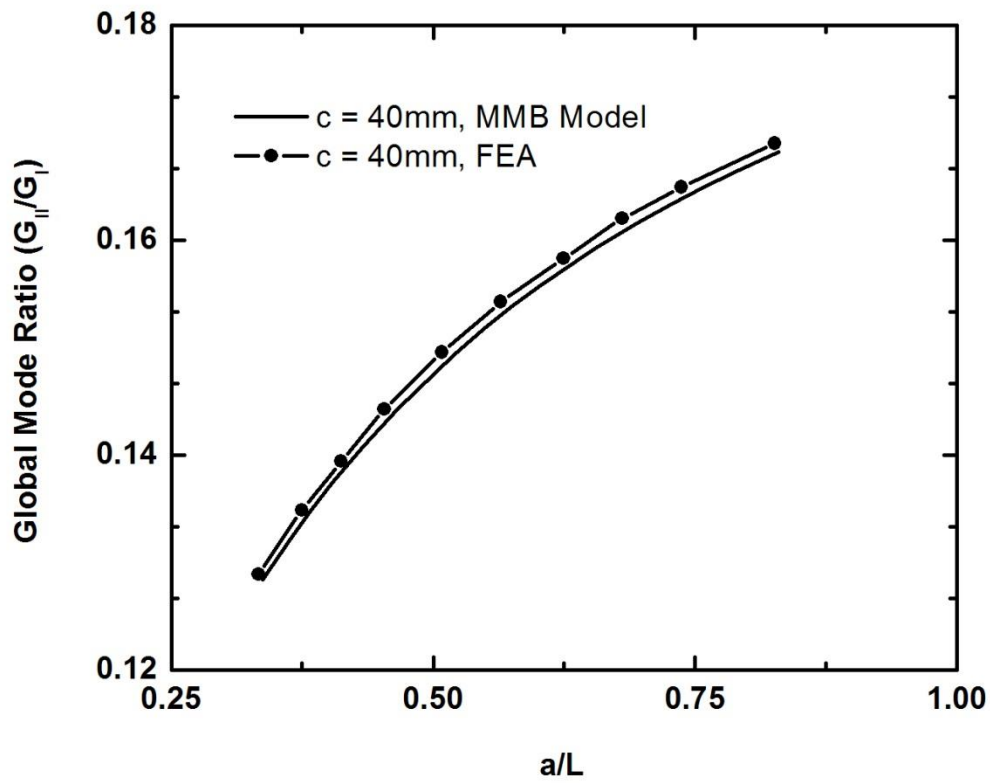


Figure 6.16: Global mode ratio versus crack length ( $a/L$ ) at a lever arm distance ( $c = 40 \text{ mm}$ ) for E-glass face sheet/foam core sandwich composite specimen.



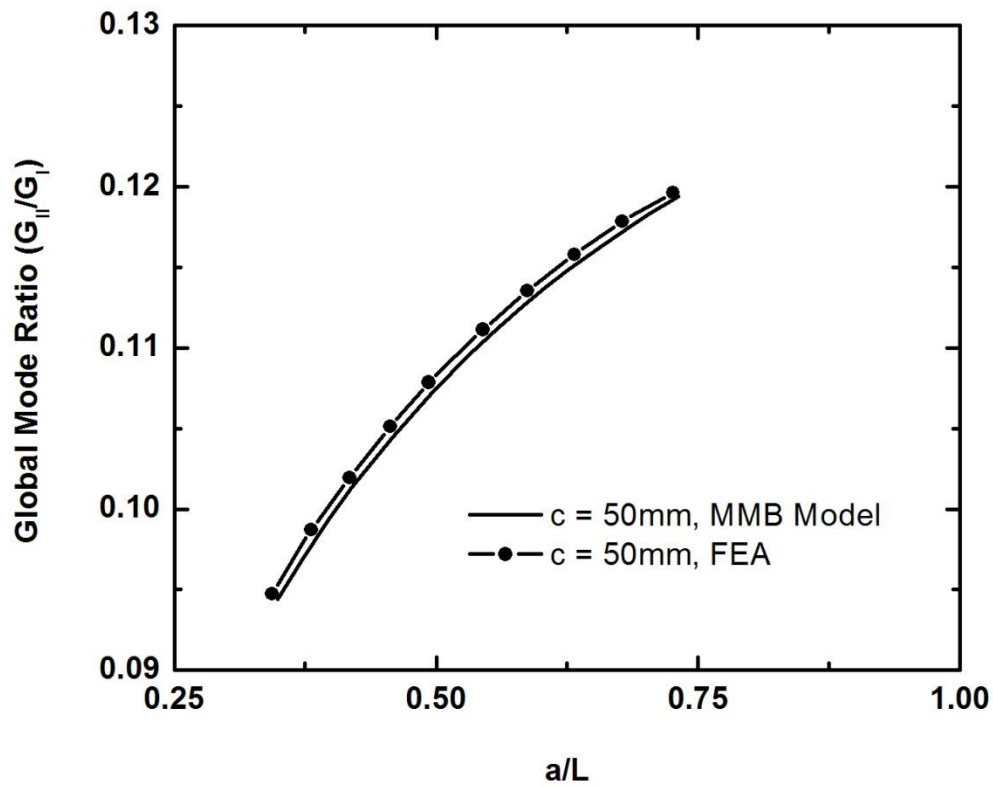


Figure 6.17: Global mode ratio versus crack length ( $a/L$ ) at a lever arm distance ( $c = 50 \text{ mm}$ ) for E-glass face sheet/foam core sandwich composite specimen.

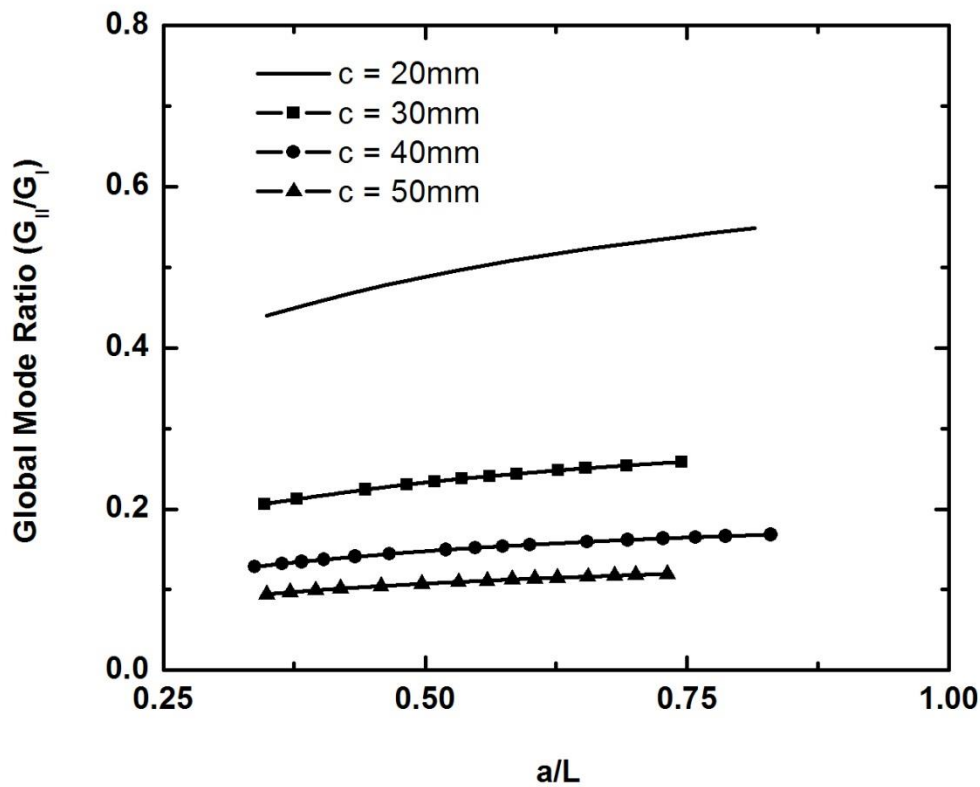


Figure 6.18: Comparison of global mode ratio versus crack length ( $a/L$ ) at a lever arm distance ( $c = 20, 30, 40$  and  $50$  mm) for E-glass face sheet/foam core sandwich composite specimen.

### 6.3. Fatigue test using single cantilever beam (SCB)

The delamination growth rates versus energy release rate ( $\Delta G_I$ ) and delamination growth rates versus number of cycles, plotted on log-log scale, are shown in figure 6.19 and 6.20, respectively. The crack propagated in the core 0.5 mm below and parallel to the interface in both static fracture and fatigue test. It was seen the crack propagated only up to a certain length after that no crack growth occurred in all specimens which were run at

different displacement levels. This is expected as in displacement control tests, the load continues to drop and can reach a level where fatigue crack extension is no longer possible. The polyurethane core sandwich composite studied in this effort fits Paris law well. The value of Paris law constant ( $C$ ) and exponent ( $m$ ) were  $6.22 \times 10^{-2}$  and 5.12, respectively. The scatter of data points was greater than normal as seen in metals because closed cell foams are very inhomogeneous in the structure. The high value of the slope indicates low crack growth resistance due to the high brittleness of the material under investigation.

For a different material system, e.g. a carbon fiber reinforced polymer (CFRP)/ polymethacrylimide (PMI) sandwich structure, the constant ( $C$ ) =  $1.26 \times 10^{-43}$  and exponent ( $m$ ) = 14.55 were reported by Rinker et al. [13]. This sandwich composite has a higher delamination crack growth rate than the polyurethane foam core sandwich composite investigated in this study.

The Negative slope of delamination growth rate versus number of cycles plotted represents relaxation controlled delamination growth. This slows down the delamination crack. This behavior is very different from the stress controlled behavior.

Newaz et al. [34] modeled this behavior as expressed in equation 6.1.

$$\frac{d\alpha}{dN} = 2n(1 - n)^2 \frac{\pi K^2}{8 \sigma_o^2} N^{2n-1} \quad (6.1)$$

Where,  $K$  is the stress intensity factor,  $\sigma_o$  is the initial yield strength,  $n$  is the material parameter and  $N$  is number of fatigue cycles.

We can use this model to describe our results. In data analysis, we find in our case, the material parameter ( $n$ ) = 0.023 obtained for glass fiber/ foam sandwich structure under investigation was in close agreement with the value of material parameter ( $n = 0.315$ ) in literature for unidirectional carbon/polyetheretherketone (PEEK) composites [34].

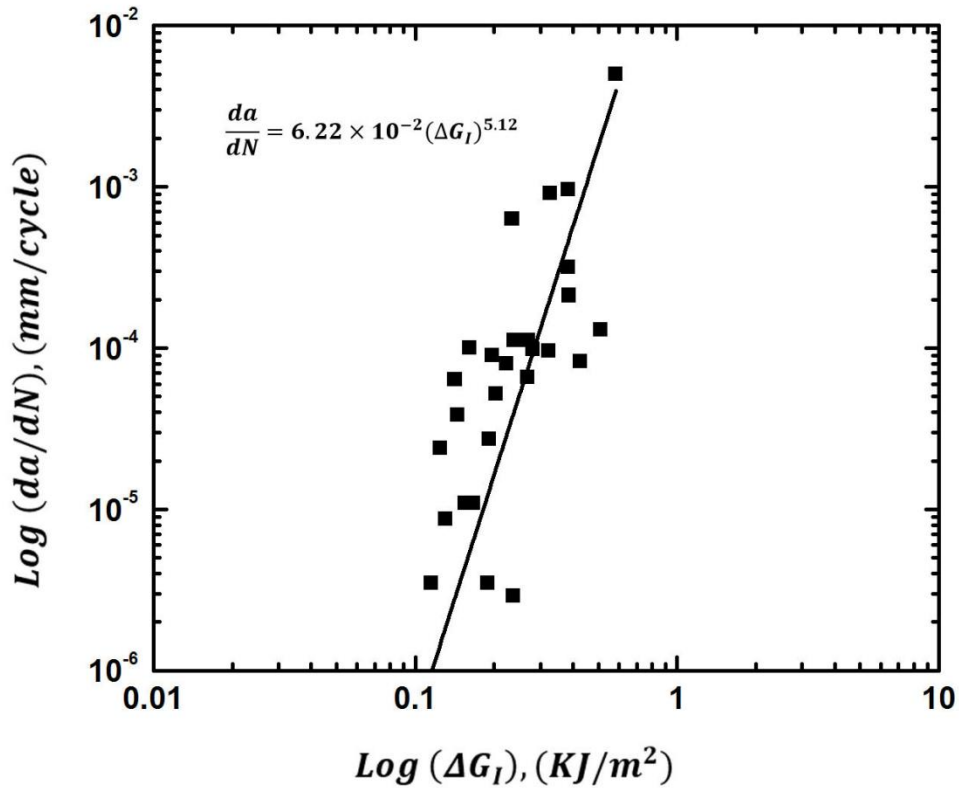


Figure 6.19: Crack growth rate versus energy release rate for E-glass face sheet/foam core sandwich composite specimens.

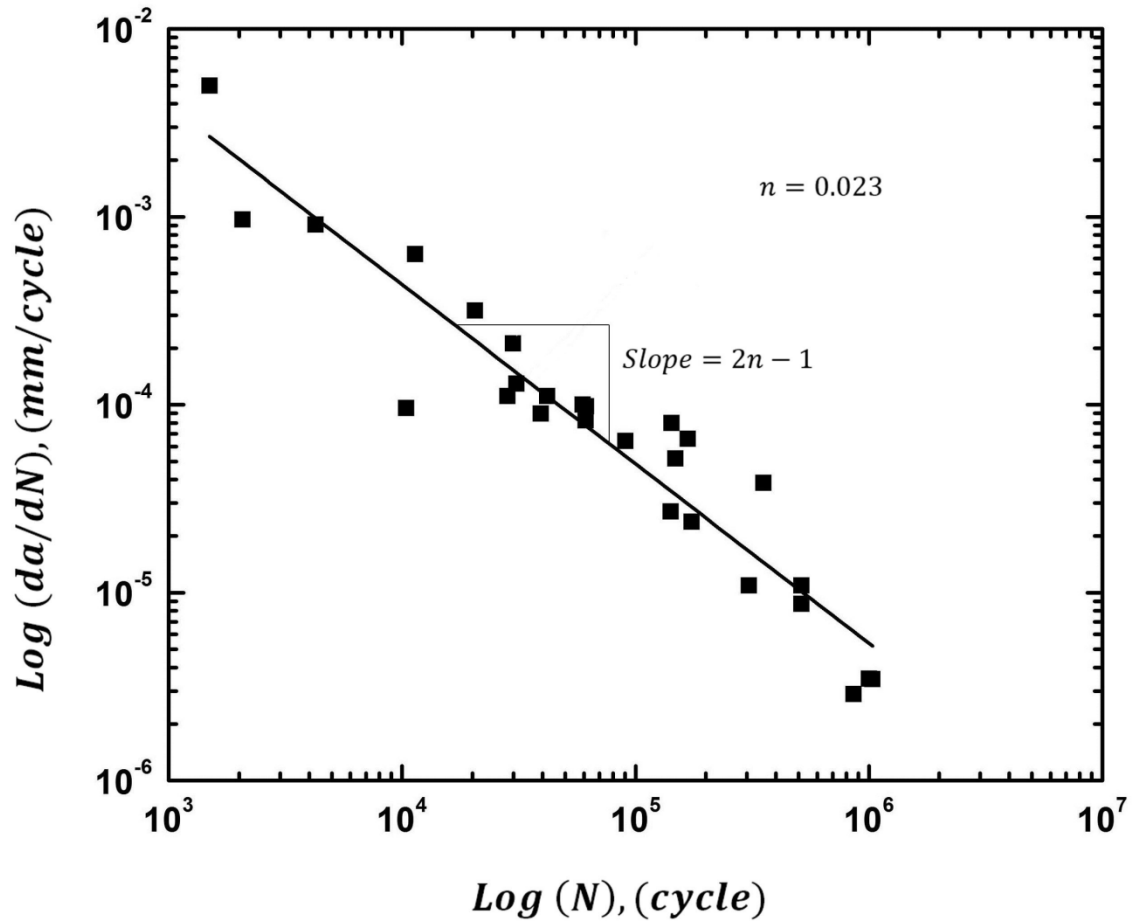


Figure 6.20: Crack growth rate versus number of cycles for E-glass face sheet/foam core sandwich composite specimens.

#### 6.4. Fatigue test using mixed mode bending (MMB)

The delamination growth rates versus energy release rate ( $\Delta G$ ) at different value of lever arm distance ( $c$ ), plotted on log-log scale, and are shown in figure 6.21-6.24. The crack propagated in the core 0.5 mm below and parallel to the interface in both static fracture and fatigue test. It was seen the crack propagated only up to a certain length after that no crack growth occurred in all specimens. This is expected as in displacement

control tests, the load continues to drop and can reach a level where fatigue crack extension is no longer possible. The polyurethane core sandwich composite studied in this effort fits Paris law well. The value of Paris law constant( $C$ ) and exponent ( $m$ ) were  $6.42 \times 10^{-1}$  and 3.24 at lever arm distance( $c = 20 \text{ mm}$ ), 1.10 and 5.06 at lever arm distance( $c = 30 \text{ mm}$ ), 3.92 and 7.51 at lever arm distance( $c = 40 \text{ mm}$ ) and 907.78 and 14.45 at lever arm distance( $c = 50 \text{ mm}$ ). It was seen that Paris law constant ( $C$ ) and exponent ( $m$ ) decreases with increase in lever arm distance. The scatter of data points was greater than normal as seen in metals because closed cell foams are very inhomogeneous in the structure. The high value of the slope indicates low crack growth resistance due to the high brittleness of the material under investigation.

For a different material system, e.g. an E-glass/polyester face sheet/PVC foam core sandwich structure, the constant( $C$ ) =  $1.825 \times 10^{-27}$  and exponent ( $m$ ) = 11.28 were reported by Manca et al. [63]. This sandwich composite has a lower delamination crack growth rate than the polyurethane foam core sandwich composite investigated in this study.

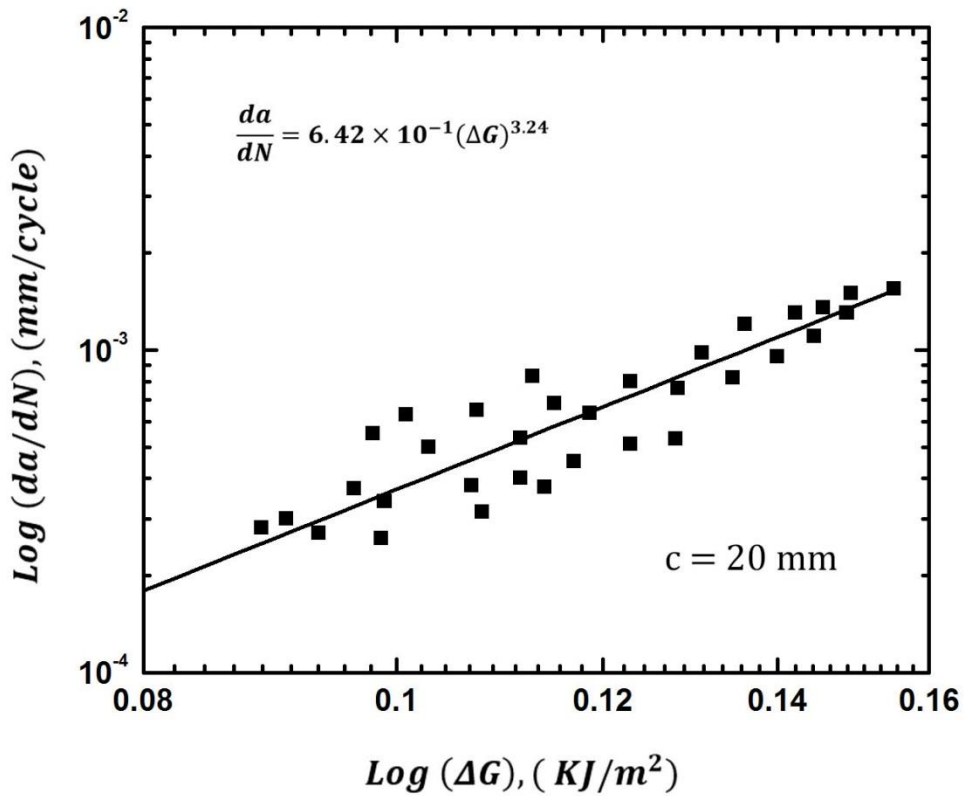


Figure 6.21: Crack growth rate versus energy release rate for E-glass face sheet/foam core at a lever arm distance ( $c = 20 \text{ mm}$ ) for sandwich composite specimens.

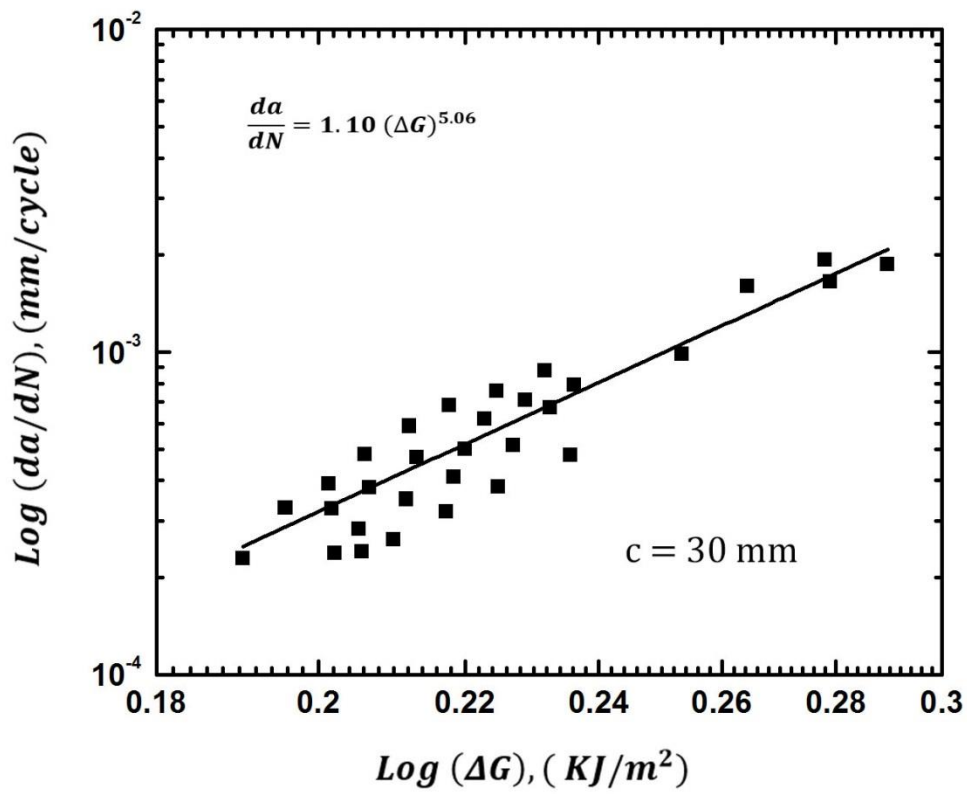


Figure 6.22: Crack growth rate versus energy release rate for E-glass face sheet/foam core at a lever arm distance ( $c = 30 \text{ mm}$ ) for sandwich composite specimens.



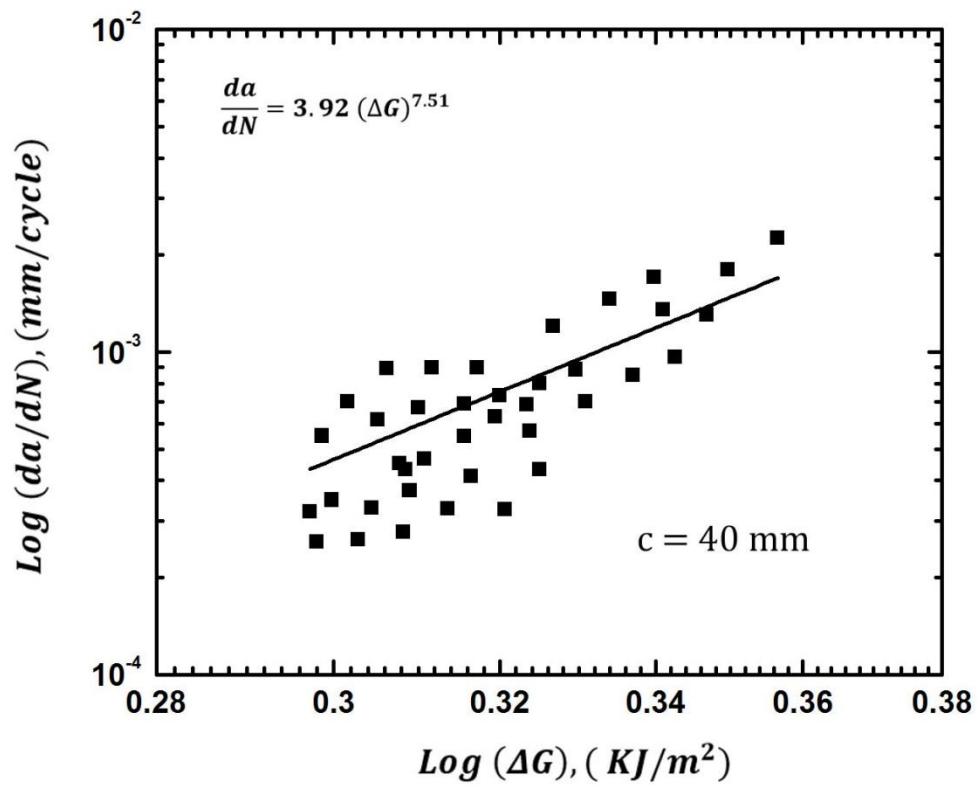


Figure 6.23: Crack growth rate versus energy release rate for E-glass face sheet/foam core at a lever arm distance ( $c = 40 \text{ mm}$ ) for sandwich composite specimens.

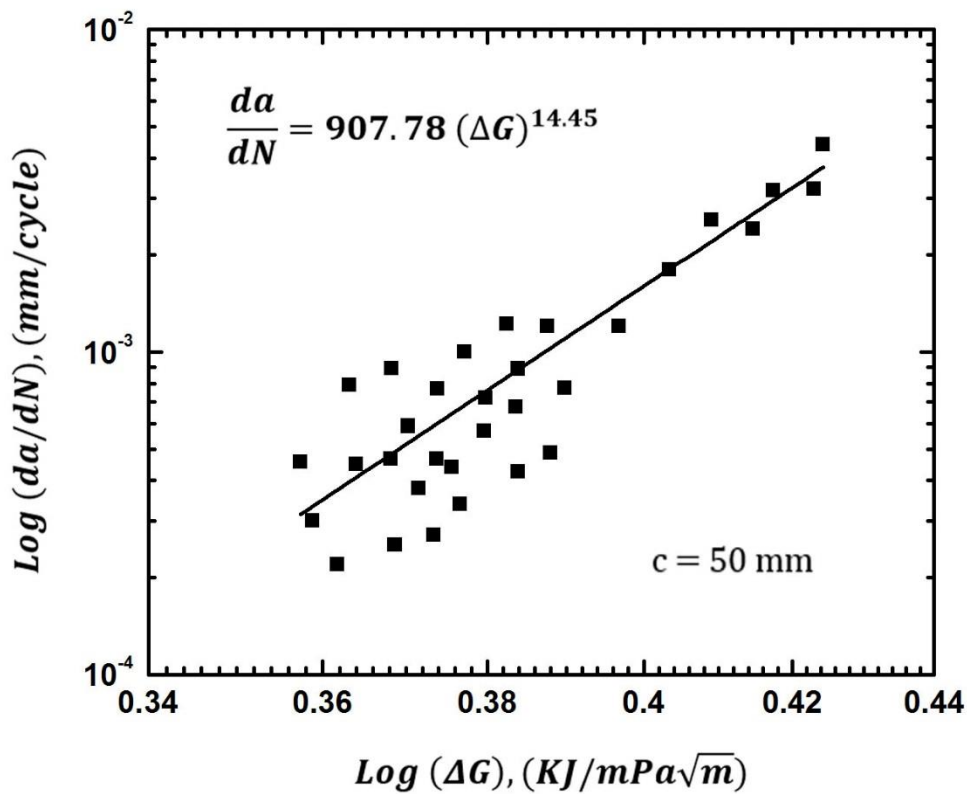


Figure 6.24: Crack growth rate versus energy release rate for E-glass face sheet/foam core at a lever arm distance ( $c = 50 \text{ mm}$ ) for sandwich composite specimens.

### 6.5. Failure modes of sandwich composite

The digital photograph of the fracture surfaces of face sheet and core at room temperature and humidity under Mode I and mixed mode for static and fatigue loading is shown in figure 6.25. The fracture surface of face sheet is completely covered with a very thin layer (thickness 0.5 mm) of the foam material. The resin impregnation after processing extended into the foam material about 0.5 mm and was confirmed via edge-wise examination under microscope. Our careful observations show that the fracture

surfaces of the face sheet and core are almost similar under static and fatigue loading. This indicates that fracture mechanism is quite the same for static and fatigue fracture. The crack propagated in the core parallel to interface in a slow and stable manner for both static and fatigue under mode I and mixed mode loading. Brittle fracture was dominant in both static and fatigue fracture cases. The cohesive brittle fracture indicates that the fracture toughness of core material is lower compared to the interface as crack propagated through the weaker medium. This is a unique feature of some foam core composites and has been reported earlier by Kulkarni et al. [70].

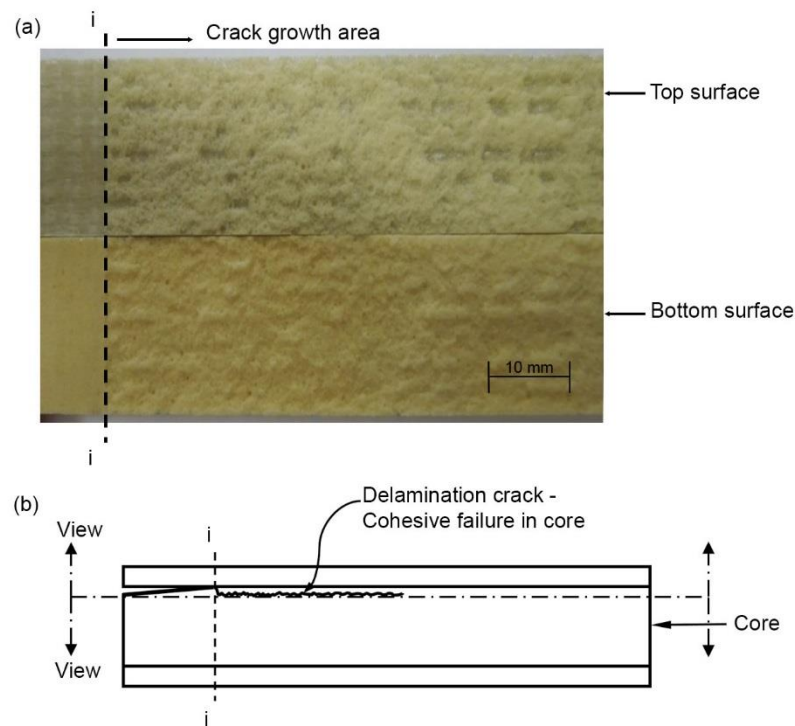


Figure 6.25: Fracture surfaces of top and bottom foam surfaces showing foam material indicative of 'cohesive failure'.

## CHAPTER 7

### CONCLUSIONS AND RECOMMENDATIONS

#### 7.1 Conclusions

E-glass facesheet/polyurethane foam core sandwich composites were investigated for mode I and mixed mode under static and fatigue loading to evaluate fracture toughness, energy release rate and characterize the delamination crack growth behavior. The effect of lever arm distance( $c$ ) on global mode ratio ( $G_{II}/G_I$ ) under mixed mode static loading was studied. The following conclusions can be made for E-glass facesheet/polyurethane foam core sandwich composite.

- **Mode I and mixed mode static test**
  - a) The fracture toughness value estimated from two different types of test for Mode I static loading namely T-peel test and wedge test are in close agreement.
  - b) The fracture toughness calculated using the energy release rate expression derived on the basis on elastic foundation analysis for double cantilever beam (DCB) specimen by Aviles and Carlsson [14] is in close agreement with the fracture toughness estimated using T-peel test.
  - c) The fracture toughness calculated using the energy release rate expression derived on the basis on elastic foundation analysis for tilted sandwich debond (TSD) specimen by Li and Carlsson [20] is in close agreement with the fracture toughness estimated using T-peel test.

- d) The crack growth was stable in wedge test. However, stick-slip behavior was noted in T-peel test.
- e) The compliance ( $C_{MMB}$ ), energy release rate ( $G_{MMB}$ ) and a global mode ratio ( $G_{II}/G_I$ ) of the mixed mode bending (MMB) specimen increases with increasing crack length.
- f) The compliance ( $C_{MMB}$ ) and energy release rate ( $G_{MMB}$ ) of the mixed mode bending (MMB) specimen increases and global mode ratio ( $G_{II}/G_I$ ) decreases with an increase in a lever arm distance ( $c$ ), respectively and Mode I become more dominant.
- g) The fracture toughness obtained from finite element analysis by employing virtual crack closure (VCCT) technique, crack surface displacement extrapolation (CSDE) method and direct J-integral evaluation method is in excellent agreement for both the T-peel test and wedge test.
- h) The compliance, energy release rate and global mode ratio of the mixed mode bending (MMB) specimen obtained from finite element analysis by employing virtual crack closure (VCCT) technique are in excellent agreement for MMB test.
- i) The fracture toughness of sandwich structure was considerably higher than the fracture toughness value ( $0.32KJ/m^2$ ) of core material for mode I and mixed mode loading.
- j) The fracture toughness is independent of initial crack length for mode I and mixed mode loading.

- k) The delamination crack growth was found to be cohesive in nature within the core but close to the interface.
  - l) Brittle fracture was dominant for mode I and mixed mode loading.
- **Mode I and mixed mode fatigue test**
    - a) Delamination crack growth behavior for E-glass face sheet/polyurethane foam core sandwich composite under displacement controlled condition for mode I and mixed mode loading was characterized.
    - b) Crack growth rate versus energy release rate for the mode I and mixed mode loading were plotted on log-log scale to determine the Paris law constant and exponent to predict the failure for E-glass face sheet/polyurethane foam core sandwich composite under investigation. The slope of Paris law is 5.12 and 14.55 for mode I and mixed mode loading, respectively. The constants are low for polyurethane foam core sandwich composites as compared to PVC core sandwich composites.
    - c) The threshold energy release rate ( $\Delta G_I = 0.12 \text{ KJ}/\text{m}^2$ ) was determined for  $R = 0.1$  by using load-shedding technique for mode I.
    - d) The energy release rate decreases with increasing crack length for mode I and mixed mode loading.
    - e) The Paris law constant and exponent increases with an increase in a lever arm distance(c).
    - f) The fracture mechanism is quite the same as for static fracture.

g) The crack growth rate is characterized by relaxation controlled growth model.

## 7.2 Recommendations for future work

- a) The effect of face sheet and core thickness on the fracture toughness and energy release rate for the mode I and mixed mode under static and fatigue loading for E-glass face sheet/ polyurethane foam core sandwich structures should be studied.
- b) The fatigue test under mode I and mixed mode loading should be conducted for a range load ratio ( $R$ ) and threshold energy relapse rate should be estimated to predict the life of E-glass face sheet/ polyurethane foam core sandwich composite under very critical applications.
- c) The experiments should be conducted at freezing and elevated temperature to study the effect of temperature on the fracture toughness and energy release rate for the mode I and mixed mode under static and fatigue loading for E-glass face sheet/ polyurethane foam core sandwich structures.
- d) Three dimensional finite element models should be used to predict accurate energy release rate and stress distribution in the vicinity of the crack tip and through the thickness.

## REFERENCES

- [1] Riley, A., Aardema, B., Vosbury, P., Eiff, M., Frautschy, H., Serkenburg, R., Shaffer, D., Wild, T., and Michmerhuizen, T., 2008, "Aviation Maintenance Technician Handbook," US Department of Transportation: Federal Aviation Administration.
- [2] Bitzer, T., 1997, Honeycomb technology: materials, design, manufacturing, applications and testing, Springer Science & Business Media.
- [3] Zenkert, D., "The Handbook of Sandwich Construction,(1997)," Engineering Materials Advisory Chameleon Press Ltd, London, UK.
- [4] Zenkert, D., 1997, An introduction to sandwich construction, Engineering materials advisory services.
- [5] Plantema, F. J., 1966, Sandwich construction: the bending and buckling of sandwich beams, plates, and shells, Wiley.
- [6] Hoff, N. J., 1950, "Bending and buckling of rectangular sandwich plates."
- [7] Timoshenko, S., 2008, Vibration Problems in Engineering, Read Books.
- [8] Hellbratt, S.-E., 1993, Design and Production of GRP Sandwich Vessels.
- [9] Pickett, B. E., 1995, "A medium life helicopter for a unique mission," Materials Challenge: Diversification and the Future., 40, pp. 410-420.
- [10] Turner, G. F., 1995, "Advanced composite materials in European aircraft present and future," Materials Challenge: Diversification and the Future., 40, pp. 366-380.
- [11] Olsson, K.-A., 1986, GRP-sandwich design and production in Sweden.
- [12] van Tooren, M., 1989, "A new step to easier production of high quality sandwich structures," Engineering Materials Advisory Services Ltd.(UK), pp. 577-597.



- [13] Rinker, M., John, M., Zahlen, P. C., and Schäuble, R., 2011, "Face sheet debonding in CFRP/PMI sandwich structures under quasi-static and fatigue loading considering residual thermal stress," *Engineering Fracture Mechanics*, 78(17), pp. 2835-2847.
- [14] Aviles, F., and Carlsson, L., 2008, "Analysis of the sandwich DCB specimen for debond characterization," *Engineering Fracture Mechanics*, 75(2), pp. 153-168.
- [15] Quispitupa, A., Berggreen, C., and Carlsson, L. A., 2009, "On the analysis of a mixed mode bending sandwich specimen for debond fracture characterization," *Engineering Fracture Mechanics*, 76(4), pp. 594-613.
- [16] Saha, M., Kabir, E., and Jeelani, S., 2008, "Study of debond fracture toughness of sandwich composites with nanophased core," *Materials Letters*, 62(4), pp. 567-570.
- [17] Wang, X., Wu, L., and Wang, S., 2009, "Study of debond fracture toughness of sandwich composites with metal foam core," *Journal of materials science & technology*, 25(5), pp. 713-716.
- [18] Ural, A., Zehnder, A. T., and Ingrassia, A. R., 2003, "Fracture mechanics approach to facesheet delamination in honeycomb: measurement of energy release rate of the adhesive bond," *Engineering Fracture Mechanics*, 70(1), pp. 93-103.
- [19] Liechti, K. M., and Marton, B., 2002, "Delamination of a high-temperature sandwich plate," *Experimental mechanics*, 42(2), pp. 206-213.
- [20] Li, X., and Carlsson, L. A., 2000, "Elastic foundation analysis of tilted sandwich debond (TSD) specimen," *Journal of Sandwich Structures and Materials*, 2(1), pp. 3-32.

- [21] Li, X., and Carlsson, L. A., 1999, "The tilted sandwich debond (TSD) specimen for face/core interface fracture characterization," *Journal of Sandwich Structures and Materials*, 1(1), pp. 60-75.
- [22] Smith, S., and Shivakumar, K., 2001, "Modified mode-I cracked sandwich beam (CSB) fracture test," AIAA paper, 1221(2).
- [23] Berggreen, C., and Carlsson, L. A., 2010, "A modified TSD specimen for fracture toughness characterization-fracture mechanics analysis and design," *Journal of Composite Materials*, 44(15), pp. 1893-1912.
- [24] Prasad, S., and Carlsson, L. A., 1994, "Debonding and crack kinking in foam core sandwich beams—I. Analysis of fracture specimens," *Engineering Fracture Mechanics*, 47(6), pp. 813-824.
- [25] Prasad, S., and Carlsson, L. A., 1994, "Debonding and crack kinking in foam core sandwich beams—II. Experimental investigation," *Engineering Fracture Mechanics*, 47(6), pp. 825-841.
- [26] Berggreen, C., Simonsen, B. C., and Borum, K. K., 2007, "Experimental and numerical study of interface crack propagation in foam-cored sandwich beams," *Journal of Composite Materials*, 41(4), pp. 493-520.
- [27] Lundsgaard-Larsen, C., Berggreen, C., and Carlsson, L. A., "On the use of a woven mat to control the crack path in composite sandwich specimens with foam core," *Proc. ASME 2007 International Mechanical Engineering Congress and Exposition*, American Society of Mechanical Engineers, pp. 975-976.

- [28] Gdoutos, E., "DEBONDING OF INTERFACIAL CRACKS IN SANDWICH BEAMS."
- [29] Hojo, M., Ando, T., Tanaka, M., Adachi, T., Ochiai, S., and Endo, Y., 2006, "Modes I and II interlaminar fracture toughness and fatigue delamination of CF/epoxy laminates with self-same epoxy interleaf," *International Journal of Fatigue*, 28(10), pp. 1154-1165.
- [30] Hojo, M., Nakashima, K., Kusaka, T., Tanaka, M., Adachi, T., Fukuoka, T., and Ishibashi, M., 2010, "Mode I fatigue delamination of Zanchor-reinforced CF/epoxy laminates," *International journal of fatigue*, 32(1), pp. 37-45.
- [31] Shipsha, A., Burman, M., and Zenkert, D., 1999, "Interfacial fatigue crack growth in foam core sandwich structures," *Fatigue and Fracture of Engineering Materials and Structures*, 22(2), pp. 123-132.
- [32] Berkowitz, C. K., and Johnson, W. S., 2005, "Fracture and fatigue tests and analysis of composite sandwich structure," *Journal of composite materials*, 39(16), pp. 1417-1431.
- [33] Kanny, K., and Mahfuz, H., 2005, "Flexural fatigue characteristics of sandwich structures at different loading frequencies," *Composite Structures*, 67(4), pp. 403-410.
- [34] Newaz, G. M., Lustiger, A., and Yung, J.-Y., 1989, "Delamination growth under cyclic loading at elevated temperature in thermoplastic composites," *Advances in thermoplastic matrix composite materials*, pp. 264-278.

- [35] Trethewey, B. R., Gillespie, J. W., and Carlsson, L. A., 1988, "Mode II cyclic delamination growth," *Journal of composite materials*, 22(5), pp. 459-483.
- [36] Peng, L., Zhang, J., Zhao, L., Bao, R., Yang, H., and Fei, B., 2011, "Mode I delamination growth of multidirectional composite laminates under fatigue loading," *Journal of composite materials*, 45(10), pp. 1077-1090.
- [37] Shivakumar, K., Chen, H., Abali, F., Le, D., and Davis, C., 2006, "A total fatigue life model for mode I delaminated composite laminates," *International Journal of Fatigue*, 28(1), pp. 33-42.
- [38] Nakai, Y., and Hiwa, C., 2002, "Effects of loading frequency and environment on delamination fatigue crack growth of CFRP," *International Journal of Fatigue*, 24(2), pp. 161-170.
- [39] Sjögren, A., and Asp, L. E., 2002, "Effects of temperature on delamination growth in a carbon/epoxy composite under fatigue loading," *International Journal of Fatigue*, 24(2), pp. 179-184.
- [40] Shindo, Y., Inamoto, A., Narita, F., and Horiguchi, K., 2006, "Mode I fatigue delamination growth in GFRP woven laminates at low temperatures," *Engineering Fracture Mechanics*, 73(14), pp. 2080-2090.
- [41] Shipsha, A., Burman, M., and Zenkert, D., 2000, "On mode I fatigue crack growth in foam core materials for sandwich structures," *Journal of Sandwich Structures and Materials*, 2(2), pp. 103-116.
- [42] Hojo, M., Matsuda, S., Fiedler, B., Kawada, T., Moriya, K., Ochiai, S., and Aoyama, H., 2002, "Mode I and II delamination fatigue crack growth behavior of alumina

- fiber/epoxy laminates in liquid nitrogen," *International journal of fatigue*, 24(2), pp. 109-118.
- [43] Hirose, Y., Hojo, M., Fujiyoshi, A., and Matsubara, G., 2007, "Suppression of interfacial crack for foam core sandwich panel with crack arrester," *Advanced Composite Materials*, 16(1), pp. 11-30.
- [44] Hirose, Y., Matsuda, H., Matsubara, G., Inamura, F., and Hojo, M., 2009, "Evaluation of new crack suppression method for foam core sandwich panel via fracture toughness tests and analyses under mode-I type loading," *Journal of Sandwich Structures and Materials*.
- [45] Hirose, Y., and Hojo, M., 2010, "Peel progression preventing structure of sandwich panel," *Google Patents*.
- [46] Minakuchi, S., Yamauchi, I., Takeda, N., and Hirose, Y., 2009, "Detection of arrested crack for foam core sandwich structures using optical fiber sensors embedded in a crack arrester," *ICAF 2009, Bridging the Gap between Theory and Operational Practice*, pp. 209-221.
- [47] Carlsson, L. A., and Kardomateas, G. A., 2011, *Structural and failure mechanics of sandwich composites*, Springer Science & Business Media.
- [48] Krueger, R., 2004, "Virtual crack closure technique: history, approach, and applications," *Applied Mechanics Reviews*, 57(2), pp. 109-143.
- [49] Cantwell, W., and Davies, P., 1994, "A test technique for assessing core-skin adhesion in composite sandwich structures," *Journal of materials science letters*, 13(3), pp. 203-205.

- [50] Cantwell, W., and Davies, P., 1996, "A study of skin-core adhesion in glass fibre reinforced sandwich materials," *Applied Composite Materials*, 3(6), pp. 407-420.
- [51] Prasad, S., and Carlson, L., 1994, "Debonding and crack kinking in foam core sandwich beams-II," *Experimental investigation, Engng. Fracture Mech*, 47(6), pp. 825-841.
- [52] Kanninen, M., 1973, "An augmented double cantilever beam model for studying crack propagation and arrest," *International Journal of fracture*, 9(1), pp. 83-92.
- [53] Allen, H. G., 2013, *Analysis and Design of Structural Sandwich Panels: The Commonwealth and International Library: Structures and Solid Body Mechanics Division*, Elsevier.
- [54] Carlsson, L. A., Sendlein, L. S., and Merry, S. L., 1991, "Characterization of face sheet/core shear fracture of composite sandwich beams," *Journal of Composite Materials*, 25(1), pp. 101-116.
- [55] Barrett, J., and Foschi, R., 1977, "Mode II stress-intensity factors for cracked wood beams," *Engineering Fracture Mechanics*, 9(2), pp. 371-378.
- [56] Russell, A., and Street, K., 1982, "Factors affecting the interlaminar fracture energy of graphite/epoxy laminates," *Progress in science and Engineering of Composites*, pp. 279-286.
- [57] Reeder, J. R., and REWS, J. H., 1990, "Mixed-mode bending method for delamination testing," *AiAA Journal*, 28(7), pp. 1270-1276.

- [58] Ozdil, F., and Carlsson, L., 2000, "Characterization of mixed mode delamination growth in glass/epoxy composite cylinders," *Journal of composite materials*, 34(5), pp. 420-441.
- [59] Phadatare, A. S., 2012, Flexural analysis of balsa core sandwich composite: Failure mechanisms, core grain orientation and padding effect, WAYNE STATE UNIVERSITY.
- [60] Anderson, T., "Fracture Mechanics Fundamentals and Applications, 2005," CRC press, Taylor and Francis Group, ISBN, 10, pp. 0-8493.
- [61] Lawn, B. R., 1993, Fracture of brittle solids, Cambridge university press.
- [62] 6671-01, A. D. Standard test method for mixed mode I-mode II interlaminar fracture of unidirectional fiber-reinforced polymer matrix composites, D 6671-01. ASTM Standards; 2003
- [63] Manca, M., Quispitupa, A., Berggreen, C., and Carlsson, L. A., 2012, "Face/core debond fatigue crack growth characterization using the sandwich mixed mode bending specimen," *Composites Part A: Applied Science and Manufacturing*, 43(11), pp. 2120-2127.
- [64] ABAQUS, V., 2011, "6.10. 3 Documentation," Dassault Systems.
- [65] Hutchinson, J. W., and Suo, Z., 1992, "Mixed mode cracking in layered materials," *Advances in applied mechanics*, 29(63), p. 191.
- [66] Dundurs, J., 1967, "Effect of elastic constants on stress in a composite under plane deformation," *Journal of Composite Materials*, 1(3), pp. 310-322.

- [67] Liechti, K., and Chai, Y., 1992, "Asymmetric shielding in interfacial fracture under in-plane shear," *Journal of applied mechanics*, 59(2), pp. 295-304.
- [68] HyperMesh, A., "11.0, Altair Engineering," Inc., Troy, MI, USA.
- [69] Krueger, R., 2010, "Development of a benchmark example for delamination fatigue growth prediction."
- [70] Kulkarni, N., Mahfuz, H., Jeelani, S., and Carlsson, L. A., 2003, "Fatigue crack growth and life prediction of foam core sandwich composites under flexural loading," *Composite Structures*, 59(4), pp. 499-505.



**ABSTRACT****FACE SHEET/CORE DEBONDING IN SANDWICH COMPOSITES UNDER  
STATIC AND FATIGUE LOADING**

by

**MANJINDER SINGH WARRIACH****December 2015****Advisor:** Professor Golam Newaz**Major:** Mechanical Engineering**Degree:** Doctor of Philosophy

Delamination growth due to face sheet/core debonding is a major concern due to its inherent weakness in sandwich composites which can be exacerbated due to the presence of flaws. In this research work The primary objective of this research was to characterize the delamination crack growth behavior in E-glass face sheet/polyurethane foam core sandwich composite with pre-existing initial delamination crack at a face sheet/core interface under static and fatigue for mode I and mixed mode loading. For mode I static loading two types of delamination experiments, namely T-peel test and wedge test were implemented to evaluate fracture toughness in polyurethane foam core sandwich composites. It is shown that both tests can provide reliable values for mode I fracture toughness. Two analytical solutions for models (double cantilever beam (DCB) specimen and tilted debond specimen (TDS) test) based on elastic foundation analysis are

modified and validated for mode I loading. For mixed mode static loading, mixed mode bending (MMB) specimen was employed to evaluate energy release rate, compliance and global mode ratio for composite under investigation. It was observed that energy release rate, compliance and global mode ratio increases with increase in crack length. For fatigue life is investigated for constant displacement amplitude for mode I and mixed mode loading using single cantilever beam (SCB) specimen and mixed mode bending (MMB) specimen, respectively. The fatigue test results are in terms of crack growth rate versus energy release rate and Paris law constants are estimated to predict failure of polyurethane foam core sandwich composite. Decreasing crack growth rate as a function of fatigue cycles was attributed to stress relaxation at delamination crack tip. The effect of lever arm distance ( $c$ ) for mixed mode loading is investigated. It is shown that both compliance and energy release increases with an increase in the lever arm distance ( $c$ ) and global mode ratio decreases and mode I become more dominant. The polyurethane foam core sandwich composites results are new. The energy release rate and Paris law constants for a growing crack are low for polyurethane foam core sandwich composites as compared to PVC core sandwich composites. Finally, finite element analyses are conducted to validate the experimental results. The results obtained from experiments and finite element analysis showed good agreement.

**AUTOBIOGRAPHICAL STATEMENT****MANJINDER SINGH WARRIACH****EDUCATION:**

- Ph.D., Mechanical Engineering, Wayne State University, Detroit, Michigan, 2015.
- M.S., Mechanical Engineering, Wayne State University, Detroit, Michigan, 2007.
- B.E., Mechanical Engineering, Pune University, Pune, India, 2004.

**EXPERIENCE:**

- Graduate Teaching Assistant, Mechanical Engineering Department 08/10 - 08/15  
College of Engineering, Wayne State University, Detroit, MI
- Finite Element Analyst, Construction Equipment Group 07/08 - 12/08  
Case New Holland (CNH), Burr Ridge, IL